

A DISTURBANCE-REJECTION PROBLEM  
FOR A 2-D AIRFOIL

by

Thomas R. Bail

Thesis submitted to the Faculty of the Virginia Polytechnic Institute and State  
University in partial fulfillment of the requirements for the degree of

MASTER OF SCIENCE IN MATHEMATICS

APPROVED:

Dr. John Burns, Chairman

Dr. Terry Herdman

Dr. Robert Rogers

April 1997

Blacksburg, VA

Keywords:  $LQG$ ,  $H^\infty$ , flutter, singular values

Copyright 1997, Thomas R. Bail

## A Disturbance-Rejection Problem For a 2-D Airfoil Exhibiting Flutter

Thomas R. Bail

(ABSTRACT)

Flutter suppression is a problem of considerable interest in modern avionics. Flutter is a vibration caused by energy in the airstream being absorbed by a non-rigid wing. Active control is one possible method of suppressing flutter. However, due to unmeasurable aerodynamic-lag states, developing an active control using full-state feedback is not viable. The use of a state-estimator is a more practical way of developing active controllers. In this paper we investigate two control methods using state-estimators. We also use simple models of disturbances to test attenuation and robustness of each control method. Finally, a method of quantitative robust analysis is reviewed and then applied to each of the controlled systems.

## ACKNOWLEDGEMENTS

First, I would like to thank Dr. Burns. The support and enthusiasm he has always offered helped me through many trying times. Second, I wish to thank Dr. Rogers. Through Dr. Rogers I realized what I want to accomplish as a mathematician. Also, a thank you goes out to Dr. Herdman. I appreciate the time and effort he put forth sitting on my committee.

I would like to thank my parents for having me. Whenever I have dreamed they have always allowed me to keep dreaming. All my dreaming is starting to pay off and for this I love them. A special thanks to Dave McKee. The time spent on the field and in the rehearsal room allowed me to release plenty of unwanted stress. Last but not least I thank Shana Olds. Without her I know I would have quit long before I started.

# Contents

<b>1</b>	<b>Introduction</b>	<b>1</b>
<b>2</b>	<b>The Disturbance-Input System</b>	<b>2</b>
2.1	The Airfoil Model . . . . .	2
2.2	The Disturbance-Input Formulation . . . . .	6
<b>3</b>	<b>The Control Problems</b>	<b>9</b>
3.1	The LQG Problem . . . . .	9
3.2	The $H^\infty$ Problem . . . . .	15
<b>4</b>	<b>System Simulations</b>	<b>19</b>
4.1	Open-Loop Simulations . . . . .	20
4.2	Closed-Loop Simulations . . . . .	31
4.2.1	The Stable Case . . . . .	31
4.2.2	The Marginally Stable Case . . . . .	38
4.2.3	The Unstable Case . . . . .	44
4.3	Remarks on Controller Performance . . . . .	52
<b>5</b>	<b>Analysis of Robustness</b>	<b>53</b>
<b>6</b>	<b>Conclusions</b>	<b>64</b>
<b>A</b>	<b>Symbols</b>	<b>65</b>
<b>B</b>	<b>Constants and Matrices</b>	<b>68</b>
<b>C</b>	<b>MATLAB Codes</b>	<b>71</b>

# List of Figures

2.1	2-D Airfoil . . . . .	2
4.1	No Disturbance, $V = 950\text{ft}/\text{sec}$ , Open Loop, $\dot{h}$ , $\dot{\alpha}$ and $\dot{\beta}$ . . . . .	21
4.2	No Disturbance, $V = 950\text{ft}/\text{sec}$ , Open Loop, $h$ , $\alpha$ and $\beta$ . . . . .	22
4.3	No Disturbance, $V = 950\text{ft}/\text{sec}$ , Open Loop, $B_1$ , $B_2$ , $A_1$ , and $A_2$ . . . . .	22
4.4	No Disturbance, $V = 975.6\text{ft}/\text{sec}$ , Open Loop, $\dot{h}$ , $\dot{\alpha}$ and $\dot{\beta}$ . . . . .	23
4.5	No Disturbance, $V = 975.6\text{ft}/\text{sec}$ , Open Loop, $h$ , $\alpha$ and $\beta$ . . . . .	23
4.6	No Disturbance, $V = 975.6\text{ft}/\text{sec}$ , Open Loop, $B_1$ , $B_2$ , $A_1$ , and $A_2$ . . . . .	24
4.7	No Disturbance, $V = 1000\text{ft}/\text{sec}$ , Open Loop, $\dot{h}$ , $\dot{\alpha}$ and $\dot{\beta}$ . . . . .	24
4.8	No Disturbance, $V = 1000\text{ft}/\text{sec}$ , Open Loop, $h$ , $\alpha$ and $\beta$ . . . . .	25
4.9	No Disturbance, $V = 1000\text{ft}/\text{sec}$ , Open Loop, $B_1$ , $B_2$ , $A_1$ , and $A_2$ . . . . .	25
4.10	Disturbance 1, $V = 950\text{ft}/\text{sec}$ , Open Loop, $\dot{h}$ , $\dot{\alpha}$ and $\dot{\beta}$ . . . . .	26
4.11	Disturbance 1, $V = 950\text{ft}/\text{sec}$ , Open Loop, $h$ , $\alpha$ and $\beta$ . . . . .	26
4.12	Disturbance 1, $V = 950\text{ft}/\text{sec}$ , Open Loop, $B_1$ , $B_2$ , $A_1$ , and $A_2$ . . . . .	27
4.13	Disturbance 1, $V = 975.6\text{ft}/\text{sec}$ , Open Loop, $\dot{h}$ , $\dot{\alpha}$ and $\dot{\beta}$ . . . . .	27
4.14	Disturbance 1, $V = 975.6\text{ft}/\text{sec}$ , Open Loop, $h$ , $\alpha$ and $\beta$ . . . . .	28
4.15	Disturbance 1, $V = 975.6\text{ft}/\text{sec}$ , Open Loop, $B_1$ , $B_2$ , $A_1$ , and $A_2$ . . . . .	28
4.16	Disturbance 1, $V = 1000\text{ft}/\text{sec}$ , Open Loop, $\dot{h}$ , $\dot{\alpha}$ and $\dot{\beta}$ . . . . .	29
4.17	Disturbance 1, $V = 1000\text{ft}/\text{sec}$ , Open Loop, $h$ , $\alpha$ and $\beta$ . . . . .	29
4.18	Disturbance 1, $V = 1000\text{ft}/\text{sec}$ , Open Loop, $B_1$ , $B_2$ , $A_1$ , and $A_2$ . . . . .	30
4.19	No Disturbance, $V = 950\text{ft}/\text{sec}$ , $LQG$ Closed-Loop System . . . . .	33
4.20	No Disturbance, $V = 950\text{ft}/\text{sec}$ , $H^\infty$ Closed-Loop System . . . . .	33
4.21	Disturbance 1, $V = 950\text{ft}/\text{sec}$ , $LQG$ Closed-Loop System . . . . .	34
4.22	Disturbance 1, $V = 950\text{ft}/\text{sec}$ , $H^\infty$ Closed-Loop System . . . . .	34
4.23	Disturbance 2, $V = 950\text{ft}/\text{sec}$ , Open-Loop System . . . . .	35
4.24	Disturbance 2, $V = 950\text{ft}/\text{sec}$ , $LQG$ Closed-Loop System . . . . .	35
4.25	Disturbance 2, $V = 950\text{ft}/\text{sec}$ , $H^\infty$ Closed-Loop System . . . . .	36
4.26	Disturbance 3, $V = 950\text{ft}/\text{sec}$ , Open-Loop System . . . . .	36
4.27	Disturbance 3, $V = 950\text{ft}/\text{sec}$ , $LQG$ Closed-Loop System . . . . .	37
4.28	Disturbance 3, $V = 950\text{ft}/\text{sec}$ , $H^\infty$ Closed-Loop System . . . . .	37
4.29	No Disturbance, $V = 975.6\text{ft}/\text{sec}$ , $LQG$ Closed-Loop System . . . . .	38

4.30	No Disturbance, $V = 975.6ft/sec$ , $H^\infty$ Closed-Loop System . . . . .	39
4.31	Disturbance 1, $V = 975.6ft/sec$ , $LQG$ Closed-Loop System . . . . .	39
4.32	Disturbance 1, $V = 975.6ft/sec$ , $H^\infty$ Closed-Loop System . . . . .	40
4.33	Disturbance 2, $V = 975.6ft/sec$ , Open-Loop System . . . . .	40
4.34	Disturbance 2, $V = 975.6ft/sec$ , $LQG$ Closed-Loop System . . . . .	41
4.35	Disturbance 2, $V = 975.6ft/sec$ , $H^\infty$ Closed-Loop System . . . . .	41
4.36	Disturbance 3, $V = 975.6ft/sec$ , Open-Loop System . . . . .	42
4.37	Disturbance 3, $V = 975.6ft/sec$ , $LQG$ Closed-Loop System . . . . .	42
4.38	Disturbance 3, $V = 975.6ft/sec$ , $H^\infty$ Closed-Loop System . . . . .	43
4.39	No Disturbance, $V = 1000ft/sec$ , $LQG$ Closed-Loop System . . . . .	45
4.40	No Disturbance, $V = 1000ft/sec$ , $H^\infty$ Closed-Loop System . . . . .	45
4.41	No Disturbance, $V = 1000ft/sec$ , $\dot{\beta}$ . . . . .	46
4.42	Disturbance 1, $V = 1000ft/sec$ , $LQG$ Closed-Loop System . . . . .	46
4.43	Disturbance 1, $V = 1000ft/sec$ , $H^\infty$ Closed-Loop System . . . . .	47
4.44	Disturbance 1, $V = 1000ft/sec$ , $\dot{\beta}$ . . . . .	47
4.45	Disturbance 2, $V = 1000ft/sec$ , Open-Loop System . . . . .	48
4.46	Disturbance 2, $V = 1000ft/sec$ , $LQG$ Closed-Loop System . . . . .	48
4.47	Disturbance 2, $V = 1000ft/sec$ , $H^\infty$ Closed-Loop System . . . . .	49
4.48	Disturbance 2, $V = 1000ft/sec$ , $\dot{\beta}$ . . . . .	49
4.49	Disturbance 3, $V = 1000ft/sec$ , Open-Loop System . . . . .	50
4.50	Disturbance 3, $V = 1000ft/sec$ , $LQG$ Closed-Loop System . . . . .	50
4.51	Disturbance 3, $V = 1000ft/sec$ , $H^\infty$ Closed-Loop System . . . . .	51
4.52	Disturbance 3, $V = 1000ft/sec$ , $\dot{\beta}$ . . . . .	51
5.1	Singular Values, Open-Loop System, $V = 950ft/sec$ . . . . .	56
5.2	Singular Values, $LQG$ Closed-Loop System, $V = 950ft/sec$ . . . . .	57
5.3	Singular Values, $H^\infty$ Closed-Loop System, $V = 950ft/sec$ . . . . .	58
5.4	Singular Values, Open-Loop System, $V = 975.6ft/sec$ . . . . .	59
5.5	Singular Values, $LQG$ Closed-Loop System, $V = 975.6ft/sec$ . . . . .	60
5.6	Singular Values, $H^\infty$ Closed-Loop System, $V = 975.6ft/sec$ . . . . .	61
5.7	Singular Values, $LQG$ Closed-Loop System, $V = 1000ft/sec$ . . . . .	62
5.8	Singular Values, $H^\infty$ Closed-Loop System, $V = 1000ft/sec$ . . . . .	63

# List of Tables

4.1	Coefficients Defining the Disturbances . . . . .	21
4.2	Stable System Eigenvalues . . . . .	32
B.1	List of $R$ 's . . . . .	69
B.2	List of $\Phi$ 's . . . . .	70
B.3	List of Constants . . . . .	70

# Chapter 1

## Introduction

Physically, flutter is an in-flight vibration of the wings caused by the energy in the airstream being absorbed by a non-rigid structure. Several advantages of flutter suppression are decreasing wing fatigue, better flight comfort, and faster flight velocities. Passive and active control methods have been used to suppress flutter. Passive control can be accomplished by adding mass or stiffness to the wing. This approach adds mass to the system and is therefore undesirable. For this reason we shall consider active control.

We use a model developed by Olds [9] and York [12] for a two-dimensional cross-section of an airfoil. The model consists of an airfoil and a trailing flap. The trailing flap is the physical embodiment of the active control. We are interested in using feedback to drive the trailing flap and damp flutter. In [9] Olds used full-state feedback computed by *LQR* methods. The *LQR* control has the form  $u(t) = -Kx(t)$  and requires that all states be known at all times. In a more practical situation, sensors are used to measure the system's states. However, in many cases, several of the states are unmeasurable. Simply put, all the states are not available for feedback. Consequently, the system states need to be estimated from measured output. Two control methods that make use of a state-estimator are the *LQG* and  $H^\infty$  control methods. These control methods are the focus of this paper.

In [5], Doyle showed that the *LQG* control does not always provide a robust closed-loop system. A small perturbation to the system can cause the closed-loop system to go unstable. Real systems are always subject to many disturbances. Thus, the overall goal of robust control design is to use feedback control to achieve both good performance and robustness.

One of the goals of this paper is to construct the *LQG* and  $H^\infty$  controllers and apply them to the flutter problem. The other goal is to analyze and compare the two approaches by using the Singular Value Robustness Theorem.

# Chapter 2

## The Disturbance-Input System

### 2.1 The Airfoil Model

We consider a disturbance-rejection problem for a two-dimensional airfoil exhibiting flutter. The typical airfoil is viewed as a flat plate suspended from a fixed object by a spring. The basic model is illustrated by Figure 2.1.

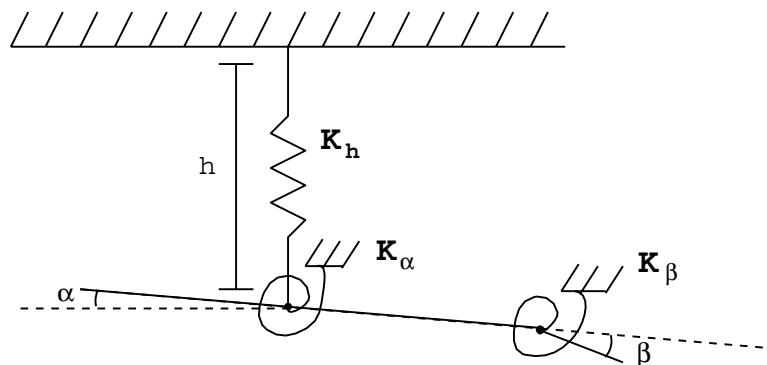


Figure 2.1: 2-D Airfoil

The control flap is located at the trailing edge. The goal is to design a controller that utilizes the control flap to suppress flutter and deal with internal and external disturbances. Referring to Figure 2.1, we let  $h$  denote the plunge,  $\alpha$  the angle of attack and  $\beta$  the flap angle of the controlling flap. The plunge is measured positive downward. The angle of attack, or pitch, is measured from the horizontal at the shear center of the airfoil. The flap angle is measured from the axis created by the airfoil at the control flap hinge. In order to provide the proper restraining forces so that the airfoil behaves as part of an attached wing, one assumes the existence of linear and torsional springs. The stiffness coefficients for these springs are given by  $K_h$  and  $K_\alpha$ , respectively. The torsional flap spring with

stiffness coefficient  $K_\beta$  provides a restraining force on the control flap. The control force is given by a torque applied to this spring. We refer to the paper by Olds [9] for a detailed construction of the model. For this paper we start with the state-space model of the form

$$\dot{x}(t) = Ax(t) + Bu(t) + Gw_1(t). \quad (2.1)$$

Here, the state vector is given by

$$x(t) = \left[ \dot{h}(t) \quad \dot{\alpha}(t) \quad \dot{\beta}(t) \quad h(t) \quad \alpha(t) \quad \beta(t) \quad B_1(t) \quad B_2(t) \quad A_1(t) \quad A_2(t) \right]^T \quad (2.2)$$

where the last four states,  $B_1$ ,  $B_2$ ,  $A_1$ , and  $A_2$ , are called aerodynamic-lag states. The control input  $u(t)$  is the torque applied to the flap. The input  $w_1(t)$  is an external disturbance and the disturbance-input matrix,  $G$  is developed below.

The state matrix,  $A$ , is a  $10 \times 10$  matrix, of the form

$$A = \begin{bmatrix} A_{11} & A_{12} & A_{13} \\ A_{21} & A_{22} & A_{23} \\ A_{31} & A_{32} & A_{33} \end{bmatrix}. \quad (2.3)$$

The exact form of  $A_{ij}$  is derived in [9] and in the thesis by York [12]. For completeness, each  $A_{ij}$  is presented in Appendix B.

The input matrix,  $B$ , is given by

$$B = \frac{1}{I_\beta} \left[ \left( (M')^{-1} \begin{bmatrix} 0 \\ 0 \\ 1 \end{bmatrix} \right)^T \quad 0 \right]^T, \quad (2.4)$$

where  $M'$  is given in Appendix B.

It is useful to write the system in the block form

$$\frac{d}{dt} \begin{bmatrix} \dot{Y}(t) \\ Y(t) \\ x_A(t) \end{bmatrix} = \begin{bmatrix} A_{11} & A_{12} & A_{13} \\ A_{21} & A_{22} & A_{23} \\ A_{31} & A_{32} & A_{33} \end{bmatrix} \begin{bmatrix} \dot{Y}(t) \\ Y(t) \\ x_A(t) \end{bmatrix} + Bu(t) + Gw_1(t) \quad (2.5)$$

where

$$Y(t) = \begin{bmatrix} h(t) \\ \alpha(t) \\ \beta(t) \end{bmatrix} \text{ and } x_A(t) = \begin{bmatrix} A_1(t) \\ A_2(t) \\ B_1(t) \\ B_2(t) \end{bmatrix}. \quad (2.6)$$

Using this block form, the external disturbance is developed. For this paper, the external disturbance is modeled by a wind gust. From Dowell [4] we introduce the lift, moment and

control-flap disturbances due to a gust given by

$$w_L(t) = \int_0^t I_{LG}(t - \sigma) \frac{w_G}{V} d\sigma \quad (2.7)$$

$$w_M(t) = \int_0^t I_{MG}(t - \sigma) \frac{w_G}{V} d\sigma \quad (2.8)$$

$$w_f(t) = \int_0^t I_{fG}(t - \sigma) \frac{w_G}{V} d\sigma, \quad (2.9)$$

where  $w_G$  is the gust vertical velocity. These components are built into the system by adding them to the lift,  $L(t)$ , moment,  $M(t)$ , and torque,  $T(t)$ , developed in the paper by Olds [9].

We start with the new lift, moment and torque given by

$$L_{new}(t) = L(t) + w_L(t) \quad (2.10)$$

$$M_{new}(t) = M(t) + w_M(t) \quad (2.11)$$

$$T_{new}(t) = T(t) + w_f(t). \quad (2.12)$$

From [9] it follows that

$$M'\ddot{Y}(t) + KY(t) = - \begin{bmatrix} L_{new}(t) \\ M_{new}(t) \\ T_{new}(t) \end{bmatrix}, \quad (2.13)$$

which yields

$$\begin{aligned} M'\ddot{Y}(t) + KY(t) &= -\pi\rho b^2 \left[ Z_1\ddot{Y}(t) + Z_2\dot{Y}(t) + Z_3Y(t) + Z_4x_A(t) \right] \\ &\quad - \begin{bmatrix} w_L(t) \\ w_M(t) \\ w_f(t) \end{bmatrix} \\ &= -\pi\rho b^2 \left[ Z_1\ddot{Y}(t) + Z_2\dot{Y}(t) + Z_3Y(t) + Z_4x_A(t) \right] \\ &\quad - \begin{bmatrix} 1 & 0 & 0 \\ 0 & 1 & 0 \\ 0 & 0 & 1 \end{bmatrix} \begin{bmatrix} w_L(t) \\ w_M(t) \\ w_f(t) \end{bmatrix}. \end{aligned} \quad (2.14)$$

Solving for  $\ddot{Y}(t)$ , we have that

$$\begin{aligned} M'\ddot{Y}(t) + \pi\rho b^2 Z_1\ddot{Y}(t) &= -KY(t) - \pi\rho b^2 \left[ Z_2\dot{Y}(t) + Z_3Y(t) + Z_4x_A(t) \right] \\ &\quad - \begin{bmatrix} 1 & 0 & 0 \\ 0 & 1 & 0 \\ 0 & 0 & 1 \end{bmatrix} \begin{bmatrix} w_L(t) \\ w_M(t) \\ w_f(t) \end{bmatrix}, \end{aligned}$$

or equivalently

$$\begin{aligned} [M' + \pi\rho b^2 Z_1] \ddot{Y}(t) &= -KY(t) - \pi\rho b^2 [Z_2 \dot{Y}(t) + Z_3 Y(t) + Z_4 x_A(t)] \\ &\quad - \begin{bmatrix} 1 & 0 & 0 \\ 0 & 1 & 0 \\ 0 & 0 & 1 \end{bmatrix} \begin{bmatrix} w_L(t) \\ w_M(t) \\ w_f(t) \end{bmatrix}. \end{aligned}$$

Hence, it follows that

$$\begin{aligned} \ddot{Y}(t) &= [M' + \pi\rho b^2 Z_1]^{-1} \left( -KY(t) - \pi\rho b^2 [Z_2 \dot{Y}(t) + Z_3 Y(t) + Z_4 x_A(t)] \right) \\ &\quad - [M' + \pi\rho b^2 Z_1]^{-1} \begin{bmatrix} 1 & 0 & 0 \\ 0 & 1 & 0 \\ 0 & 0 & 1 \end{bmatrix} \begin{bmatrix} w_L(t) \\ w_M(t) \\ w_f(t) \end{bmatrix} \\ &= - [M' + \pi\rho b^2 Z_1]^{-1} \left( \pi\rho b^2 Z_2 \dot{Y}(t) + (K + \pi\rho b^2 Z_3) Y(t) + \pi\rho b^2 Z_4 x_A(t) \right) \\ &\quad - [M' + \pi\rho b^2 Z_1]^{-1} \begin{bmatrix} 1 & 0 & 0 \\ 0 & 1 & 0 \\ 0 & 0 & 1 \end{bmatrix} \begin{bmatrix} w_L(t) \\ w_M(t) \\ w_f(t) \end{bmatrix}. \end{aligned} \quad (2.15)$$

Therefore, the model for an airfoil with a wind gust model defined by (2.10)-(2.12) is given by

$$\begin{aligned} \begin{bmatrix} \ddot{Y}(t) \\ \dot{Y}(t) \\ \dot{x}_A(t) \end{bmatrix} &= \begin{bmatrix} A_{11} & A_{12} & A_{13} \\ A_{21} & A_{22} & A_{23} \\ A_{31} & A_{32} & A_{33} \end{bmatrix} \begin{bmatrix} \dot{Y}(t) \\ Y(t) \\ x_A(t) \end{bmatrix} + \\ &\quad - [M' + \pi\rho b^2 Z_1]^{-1} \begin{bmatrix} 1 & 0 & 0 \\ 0 & 1 & 0 \\ 0 & 0 & 1 \\ & & & 0_{7 \times 3} \end{bmatrix} \begin{bmatrix} w_L(t) \\ w_M(t) \\ w_f(t) \end{bmatrix} + Bu(t). \end{aligned} \quad (2.16)$$

We denote the gust matrix by  $G$  and the gust-input vector by  $w_1(t)$  and note that

$$G = [M' + \pi\rho b^2 Z_1]^{-1} \begin{bmatrix} 1 & 0 & 0 \\ 0 & 1 & 0 \\ 0 & 0 & 1 \\ & & & 0_{7 \times 3} \end{bmatrix} \text{ and } w_1(t) = \begin{bmatrix} w_L(t) \\ w_M(t) \\ w_f(t) \end{bmatrix}. \quad (2.17)$$

Since a complete derivation of the model is not provided, it is important to comment on the aerodynamic-lag states. The aerodynamic-lag states represent the aerodynamic loads on the airfoil. In general, it is not possible to directly measure (or sense) these states. Consequently, one must construct estimators for these lag states from the states that are measurable. For this study it is assumed that measurements of  $\dot{h}$ ,  $\dot{\alpha}$ ,  $\dot{\beta}$ ,  $h$ ,  $\alpha$ , and  $\beta$  exist. We see how the unmeasured states affect the formulation for the disturbance-input system in the next section.

## 2.2 The Disturbance-Input Formulation

Consider a disturbance-rejection problem defined by the system

$$\begin{aligned} \dot{x}(t) &= Ax(t) + B_1w(t) + B_2u(t) \\ z(t) &= C_1x(t) + D_{11}w(t) + D_{12}u(t) \\ y(t) &= C_2x(t) + D_{21}w(t) + D_{22}u(t) \end{aligned} \quad (2.18)$$

where  $x(t)$  is the state,  $z(t)$  is the controlled output,  $y(t)$  is the measured output,  $w(t)$  is the disturbance input (external and internal), and  $u(t)$  is the control input. We call the system (2.18) a disturbance-input system. In this section the flutter problem is formulated as a system of the form (2.18).

The state matrix,  $A$ , is defined by (2.3) above. Also, the control-input matrix,  $B_2$  is given by  $B_2 = B$ , where  $B$  is defined by (2.4).

In this study the internal disturbance used is sensor noise. Since measured output is used to derive a control law, sensors are required to measure the system states. It is assumed that the six states,  $\dot{h}$ ,  $\dot{\alpha}$ ,  $\dot{\beta}$ ,  $h$ ,  $\alpha$ , and  $\beta$ , can be sensed. Six separate hypothetical sensors are used to measure each of these states. For each of these sensors, a sinusoidal noise is present. The sensor noise vector,  $w_2(t)$ , is given by

$$w_2(t) = \begin{bmatrix} a_1 \cos(p_1 t) \\ a_2 \cos(p_1 t) \\ a_3 \cos(p_1 t) \\ a_4 \cos(p_2 t) \\ a_5 \cos(p_2 t) \\ a_6 \cos(p_2 t) \end{bmatrix} \quad (2.19)$$

where  $a_i$  and  $p_j$  are selected randomly.

Combining the internal and external disturbance inputs into one vector provides the disturbance input used in system (2.18)

$$w(t) = \begin{bmatrix} w_1(t) \\ w_2(t) \end{bmatrix} = \begin{bmatrix} w_L(t) \\ w_M(t) \\ w_f(t) \\ a_1 \cos(p_1 t) \\ a_2 \cos(p_1 t) \\ a_3 \cos(p_1 t) \\ a_4 \cos(p_2 t) \\ a_5 \cos(p_2 t) \\ a_6 \cos(p_2 t) \end{bmatrix}. \quad (2.20)$$

Now that the disturbance input  $w(t)$  is known,  $B_1$  is known. The disturbance matrix  $B_1$  is given by

$$B_1 = \begin{bmatrix} G_{10 \times 3} & 0_{10 \times 6} \end{bmatrix}. \quad (2.21)$$

The form of this matrix implies that the gust disturbance acts only on the system states.

The controlled output,  $z(t)$  has the form

$$z(t) = C_1x(t) + D_{11}w(t) + D_{12}u(t).$$

The matrix  $C_1$  is given by

$$C_1 = \begin{bmatrix} 1 & 0 & 0 & 0 & 0 & 0 & 0 & 0 & 0 & 0 \\ 0 & 1 & 0 & 0 & 0 & 0 & 0 & 0 & 0 & 0 \\ 0 & 0 & 1 & 0 & 0 & 0 & 0 & 0 & 0 & 0 \\ 0 & 0 & 0 & 1 & 0 & 0 & 0 & 0 & 0 & 0 \\ 0 & 0 & 0 & 0 & 1 & 0 & 0 & 0 & 0 & 0 \\ 0 & 0 & 0 & 0 & 0 & 1 & 0 & 0 & 0 & 0 \\ 0 & 0 & 0 & 0 & 0 & 0 & .0001 & 0 & 0 & 0 \\ 0 & 0 & 0 & 0 & 0 & 0 & 0 & .0001 & 0 & 0 \\ 0 & 0 & 0 & 0 & 0 & 0 & 0 & 0 & .0001 & 0 \\ 0 & 0 & 0 & 0 & 0 & 0 & 0 & 0 & 0 & .0001 \\ 0 & 0 & 0 & 0 & 0 & 0 & 0 & 0 & 0 & 0 \end{bmatrix}. \quad (2.22)$$

The disturbance matrix  $D_{11}$  is given by

$$D_{11} = \begin{bmatrix} 0_{11 \times 9} \end{bmatrix} \quad (2.23)$$

and the matrix  $D_{12}$  is defined by

$$D_{12} = \begin{bmatrix} 0_{10 \times 1} \\ 1 \end{bmatrix}. \quad (2.24)$$

The above matrices define the controlled output. The disturbance input has no affect on the controlled output and minimal weighting is added to either the system states or to the control. The weighting applied to the lag states provides a reduction of their impact on the controlled output. From the above matrices the controlled output has the form

$$z(t) = \begin{bmatrix} \dot{h}(t) \\ \dot{\alpha}(t) \\ \dot{\beta}(t) \\ h(t) \\ \alpha(t) \\ \beta(t) \\ .0001B_1(t) \\ .0001B_2(t) \\ .0001A_1(t) \\ .0001A_2(t) \\ u(t) \end{bmatrix}. \quad (2.25)$$

The measured output has the form

$$y(t) = C_2x(t) + D_{21}w(t) + D_{22}u(t).$$

The matrices  $C_2$ ,  $D_{21}$  and  $D_{22}$  are given by

$$C_2 = \begin{bmatrix} I_{6 \times 10} & 0_{6 \times 4} \end{bmatrix}, \quad (2.26)$$

$$D_{21} = \begin{bmatrix} 0_{6 \times 3} & I_{6 \times 6} \end{bmatrix}, \quad (2.27)$$

and

$$D_{22} = \begin{bmatrix} 0_{6 \times 1} \end{bmatrix}. \quad (2.28)$$

Using these matrices one observes that only the first six states and the sensor noise are present in the measured output. The form of  $C_2$  implies that the control input has no direct affect on the measured output. Also, the form of  $D_{21}$  implies that the sensor noise is explicitly present in the measured output and the gust enters the measured input indirectly. Using the system matrices defined above, the measured output has the specific form

$$y(t) = \begin{bmatrix} \dot{h}(t) + (a_1 \cos(p_1 t)) \\ \dot{\alpha}(t) + (a_2 \cos(p_1 t)) \\ \dot{\beta}(t) + (a_3 \cos(p_1 t)) \\ h(t) + (a_4 \cos(p_2 t)) \\ \alpha(t) + (a_5 \cos(p_2 t)) \\ \beta(t) + (a_6 \cos(p_2 t)) \end{bmatrix}. \quad (2.29)$$

A complete dynamic system involving an airfoil exhibiting flutter, wind gust and sensor noise has now been constructed. We turn now to the flutter suppression problem.

# Chapter 3

## The Control Problems

### 3.1 The LQG Problem

In [9] Olds applies an *LQR* control method to the flutter suppression problem. This control method is not practical because of the unmeasurable lag states. Also, one needs to consider the effects of internal and external disturbances. To address these issues *LQG* and  $H^\infty$  control methods are utilized. The method discussed in this section is the *LQG* method. In designing the *LQG* controller we start with the dynamic system

$$\begin{aligned} \dot{x}(t) &= Ax(t) + B_2u(t) + \xi(t) \\ z(t) &= C_1x(t) + D_{12}u(t) \\ y(t) &= C_2x(t) + D_{22}u(t) + \theta(t) \end{aligned} \tag{3.1}$$

where  $\xi(t)$ , the plant noise, and  $\theta(t)$ , the measurement noise, are white and Gaussian with joint correlation function

$$E \left\{ \begin{bmatrix} \xi(t) \\ \theta(t) \end{bmatrix} \begin{bmatrix} \xi(t) & \theta(t) \end{bmatrix} \right\} = \begin{bmatrix} \Xi & 0 \\ 0 & \Theta \end{bmatrix} \delta(t - \tau). \tag{3.2}$$

For this case  $\Xi$  and  $\Theta$  are defined to be

$$\Xi = [I_{10 \times 10}],$$

and

$$\Theta = [I_{6 \times 6}].$$

The goal is to find a control input  $u(t)$  such that the system is stabilized and the control minimizes the cost function

$$J_{LQG} = \lim_{T \rightarrow \infty} E \left\{ \int_0^T \begin{bmatrix} x(t)^T & u(t)^T \end{bmatrix} \begin{bmatrix} Q & 0 \\ 0 & R \end{bmatrix} \begin{bmatrix} x(t) \\ u(t) \end{bmatrix} dt \right\}. \tag{3.3}$$

From Rhee and Speyer [10] the matrices  $Q$  and  $R$  are defined to be

$$Q = C_1^T C_1 \quad (3.4)$$

$$R = D_{12}^T D_{12}. \quad (3.5)$$

It follows from Green and Limebeer [8] that if the pair  $(A, B_2)$  is stabilizable and the pair  $(A, C_2)$  is detectable, then a solution to the  $LQG$  problem exists. For the pair  $(A, B_2)$  to be stabilizable we have to show that there exists a  $K$  such that the real parts of the eigenvalues of  $(A - B_2 K)$  are negative. For this paper the system (2.18) is simulated at the velocities  $V = 950 \text{ ft/sec}$ ,  $V = 975.6 \text{ ft/sec}$  and  $V = 1000 \text{ ft/sec}$ . Therefore, we show the pair  $(A, B_2)$  to be stabilizable and the pair  $(A, C_2)$  to be detectable at each of these flow speeds. If  $V = 950 \text{ ft/sec}$  and  $K$  is given by

$$K = \left[ 0_{10 \times 1} \right], \quad (3.6)$$

then the eigenvalues of  $(A - B_2 K)$  are

$$\begin{aligned} \lambda_1 &= -6.20 + 563.58i \\ \lambda_2 &= -6.20 - 563.58i \\ \lambda_3 &= -2.34 + 81.63i \\ \lambda_4 &= -2.34 - 81.63i \\ \lambda_5 &= -17.84 + 66.81i \\ \lambda_6 &= -17.84 - 66.81i \\ \lambda_7 &= -93.18 \\ \lambda_8 &= -12.98 \\ \lambda_9 &= -101.33 \\ \lambda_{10} &= -12.98 \end{aligned}$$

which have all negative real parts. Therefore, the pair  $(A, B_2)$  at  $V = 950 \text{ ft/sec}$  is stabilizable.

If  $V = 975.6 \text{ ft/sec}$  and  $K$  is given by

$$K = \begin{bmatrix} .5470 & -1.5529 & 0.6858 & -38.6409 & -39.4681 \\ -27.4179 & 0.0017 & 0.0349 & 0.0001 & 0.0173 \end{bmatrix}, \quad (3.7)$$

then the eigenvalues of  $(A - B_2K)$  are

$$\begin{aligned}
\lambda_1 &= -29.05 + 562.64i \\
\lambda_2 &= -29.05 - 562.64i \\
\lambda_3 &= -0.15 + 80.32i \\
\lambda_4 &= -0.15 - 80.32i \\
\lambda_5 &= -20.95 + 67.37i \\
\lambda_6 &= -20.95 - 67.37i \\
\lambda_7 &= -95.20 \\
\lambda_8 &= -13.33 \\
\lambda_9 &= -104.06 \\
\lambda_{10} &= -13.33
\end{aligned}$$

which have all negative real parts. Therefore, the pair  $(A, B_2)$  at  $V = 975.6ft/sec$  is stabilizable.

If  $V = 1000ft/sec$  and  $K$  is given by

$$K = \begin{bmatrix} 9.5 & -33.8 & -1.7 & -1052.0 & -777.0 \\ -589.6 & 0.0 & 0.8 & 0.0 & 0.1 \end{bmatrix}, \quad (3.8)$$

then the eigenvalues of  $(A - B_2K)$  are

$$\begin{aligned}
\lambda_1 &= -29.09 + 562.41i \\
\lambda_2 &= -29.09 - 562.41i \\
\lambda_3 &= -2.09 + 79.60i \\
\lambda_4 &= -2.09 - 79.60i \\
\lambda_5 &= -23.79 + 67.33i \\
\lambda_6 &= -23.79 - 67.33i \\
\lambda_7 &= -97.10 \\
\lambda_8 &= -13.66 \\
\lambda_9 &= -106.67 \\
\lambda_{10} &= -13.67
\end{aligned}$$

which have all negative real parts. Therefore, the pair  $(A, B_2)$  at  $V = 1000ft/sec$  is stabilizable.

To show the pair  $(A, C_2)$  observable at each of the flow speeds it is necessary to find an  $L$  such that the real parts of the eigenvalues of  $(A - LC_2)$  are all negative. To show  $(A - LC_2)$  stable at  $V = 950ft/sec$ , we define  $L$  to be

$$L = \begin{bmatrix} 0_{10 \times 6} \end{bmatrix}, \quad (3.9)$$

then the eigenvalues of  $(A - LC_2)$  are

$$\begin{aligned}
\lambda_1 &= -6.20 + 563.58i \\
\lambda_2 &= -6.20 - 563.58i \\
\lambda_3 &= -2.34 + 81.63i \\
\lambda_4 &= -2.34 - 81.63i \\
\lambda_5 &= -17.84 + 66.81i \\
\lambda_6 &= -17.84 - 66.81i \\
\lambda_7 &= -93.18 \\
\lambda_8 &= -12.98 \\
\lambda_9 &= -101.33 \\
\lambda_{10} &= -12.98
\end{aligned}$$

which have all negative real parts. Therefore, the pair  $(A, C_2)$  at  $V = 950ft/sec$  is detectable.

If  $V = 975.6ft/sec$  and  $L$  is given by

$$L = \begin{bmatrix} 0.1026 & -0.0225 & -0.0045 & -0.7537 & -0.4839 & 0.2293 \\ -0.0225 & 0.3005 & 0.0434 & 1.0745 & -1.8968 & -1.8359 \\ -0.0045 & 0.0434 & 0.0212 & 0.1151 & -0.1188 & -1.3582 \\ -0.7537 & 1.0745 & 0.1151 & 17.8592 & -4.9909 & -2.7750 \\ -0.4839 & -1.8968 & -0.1188 & -4.9909 & 32.5076 & -4.8824 \\ 0.2293 & -1.8359 & -1.3582 & -2.7750 & -4.8824 & 169.7855 \\ 0 & 0 & 0 & 0 & 0 & 0 \\ 0 & 0 & 0 & 0 & 0 & 0 \\ 0 & 0 & 0 & 0 & 0 & 0 \\ 0 & 0 & 0 & 0 & 0 & 0 \end{bmatrix}, \quad (3.10)$$

then the eigenvalues of  $(A - LC_2)$  are given by

$$\begin{aligned}
\lambda_1 &= -2309.1 + 2372.0i \\
\lambda_2 &= -2309.1 - 2372.0i \\
\lambda_3 &= -459.3 + 477.9i \\
\lambda_4 &= -459.3 - 477.9i \\
\lambda_5 &= -231.3 + 237.0i \\
\lambda_6 &= -231.3 - 237.0i \\
\lambda_7 &= -105.8 \\
\lambda_8 &= -13.4 \\
\lambda_9 &= -104.1 \\
\lambda_{10} &= -13.3
\end{aligned}$$

which have all negative real parts. Therefore, the pair  $(A, C_2)$  at  $V = 975.6ft/sec$  is detectable.

Finally, if  $V = 1000$  and  $L$  is given by

$$L = \begin{bmatrix} 0.1005 & -0.0238 & -0.0047 & -0.7375 & -0.5089 & 0.2362 \\ -0.0238 & 0.3099 & 0.0446 & 1.1302 & -1.8733 & -1.8761 \\ -0.0047 & 0.0446 & 0.0214 & 0.1197 & -0.1153 & -1.3681 \\ -0.7375 & 1.1302 & 0.1197 & 18.0619 & -4.8518 & -2.8418 \\ -0.5089 & -1.8733 & -0.1153 & -4.8518 & 32.1243 & -4.9022 \\ 0.2362 & -1.8761 & -1.3681 & -2.8418 & -4.9022 & 170.2751 \\ 0 & 0 & 0 & 0 & 0 & 0 \\ 0 & 0 & 0 & 0 & 0 & 0 \\ 0 & 0 & 0 & 0 & 0 & 0 \\ 0 & 0 & 0 & 0 & 0 & 0 \end{bmatrix}, \quad (3.11)$$

then the eigenvalues of  $(A - LC_2)$  are given by

$$\begin{aligned} \lambda_1 &= -2316.1 + 2378.9i \\ \lambda_1 &= -2316.1 - 2378.9i \\ \lambda_1 &= -453.5 + 471.5i \\ \lambda_1 &= -453.5 - 471.5i \\ \lambda_1 &= -234.9 + 240.6i \\ \lambda_1 &= -234.9 - 240.6i \\ \lambda_1 &= -108.6 \\ \lambda_1 &= -13.7 \\ \lambda_1 &= -106.7 \\ \lambda_1 &= -13.7 \end{aligned}$$

which have all negative real parts. Thus, the pair  $(A, C_2)$  at  $V = 1000 \text{ ft/sec}$  is detectable. Since it has been shown that the system is both stabilizable and detectable at each of the flow speeds, solutions exist for the  $LQG$  control problem. The general solution for the  $LQG$  problem is now presented.

In  $LQG$  design the measured output is used to build a state-estimator for the system. This state estimator is of the form

$$\dot{\hat{x}} = A_0 \hat{x}(t) + K_f y(t). \quad (3.12)$$

The control law makes use of this estimator and is defined by

$$u^*(t) = -K_c \hat{x}(t). \quad (3.13)$$

If  $A_0$  and  $K_f$  are chosen correctly, then

$$\lim_{t \rightarrow \infty} \|\hat{x}(t) - x(t)\| = 0 \quad (3.14)$$

and  $\hat{x}(t)$  estimates  $x(t)$ . Hence, we expect that  $u^*(t)$  will stabilize the system much like the control law utilizing full-state feedback. The *LQG* controller is built by first solving the decoupled algebraic Riccati equations

$$A^T P + PA - PBR^{-1}B_2^T + Q = 0 \quad (3.15)$$

$$AS + SA^T + \Xi - SC_2^T \Theta^{-1} C_2 S = 0 \quad (3.16)$$

for  $P$  and  $S$ . The control gain  $K_c$  and the filter gain  $K_f$  are defined as

$$K_c = R^{-1} B_2^T P, \quad (3.17)$$

and

$$K_f = SC_2^T \Theta^{-1}, \quad (3.18)$$

respectively. Since  $K_c$  and  $K_f$  are known, the compensator matrix  $A_0$  is defined as

$$A_0 = A - B_2 K_c - K_f C_2. \quad (3.19)$$

Using the state-estimator and the control law defined by (3.12) and (3.13), respectively, one can close the loop and the system becomes

$$\dot{x}(t) = Ax(t) + B_1 w(t) + B_2 u(t) \quad (3.20)$$

$$z(t) = C_1 x(t) + D_{11} w(t) + D_{12} u(t) \quad (3.21)$$

$$y(t) = C_2 x(t) + D_{21} w(t) + D_{22} u(t) \quad (3.22)$$

$$\dot{\hat{x}}(t) = A_0 \hat{x}(t) + K_f y(t) \quad (3.23)$$

$$u^*(t) = -K_c \hat{x}(t). \quad (3.24)$$

Substituting (3.22) and (3.24) into (3.20)-(3.23) yields the closed-loop system

$$\begin{aligned} \dot{x}(t) &= Ax(t) + B_2 (-K_c \hat{x}(t)) + B_1 w(t) \\ z(t) &= C_1 x(t) + D_{12} (-K_c \hat{x}(t)) + D_{11} w(t) \\ \dot{\hat{x}}(t) &= K_f C_2 x(t) + (A_0 - D_{22} K_c) \hat{x}(t) + K_f D_{21} w(t), \end{aligned} \quad (3.25)$$

or equivalently,

$$\begin{aligned} \begin{bmatrix} \dot{x}(t) \\ \dot{\hat{x}}(t) \end{bmatrix} &= \begin{bmatrix} A & -B_2 K_c \\ K_f C_2 & A_0 - D_{22} K_c \end{bmatrix} \begin{bmatrix} x(t) \\ \hat{x}(t) \end{bmatrix} + \begin{bmatrix} B_1 \\ K_f D_{21} \end{bmatrix} w(t) \\ z(t) &= \begin{bmatrix} C & -D_{12} K_c \end{bmatrix} \begin{bmatrix} x(t) \\ \hat{x}(t) \end{bmatrix} + D_{11} w(t). \end{aligned} \quad (3.26)$$

For analysis purposes, system (3.26) is written as

$$\begin{aligned} \begin{bmatrix} \dot{x}(t) \\ \hat{x}(t) \end{bmatrix} &= \begin{bmatrix} A_{LQG} \end{bmatrix} \begin{bmatrix} x(t) \\ \hat{x}(t) \end{bmatrix} + \begin{bmatrix} B_{LQG} \end{bmatrix} w(t) \\ z(t) &= \begin{bmatrix} C_{LQG} \end{bmatrix} \begin{bmatrix} x(t) \\ \hat{x}(t) \end{bmatrix} + D_{LQG} w(t). \end{aligned} \quad (3.27)$$

We implement the LQG control in Chapter 4. However, as shown by Doyle [5] the LQG optimal control is not always robustly stable. For some problems a small perturbation can be found that causes the closed-loop system to become unstable. One of the goals of this paper is to find a controller that can withstand reasonable disturbances and keep the system stable. This is the goal of  $H^\infty$  design. In addressing the shortcomings of LQG robustness many new control schemes have been developed. The  $H^\infty$  control method is one of the more attractive schemes and is the focus of the next section.

## 3.2 The $H^\infty$ Problem

The  $H^\infty$  control method was specifically developed to produce a robustly stable closed-loop system. For any stable perturbation, additive or multiplicative, an  $H^\infty$  computed controller is designed to keep the closed-loop system from going unstable. The  $H^\infty$  norm is used as a performance measure. The  $H^\infty$  norm is defined as

$$\|G\|_\infty = \sup_\omega \bar{\sigma}(G(j\omega)) \quad (3.28)$$

where  $G$  denotes a stable Laplace matrix,  $\omega$  denotes frequency, and  $\bar{\sigma}$  denotes the maximum singular value.

After the loop is closed by substituting the controller, the closed-loop system maps the disturbance input  $w(t)$  to the controlled output  $z(t)$ . This system transfer function is denoted by  $T_{zw}$ . The goal of the  $H^\infty$  control method is to find a  $u(t)$  that minimizes

$$\|T_{zw}\|_\infty.$$

This guarantees a robustly stable optimal control. In many cases the  $H^\infty$  norm cannot be minimized. Although it may not be possible to minimize the  $H^\infty$  norm it is possible to bound it.

In the paper by Doyle, Glover, Khargonekar, and Francis [6], they show that bounding the  $H^\infty$  norm,  $\|T_{zw}\|_\infty < \gamma$ ,  $\gamma > 0$ , is equivalent to the Hamiltonian  $H$  of  $T_{zw}$  having no eigenvalues on the imaginary axis. Then a control law computed from positive semi-definite solutions to two decoupled algebraic Riccati equations provides a stable system. This system is guaranteed to remain stable when perturbed by a stable disturbance.

From Dorato, Abdallah and Cerone [3], the  $H^\infty$  problem is defined by the system

$$\begin{aligned}\dot{x}(t) &= Ax(t) + B_1w(t) + B_2u(t) \\ z(t) &= C_1x(t) + D_{11}w(t) + D_{12}u(t) \\ y(t) &= C_2x(t) + D_{21}w(t) + D_{22}u(t).\end{aligned}\tag{3.29}$$

The objective is to find a compensator that generates a control  $u(t)$  from the measured output  $y(t)$  such that

$$\|T_{zw}(s)\|_\infty < \gamma.\tag{3.30}$$

For this problem  $\gamma$  is defined to be 1.

For the special case where

$$D_{12}^T \begin{bmatrix} C_1 & D_{12} \end{bmatrix} = \begin{bmatrix} 0 & I \end{bmatrix}\tag{3.31}$$

and

$$\begin{bmatrix} B_1 \\ D_{21} \end{bmatrix} D_{21}^T = \begin{bmatrix} 0 \\ I \end{bmatrix}\tag{3.32}$$

it is known (see [3]) that a controller exists and can be found if the solutions  $X$  and  $Y$  of the two decoupled algebraic Riccati equations

$$0 = A^T X + XA + X(B_1B_1^T - B_2B_2^T)X + C_1^T C_1\tag{3.33}$$

$$0 = AY + YA^T + Y(C_1^T - C_2^T C_2)Y + B_1^T B_1\tag{3.34}$$

exists such that  $X \geq 0$ ,  $Y \geq 0$ , and  $\rho(XY) < 1$ , where  $\rho$  denotes the spectral radius of the matrix.

From the system (2.18) it is known that

$$C_1 = \begin{bmatrix} I_{10 \times 10} \\ 0_{1 \times 10} \end{bmatrix}$$

and

$$D_{12} = \begin{bmatrix} 0_{10 \times 1} \\ 1 \end{bmatrix}.$$

Therefore,

$$\begin{aligned}D_{12}^T \begin{bmatrix} C_1 & D_{12} \end{bmatrix} &= \begin{bmatrix} 0_{1 \times 10} & 1 \end{bmatrix} \begin{bmatrix} I_{10 \times 10} & 0_{10 \times 1} \\ 0_{1 \times 10} & 1 \end{bmatrix} \\ &= \begin{bmatrix} 0_{1 \times 10} & 1 \end{bmatrix} = \begin{bmatrix} 0 & I \end{bmatrix}\end{aligned}$$

and the first condition is satisfied.

Also, from the system it is known that

$$B_1 = \begin{bmatrix} G_{10 \times 3} & 0_{10 \times 6} \end{bmatrix} = \begin{bmatrix} I_{3 \times 3} & 0_{3 \times 6} \\ 0_{7 \times 3} & 0_{7 \times 6} \end{bmatrix}$$

and

$$D_{21} = \begin{bmatrix} 0_{6 \times 3} & I_{6 \times 6} \end{bmatrix}.$$

Therefore,

$$\begin{bmatrix} B_1 \\ D_{21} \end{bmatrix} D_{21}^T = \begin{bmatrix} I_{3 \times 3} & 0_{3 \times 6} \\ 0_{7 \times 3} & 0_{7 \times 6} \\ 0_{6 \times 3} & I_{6 \times 6} \end{bmatrix} \begin{bmatrix} 0_{3 \times 6} \\ I_{6 \times 6} \end{bmatrix} = \begin{bmatrix} 0_{10 \times 6} \\ I_{6 \times 6} \end{bmatrix} = \begin{bmatrix} 0 \\ I \end{bmatrix}$$

and the second condition is met. To check the conditions on the solutions to the decoupled algebraic Riccati equations we use MATLAB routines. For the problem defined by (2.18), the  $H^\infty$  control law  $u(t)$  exists and was computed using the  $H^\infty$  routine in the MATLAB Robust Control Toolbox.

From Doyle, Glover, Khargonekar, and Francis [6] it is shown that the estimator

$$\dot{\hat{x}}(t) = \hat{A}\hat{x}(t) - ZLy(t) \quad (3.35)$$

will stabilize the system if the feedback law has the form

$$u(t) = F\hat{x}(t), \quad (3.36)$$

where

$$\hat{A} = A + B_1 B_1^T X + B_2 F + ZLC_2 \quad (3.37)$$

$$F = -B_2^T X \quad (3.38)$$

$$L = -YC_2 \quad (3.39)$$

$$Z = (I - YX)^{-1}. \quad (3.40)$$

Observe that the  $H^\infty$  and  $LQG$  controllers have a similar structure. Both methods involve solving two decoupled algebraic Riccati equations to produce a control law.

The  $H^\infty$  closed-loop system is given by

$$\dot{x}(t) = Ax(t) + B_1 w(t) + B_2 u(t) \quad (3.41)$$

$$z(t) = C_1 x(t) + D_{11} w(t) + D_{12} u(t) \quad (3.42)$$

$$y(t) = C_2 x(t) + D_{21} w(t) + D_{22} u(t) \quad (3.43)$$

$$\dot{\hat{x}}(t) = \hat{A}\hat{x}(t) - ZLy(t) \quad (3.44)$$

$$u(t) = F\hat{x}(t). \quad (3.45)$$

Substituting (3.43) and (3.45) into (3.41)-(3.44) yields the closed-loop system

$$\begin{aligned}
\dot{x}(t) &= Ax(t) + B_2F\hat{x}(t) + B_1w(t) \\
\dot{\hat{x}}(t) &= -ZLC_2x(t) + (\hat{A} - ZLD_{22}F)\hat{x}(t) - ZLD_{21}w(t) \\
z(t) &= C_1x(t) + D_{12}F\hat{x}(t) + D_{11}w(t),
\end{aligned} \tag{3.46}$$

or equivalently,

$$\begin{aligned}
\begin{bmatrix} \dot{x}(t) \\ \dot{\hat{x}}(t) \end{bmatrix} &= \begin{bmatrix} A & B_2F \\ -ZLC_2 & \hat{A} - ZLD_{22}F \end{bmatrix} \begin{bmatrix} x(t) \\ \hat{x}(t) \end{bmatrix} + \begin{bmatrix} B_1 \\ -ZLD_{21} \end{bmatrix} w(t) \\
z(t) &= \begin{bmatrix} C_1 & D_{12}F \end{bmatrix} \begin{bmatrix} x(t) \\ \hat{x}(t) \end{bmatrix} + D_{11}w(t).
\end{aligned} \tag{3.47}$$

For analysis purposes, system (3.47) is written as

$$\begin{aligned}
\begin{bmatrix} \dot{x}(t) \\ \dot{\hat{x}}(t) \end{bmatrix} &= \begin{bmatrix} A_{H^\infty} \end{bmatrix} \begin{bmatrix} x(t) \\ \hat{x}(t) \end{bmatrix} + \begin{bmatrix} B_{H^\infty} \end{bmatrix} w(t) \\
z(t) &= \begin{bmatrix} C_{H^\infty} \end{bmatrix} \begin{bmatrix} x(t) \\ \hat{x}(t) \end{bmatrix} + D_{H^\infty}w(t).
\end{aligned} \tag{3.48}$$

In Chapter 4 the  $H^\infty$  and  $LQG$  closed-loop systems are implemented. These systems are simulated using MATLAB and various numerical experiments are performed.

# Chapter 4

## System Simulations

We turn now to numerical simulations of the open-loop and closed-loop systems. The goal is to test and compare the  $LQG$  and  $H^\infty$  controllers. The  $LQG$  and  $H^\infty$  controllers are constructed using the  $LQR$  package found in the MATLAB Control System Toolbox [7] and the  $H^\infty$  package found in the MATLAB Robust Control Toolbox [2], respectively. Additional MATLAB codes needed to construct the system matrices are given in Appendix C. The basic system is a linear first-order ordinary differential equation with ten states. Once the disturbance-inputs are defined the differential equations are solved using the routine ODE45 in MATLAB. The random disturbances are defined by first defining the gust function. As discussed in Section 2.2 the random gust functions are assumed to have the form

$$w_M(t) = g_L * \begin{cases} 1 & x \in [tstep, tstep + .25] \\ 0 & elsewhere \end{cases}, \quad (4.1)$$

$$w_M(t) = g_M * \begin{cases} 1 & x \in [tstep, tstep + .25] \\ 0 & elsewhere \end{cases}, \quad (4.2)$$

$$w_f(t) = g_f * \begin{cases} 1 & x \in [tstep, tstep + .25] \\ 0 & elsewhere \end{cases}, \quad (4.3)$$

where  $g_L$ ,  $g_M$ ,  $g_f$ , and  $tstep$  are defined in Table 4.1. The coefficient  $tstep$  is the time that the gust is turned on. This model represents a sharp gust function with a duration of .25 seconds. The random coefficients for the sensor noise are also defined in Table 4.1. Simulations are run for three different disturbances and for the case with no disturbance assuming the three velocities  $V = 950ft/sec$ ,  $V = 975.6ft/sec$  and  $V = 1000ft/sec$ . For the model and the parameters defined here, the flutter speed is  $V_f = 975.6ft/sec$ . The flutter speed is the velocity at which the open-loop system is marginally stable. Above the flutter speed the open-loop system is unstable and below the flutter speed the open-loop system is asymptotically stable. The velocities  $V = 950ft/sec$  and  $V = 1000ft/sec$  are used to test the performance of the controlled systems for the stable and unstable cases.

## 4.1 Open-Loop Simulations

In this section we present the results of typical simulations of the open-loop system for various flow speeds  $V$  and disturbances as defined in Table 4.1. The open-loop system is defined by setting  $u(t) = 0$ .

Figures 4.1-4.3 represent the asymptotically stable system with no disturbance. The states asymptotically approach zero. This is expected of a stable system. Figures 4.4-4.6 represent the marginally stable system with no disturbance. As one would expect, the ten states neither approach zero nor grow unbounded. Finally, Figures 4.7-4.9 represent the unstable system with no disturbance. The displacement of the plunge in Figure 4.8 is approximately  $\pm 2000 ft$  after 5 seconds. Obviously, the model is not valid. In a real system, the airfoil would have been torn from the aircraft before this point.

Figures 4.10-4.18 represent the open-loop system at the three velocities with a typical disturbance. For these particular plots Disturbance 1 is used. Figures 4.10-4.12 show the system states for the stable open-loop system. The wind gust is evident in each of the system states. One sees a sudden rise in the states at 2 seconds. This is indicative of the sharp gust function. After the wind gust hits, the stability of the system drives the states to zero.

Figures 4.13-4.15 are the system states of the marginally stable system acted upon by Disturbance 1. The wind gust causes an interesting effect on the states. Since the system is marginally stable, the solutions continue to oscillate at a specific amplitude. After the wind gust hits, the amplitude of the system is increased. As mentioned before, the states are neither asymptotically approaching zero nor growing unbounded. Therefore, the airfoil oscillates at the new amplitude.

The unstable system with Disturbance 1 is presented in Figures 4.16-4.18. The effects of the disturbance cannot be seen because the system states become too large too fast. Again, because the system states are becoming unbounded, the airfoil would have been torn from the aircraft.

Since it was shown that the system velocities and the system positions both asymptotically approach zero for the stable system, we only concentrate on the states  $h$ ,  $\alpha$  and  $\beta$  in the next sections.

No disturbance	Disturbance 1	Disturbance 2	Disturbance 3
$g_L = 0$	$g_L = 3 \times 10^8$	$g_L = 2 \times 10^8$	$g_L = 1 \times 10^8$
$g_M = 0$	$g_M = 9 \times 10^3$	$g_M = 3 \times 10^4$	$g_M = 1 \times 10^5$
$g_f = 0$	$g_f = 0$	$g_f = 0$	$g_f = 0$
$a_1 = 0$	$a_1 = 12$	$a_1 = 18$	$a_1 = 10$
$a_2 = 0$	$a_2 = 10$	$a_2 = 2$	$a_2 = 16$
$a_3 = 0$	$a_3 = 3$	$a_3 = 8$	$a_3 = 1$
$a_4 = 0$	$a_4 = .2$	$a_4 = .09$	$a_4 = .7$
$a_5 = 0$	$a_5 = .16$	$a_5 = 2$	$a_5 = .9$
$a_6 = 0$	$a_6 = .03$	$a_6 = .5$	$a_6 = .0005$
$p_1 = 0$	$p_1 = 10$	$p_1 = 15$	$p_1 = 7$
$p_2 = 0$	$p_2 = 5$	$p_2 = 2$	$p_2 = 9$
$tstep = 0$	$tstep = 2$	$tstep = 2.5$	$tstep = 1$

Table 4.1: Coefficients Defining the Disturbances

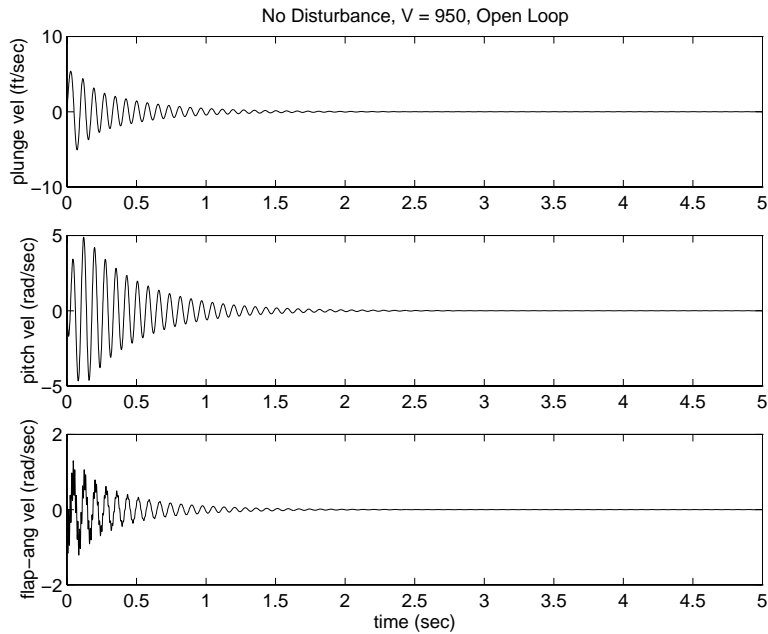


Figure 4.1: No Disturbance,  $V = 950 ft/sec$ , Open Loop,  $\dot{h}$ ,  $\dot{\alpha}$  and  $\dot{\beta}$

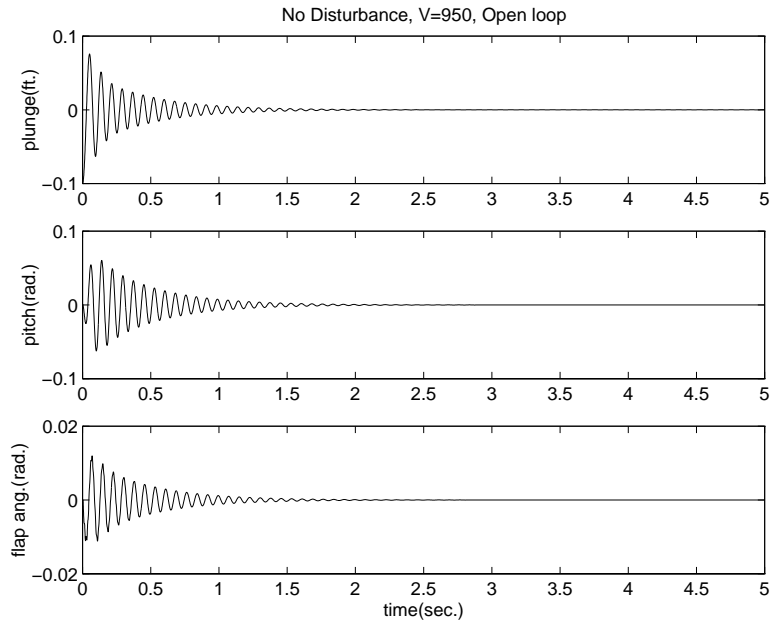


Figure 4.2: No Disturbance,  $V = 950\text{ft}/\text{sec}$ , Open Loop,  $h$ ,  $\alpha$  and  $\beta$

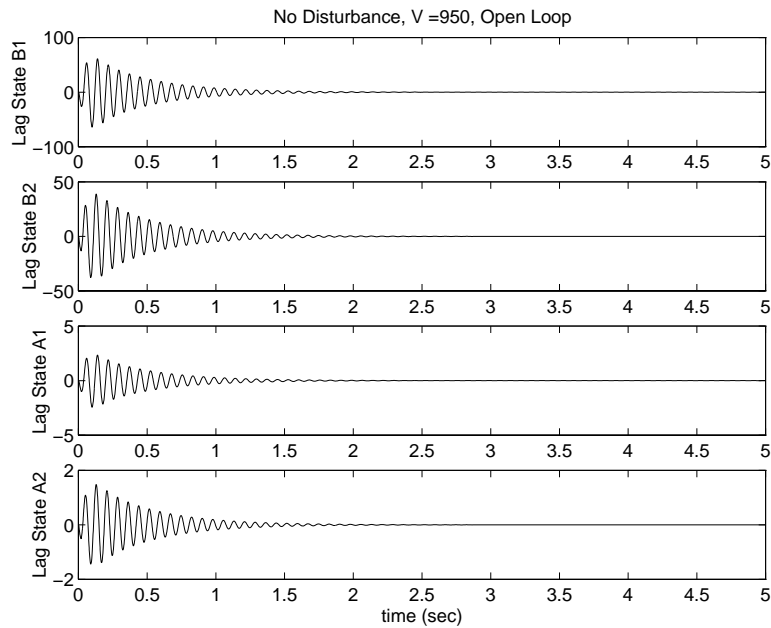


Figure 4.3: No Disturbance,  $V = 950\text{ft}/\text{sec}$ , Open Loop,  $B_1$ ,  $B_2$ ,  $A_1$ , and  $A_2$

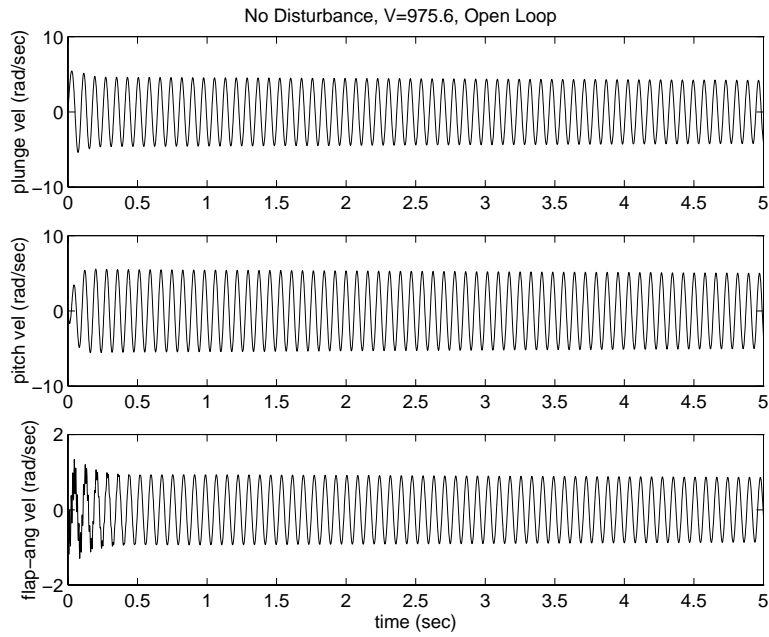


Figure 4.4: No Disturbance,  $V = 975.6 \text{ ft/sec}$ , Open Loop,  $\dot{h}$ ,  $\dot{\alpha}$  and  $\dot{\beta}$

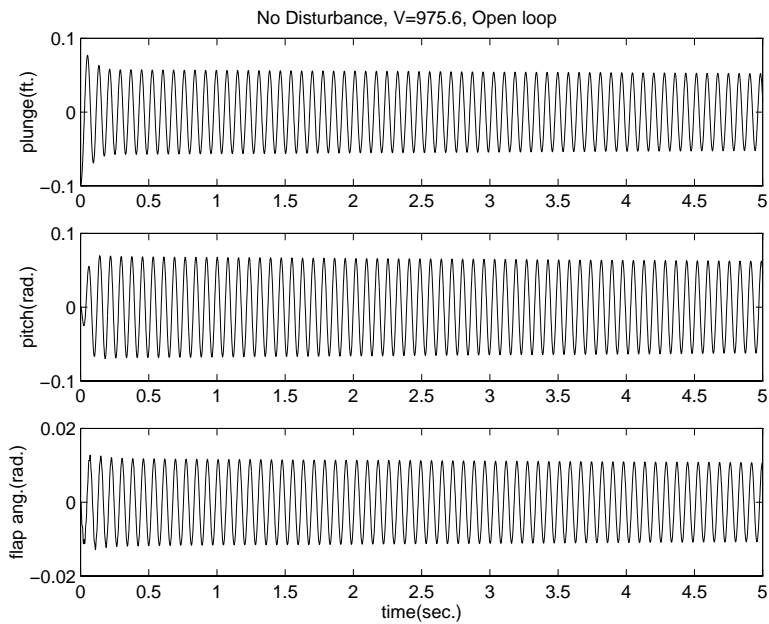


Figure 4.5: No Disturbance,  $V = 975.6 \text{ ft/sec}$ , Open Loop,  $h$ ,  $\alpha$  and  $\beta$

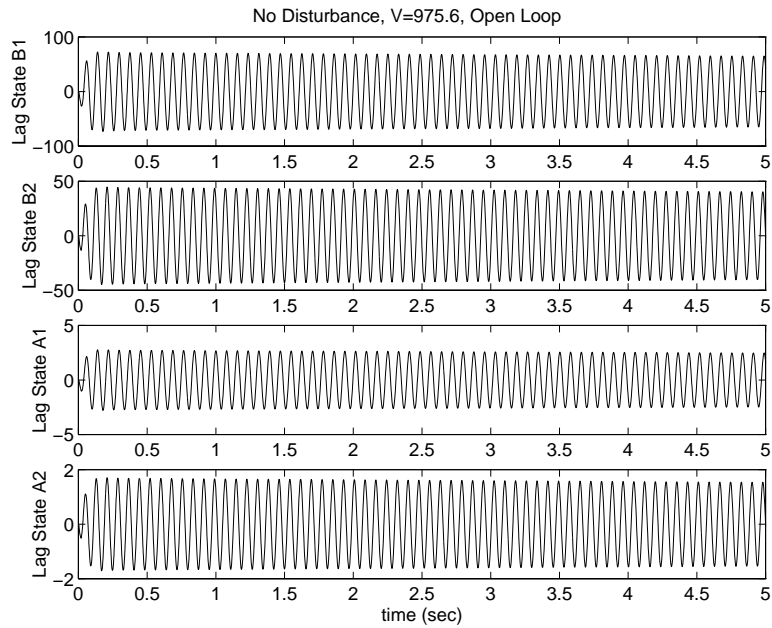


Figure 4.6: No Disturbance,  $V = 975.6 \text{ ft/sec}$ , Open Loop,  $B_1$ ,  $B_2$ ,  $A_1$ , and  $A_2$

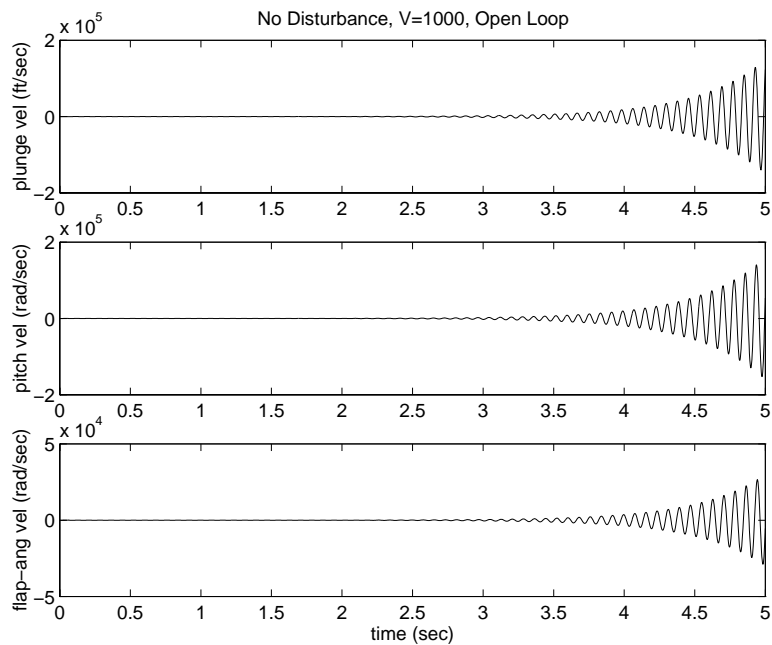


Figure 4.7: No Disturbance,  $V = 1000 \text{ ft/sec}$ , Open Loop,  $\dot{h}$ ,  $\dot{\alpha}$  and  $\dot{\beta}$

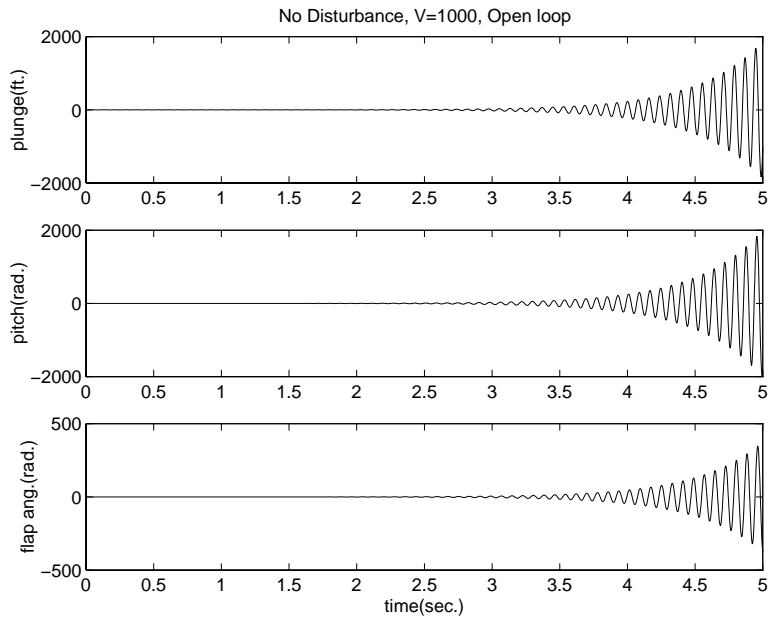


Figure 4.8: No Disturbance,  $V = 1000\text{ft}/\text{sec}$ , Open Loop,  $h$ ,  $\alpha$  and  $\beta$

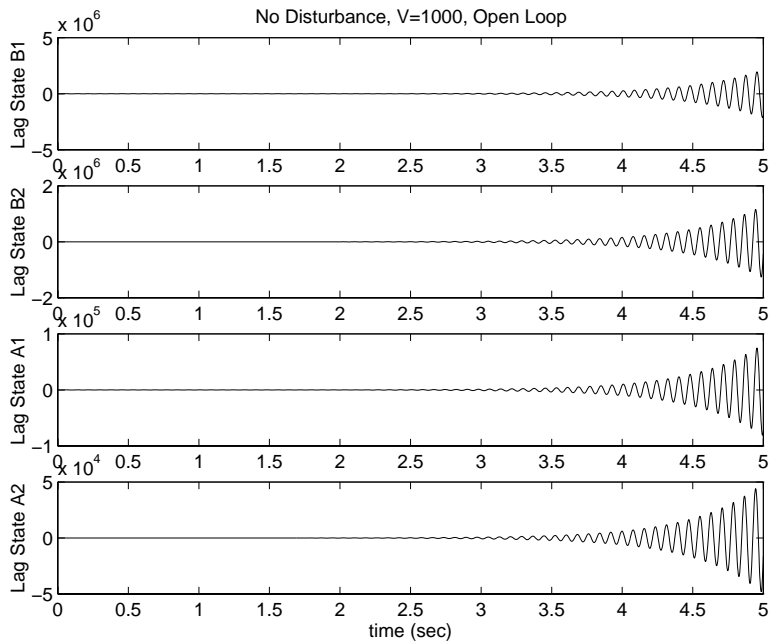


Figure 4.9: No Disturbance,  $V = 1000\text{ft}/\text{sec}$ , Open Loop,  $B_1$ ,  $B_2$ ,  $A_1$ , and  $A_2$

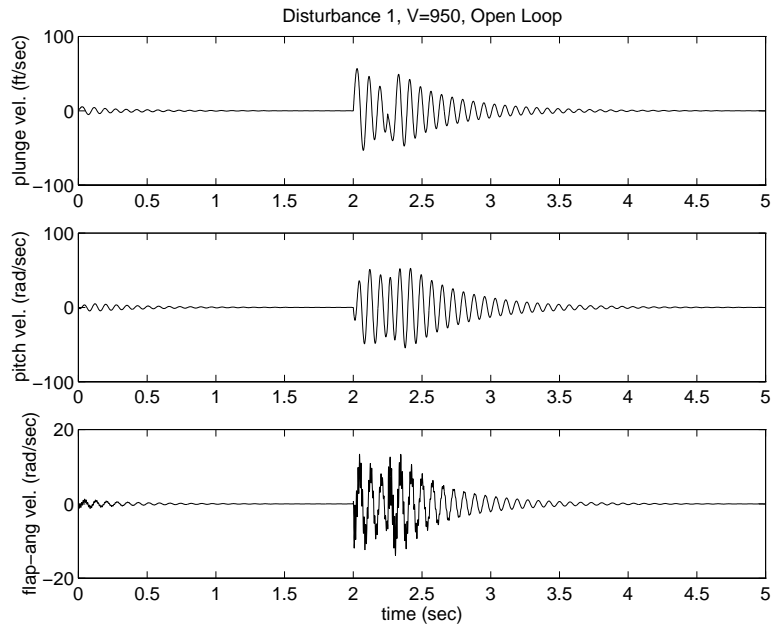


Figure 4.10: Disturbance 1,  $V = 950\text{ft}/\text{sec}$ , Open Loop,  $\dot{h}$ ,  $\dot{\alpha}$  and  $\dot{\beta}$

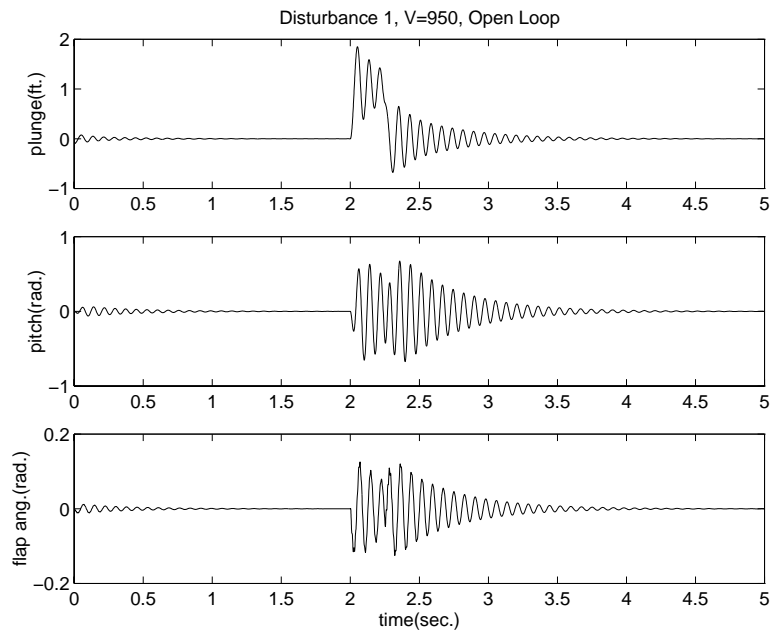


Figure 4.11: Disturbance 1,  $V = 950\text{ft}/\text{sec}$ , Open Loop,  $h$ ,  $\alpha$  and  $\beta$

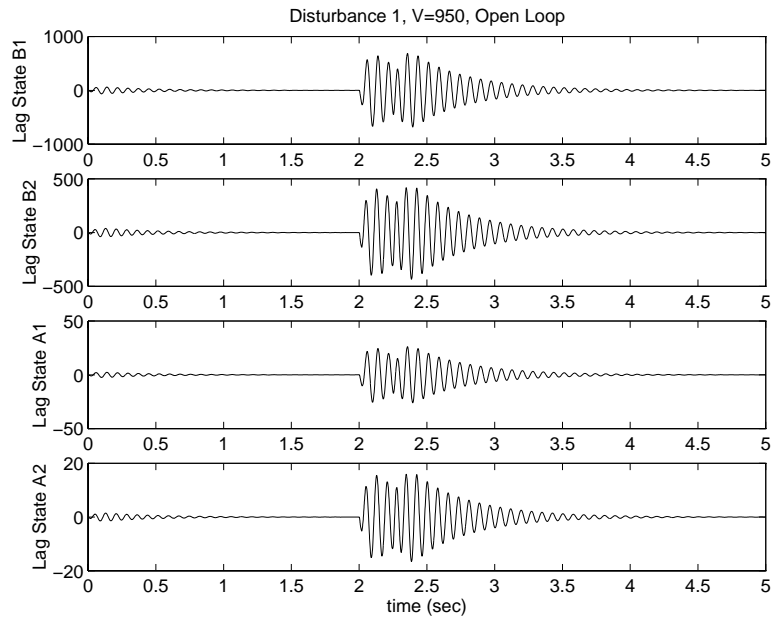


Figure 4.12: Disturbance 1,  $V = 950 ft/sec$ , Open Loop,  $B_1$ ,  $B_2$ ,  $A_1$ , and  $A_2$

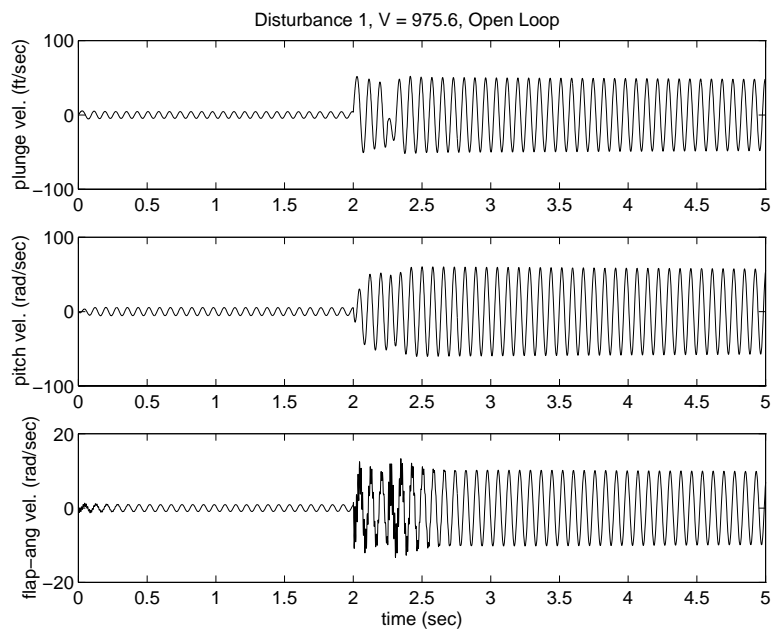


Figure 4.13: Disturbance 1,  $V = 975.6 ft/sec$ , Open Loop,  $\dot{h}$ ,  $\dot{\alpha}$  and  $\dot{\beta}$

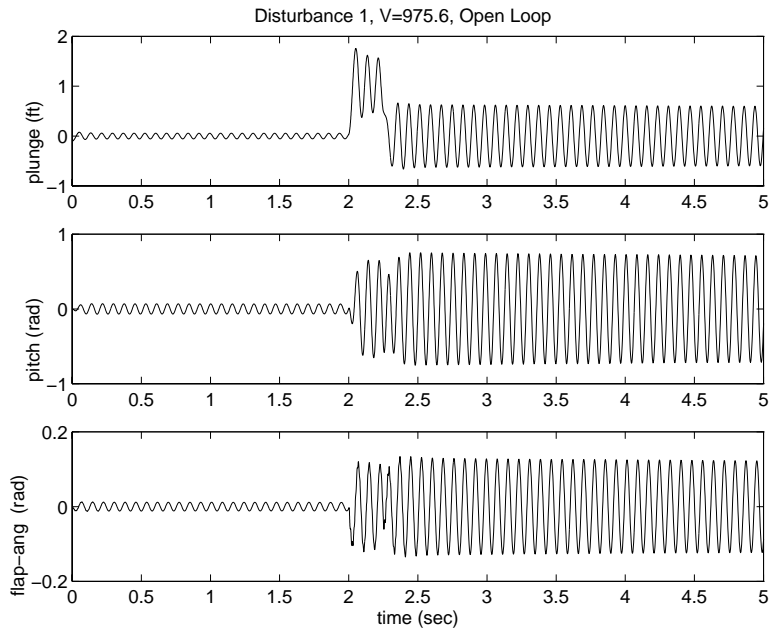


Figure 4.14: Disturbance 1,  $V = 975.6 \text{ ft/sec}$ , Open Loop,  $h$ ,  $\alpha$  and  $\beta$

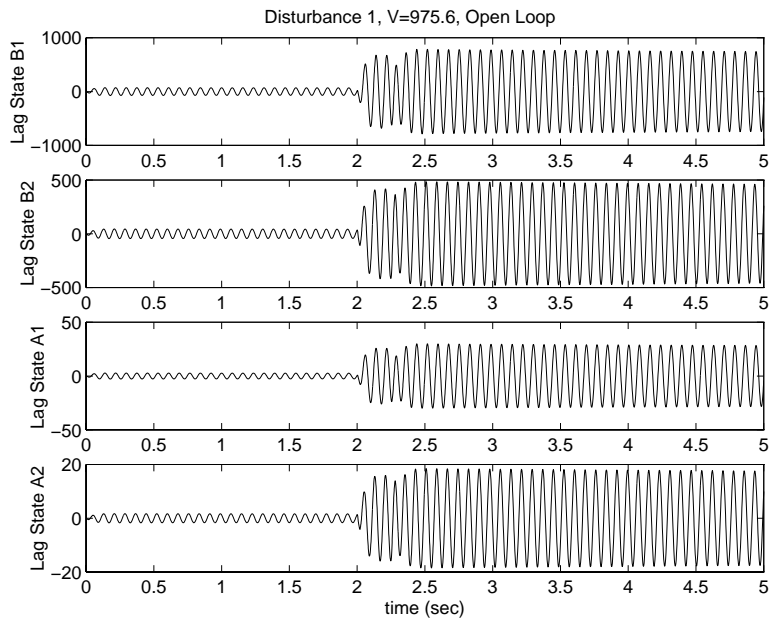


Figure 4.15: Disturbance 1,  $V = 975.6 \text{ ft/sec}$ , Open Loop,  $B_1$ ,  $B_2$ ,  $A_1$ , and  $A_2$

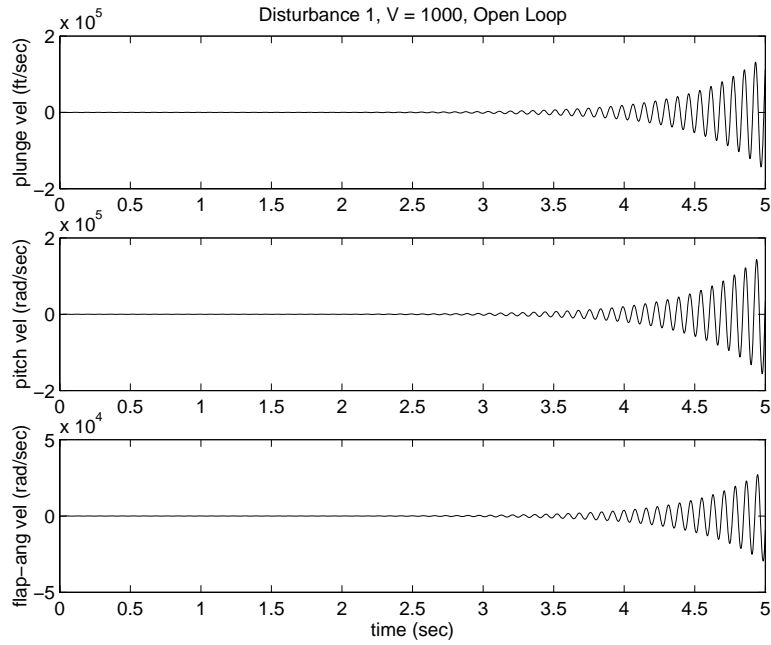


Figure 4.16: Disturbance 1,  $V = 1000\text{ft}/\text{sec}$ , Open Loop,  $\dot{h}$ ,  $\dot{\alpha}$  and  $\dot{\beta}$

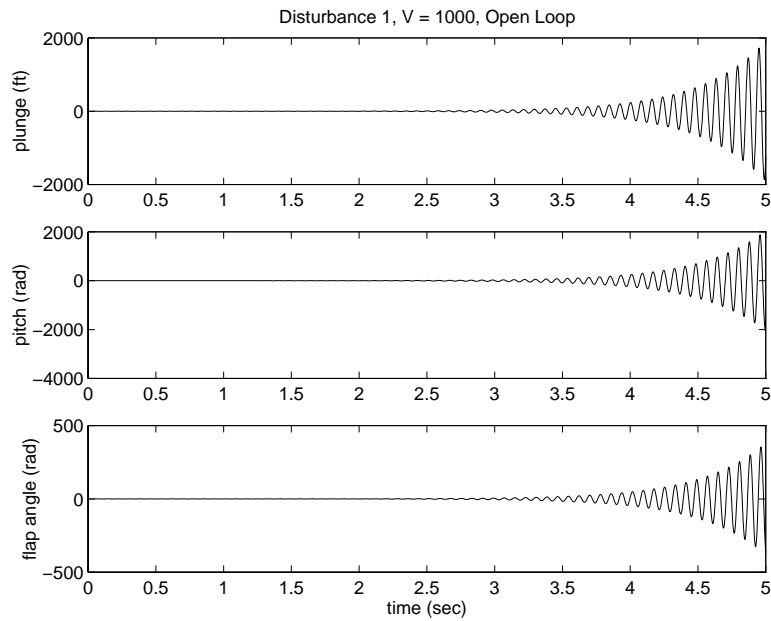


Figure 4.17: Disturbance 1,  $V = 1000\text{ft}/\text{sec}$ , Open Loop,  $h$ ,  $\alpha$  and  $\beta$

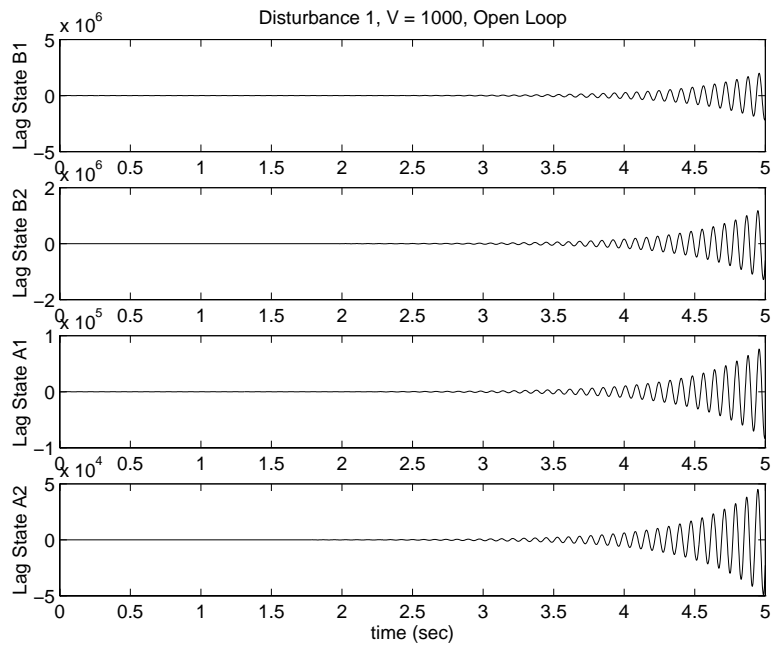


Figure 4.18: Disturbance 1,  $V = 1000 \text{ ft/sec}$ , Open Loop,  $B_1$ ,  $B_2$ ,  $A_1$ , and  $A_2$

## 4.2 Closed-Loop Simulations

In this section the open-loop,  $LQG$  and  $H^\infty$  closed-loop system simulations are presented and discussed.

### 4.2.1 The Stable Case

The open-loop and closed-loop systems for the velocity  $V = 950ft/sec$  are discussed in this section. Figures 4.2, 4.19 and 4.20 are the system states  $h$ ,  $\alpha$  and  $\beta$  for the open-loop,  $LQG$  closed-loop and  $H^\infty$  closed-loop systems, respectively (with no disturbance). The graphs provide evidence that the  $LQG$  and  $H^\infty$  controllers do not drive the system to zero any faster than the open-loop system's natural stability. Comparing the eigenvalues of the open and closed-loop system found in Table 4.2 provides a more quantitative measure of this performance. The minimum real parts of the eigenvalues for the open-loop,  $LQG$  and  $H^\infty$  closed-loops are -2.34, -2.3, and -2.34, respectively. Thus, comparable performance is achieved by these three systems.

Figures 4.11 and 4.21-4.28 present the open and closed-loop systems with the various disturbances introduced. The point of interest lies in Figures 4.23-4.25. The plunge for the open-loop system in Figure 4.23 attains a maximum of  $2ft$  when the wind gust hits the airfoil. In comparison, the plunge for the  $LQG$  and  $H^\infty$  closed-loop systems in Figures 4.24 and 4.25, respectively, reaches a maximum of  $1ft$ . Both controllers reduce the effects of the wind gust. This is also evident in the pitch and the flap angle.

Open Loop	<i>LQG</i> Closed Loop	$H^\infty$ Closed Loop
$\lambda_1 = -6.20 + 563.58i$	$\lambda_1 = -2039.2 + 2115.4i$	$\lambda_1 = -6.20 + 563.58i$
$\lambda_2 = -6.20 - 563.58i$	$\lambda_2 = -2039.2 - 2115.4i$	$\lambda_2 = -6.20 - 563.58i$
$\lambda_3 = -2.34 + 81.63i$	$\lambda_3 = -29.0 + 562.9i$	$\lambda_3 = -29.01 + 562.87i$
$\lambda_4 = -2.34 - 81.63i$	$\lambda_4 = -29.0 - 562.9i$	$\lambda_4 = -29.01 - 562.87i$
$\lambda_5 = -17.84 + 66.81i$	$\lambda_5 = -320.9 + 332.0i$	$\lambda_5 = -2.34 + 81.63i$
$\lambda_6 = -17.84 - 66.81i$	$\lambda_6 = -320.9 - 332.0i$	$\lambda_6 = -2.34 - 81.63i$
$\lambda_7 = -93.18$	$\lambda_7 = -220.1 + 226.8i$	$\lambda_7 = -2.35 + 81.63i$
$\lambda_8 = -12.98$	$\lambda_8 = -220.1 - 226.8i$	$\lambda_8 = -2.35 - 81.63i$
$\lambda_9 = -101.33$	$\lambda_9 = -2.3 + 81.6i$	$\lambda_9 = -17.84 + 66.81i$
$\lambda_{10} = -12.98$	$\lambda_{10} = -2.3 - 81.6i$	$\lambda_{10} = -17.84 - 66.81i$
	$\lambda_{11} = -17.8 + 66.8i$	$\lambda_{11} = -17.84 + 66.81i$
	$\lambda_{12} = -17.8 - 66.8i$	$\lambda_{12} = -17.84 - 66.81i$
	$\lambda_{13} = -93.2$	$\lambda_{13} = -93.18$
	$\lambda_{14} = -101.2$	$\lambda_{14} = -12.98$
	$\lambda_{15} = -13.0$	$\lambda_{15} = -93.18$
	$\lambda_{16} = -13.0$	$\lambda_{16} = -12.98$
	$\lambda_{17} = -101.3$	$\lambda_{17} = -101.33$
	$\lambda_{18} = -13.0$	$\lambda_{18} = -12.98$
	$\lambda_{19} = -101.3$	$\lambda_{19} = -101.33$
	$\lambda_{20} = -13.0$	$\lambda_{20} = -12.98$

Table 4.2: Stable System Eigenvalues

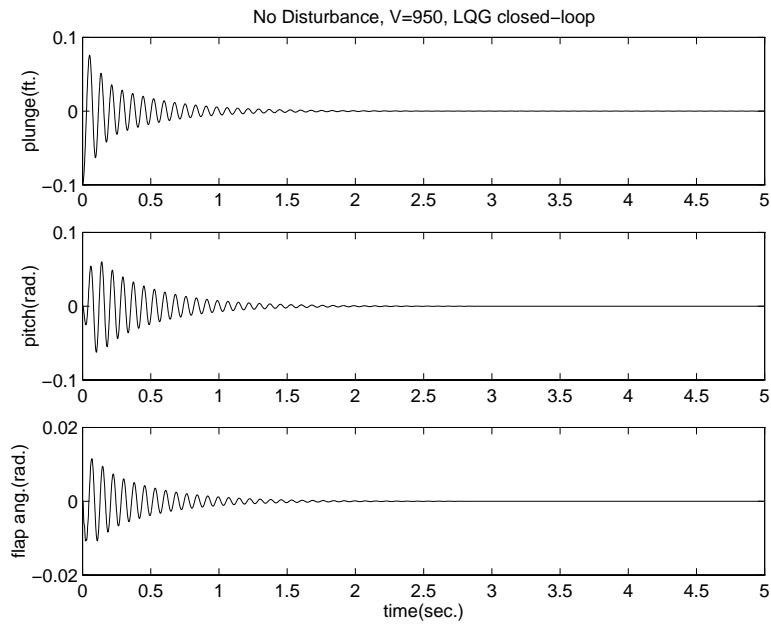


Figure 4.19: No Disturbance,  $V = 950\text{ft}/\text{sec}$ , LQG Closed-Loop System

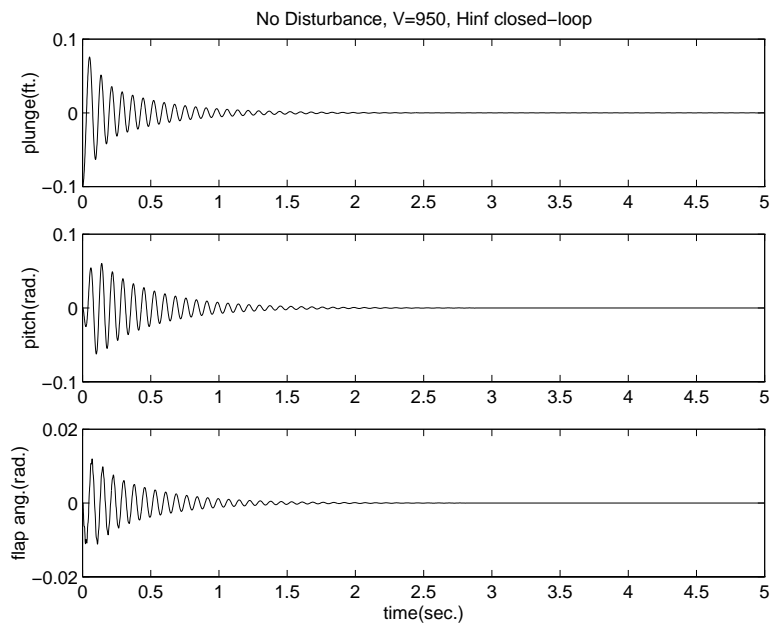


Figure 4.20: No Disturbance,  $V = 950\text{ft}/\text{sec}$ ,  $H^\infty$  Closed-Loop System

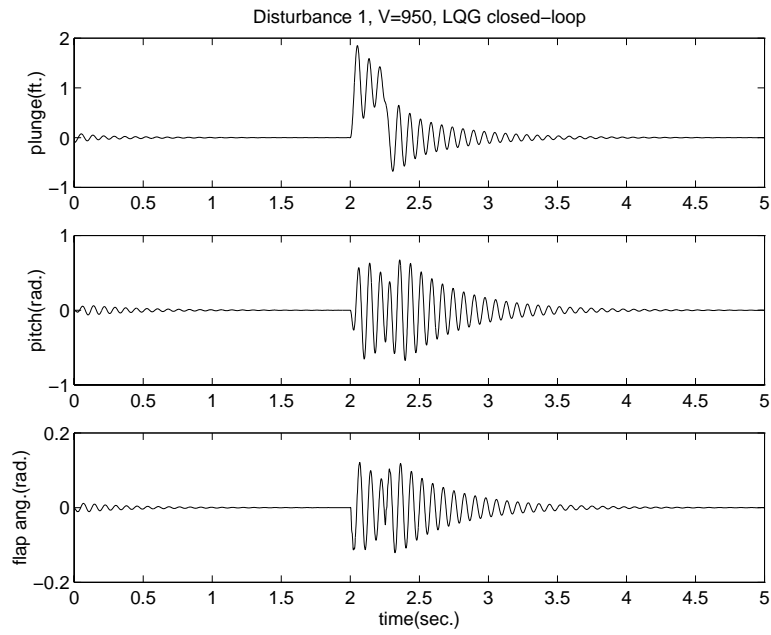


Figure 4.21: Disturbance 1,  $V = 950\text{ft}/\text{sec}$ ,  $LQG$  Closed-Loop System

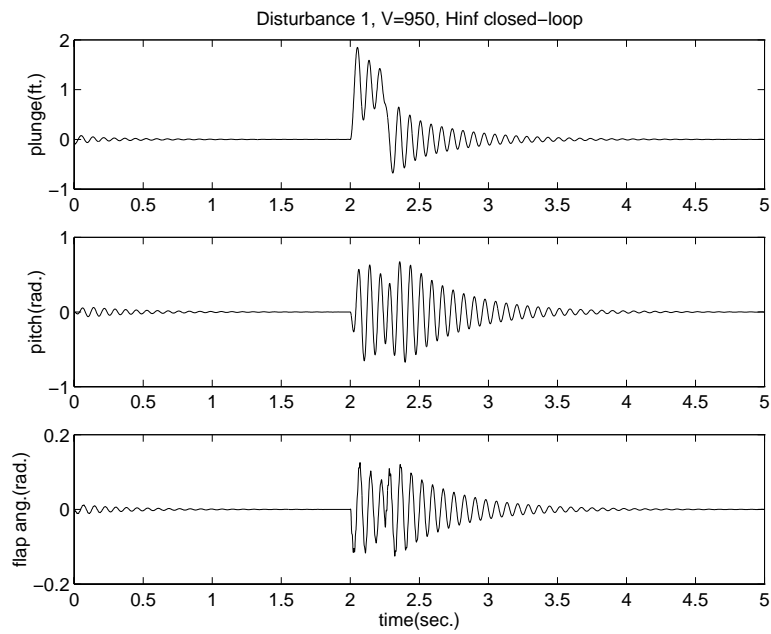


Figure 4.22: Disturbance 1,  $V = 950\text{ft}/\text{sec}$ ,  $H^\infty$  Closed-Loop System

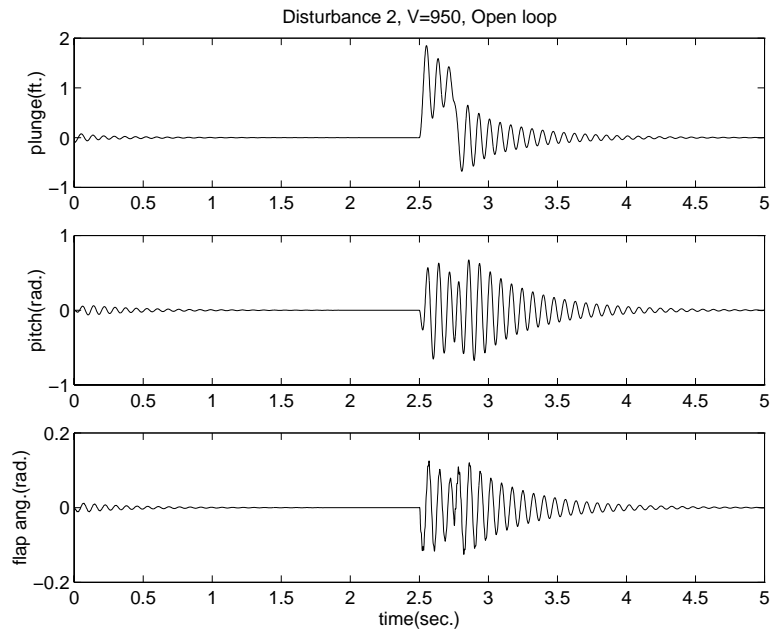


Figure 4.23: Disturbance 2,  $V = 950\text{ft}/\text{sec}$ , Open-Loop System

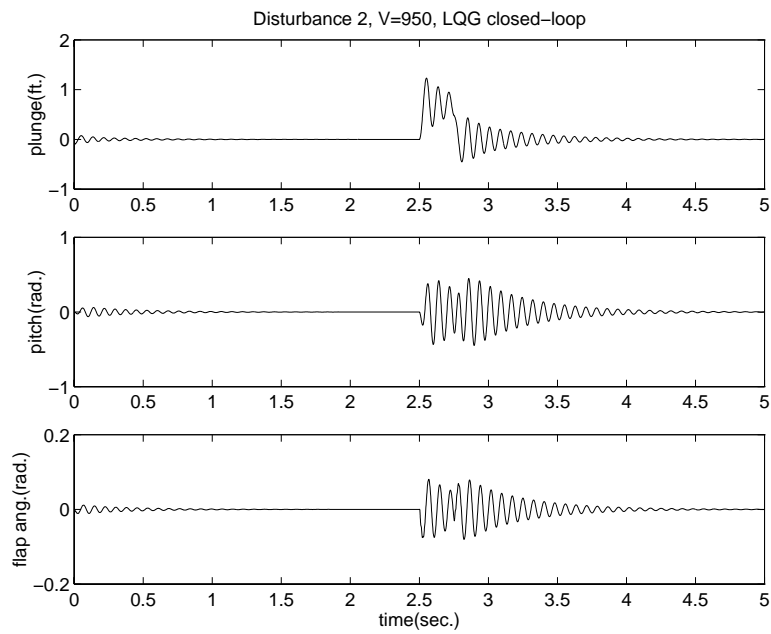


Figure 4.24: Disturbance 2,  $V = 950\text{ft}/\text{sec}$ , LQG Closed-Loop System

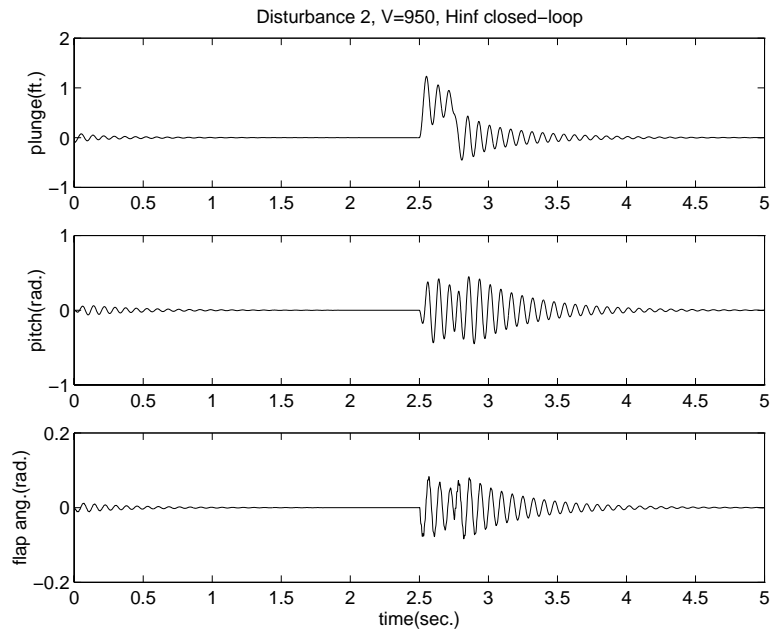


Figure 4.25: Disturbance 2,  $V = 950\text{ft}/\text{sec}$ ,  $H^\infty$  Closed-Loop System

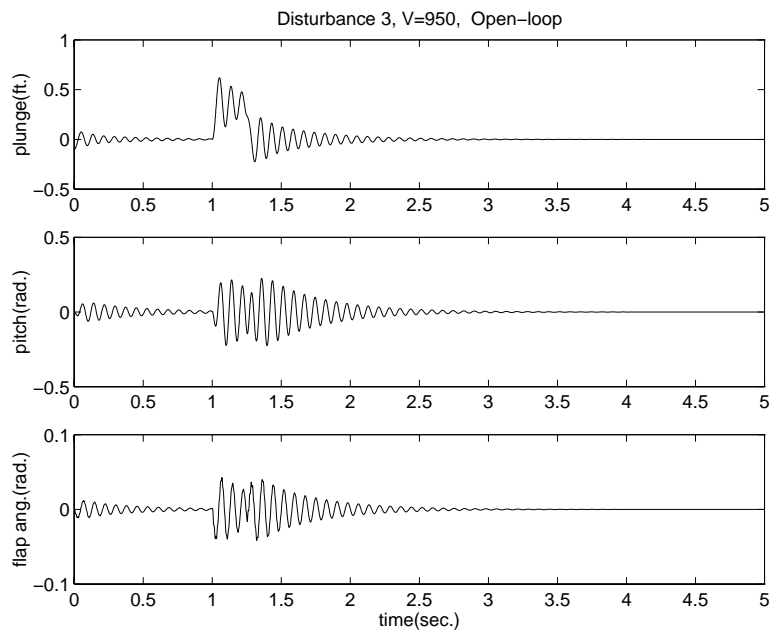


Figure 4.26: Disturbance 3,  $V = 950\text{ft}/\text{sec}$ , Open-Loop System

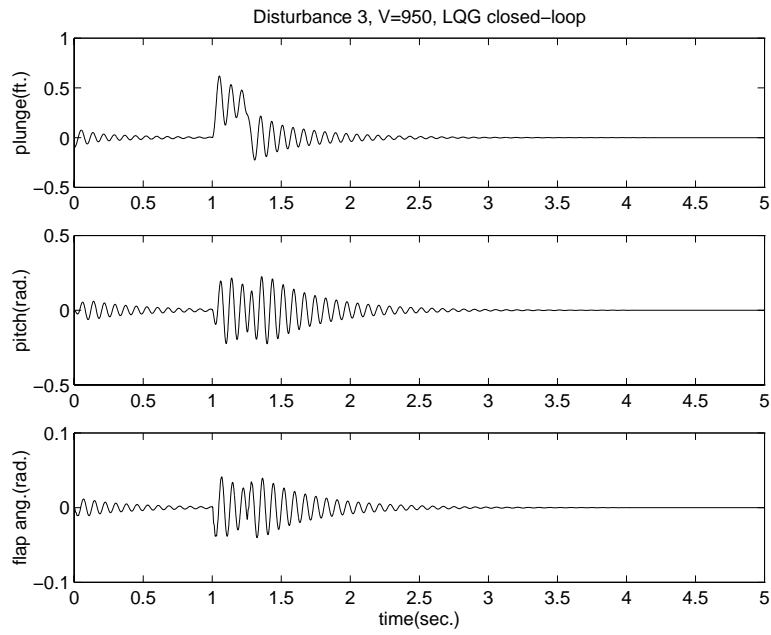


Figure 4.27: Disturbance 3,  $V = 950\text{ft/sec}$ ,  $LQG$  Closed-Loop System

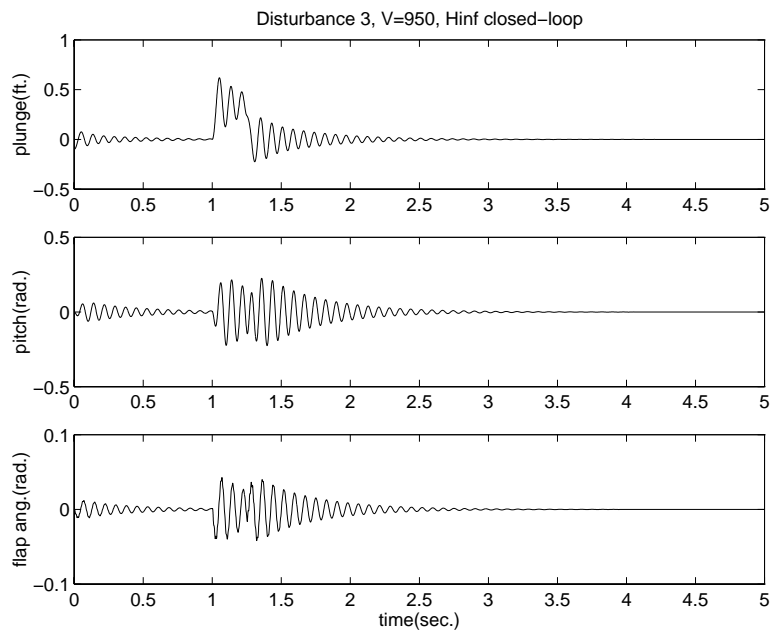


Figure 4.28: Disturbance 3,  $V = 950\text{ft/sec}$ ,  $H^\infty$  Closed-Loop System

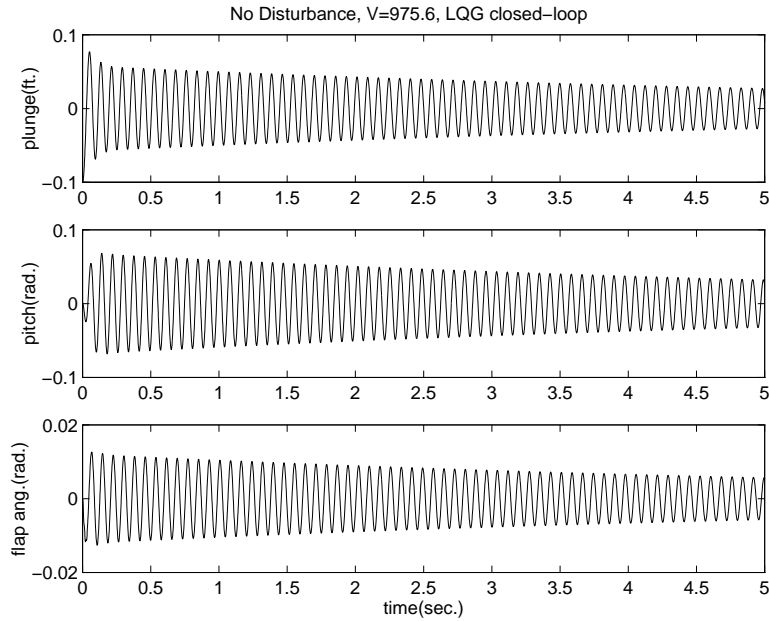


Figure 4.29: No Disturbance,  $V = 975.6 \text{ ft/sec}$ ,  $LQG$  Closed-Loop System

## 4.2.2 The Marginally Stable Case

In this section we present and compare open and closed-loop simulations for the marginally stable system. Figures 4.5, 4.29 and 4.30 are the plots of the open-loop,  $LQG$  closed-loop and  $H^\infty$  closed-loop systems, respectively (with no disturbance). In Figure 4.29 the  $LQG$  controller slowly stabilizes the system. However, the  $H^\infty$  controller has little impact on the system. To achieve better performance, one needs to develop better weightings.

Figures 4.14 and 4.33-4.38 contain the open-loop and closed-loop responses with various disturbances. In all cases, the wind gust adds energy to the system and the amplitude of the states increases. In Figure 4.31, 4.34 and 4.37, the  $LQG$  controller slowly stabilizes the system. Again, the  $H^\infty$  controller has little impact on the system. This case is interesting in that the  $LQG$  controller shows better performance than the  $H^\infty$  controller. However, the issue of robustness remains to be considered.

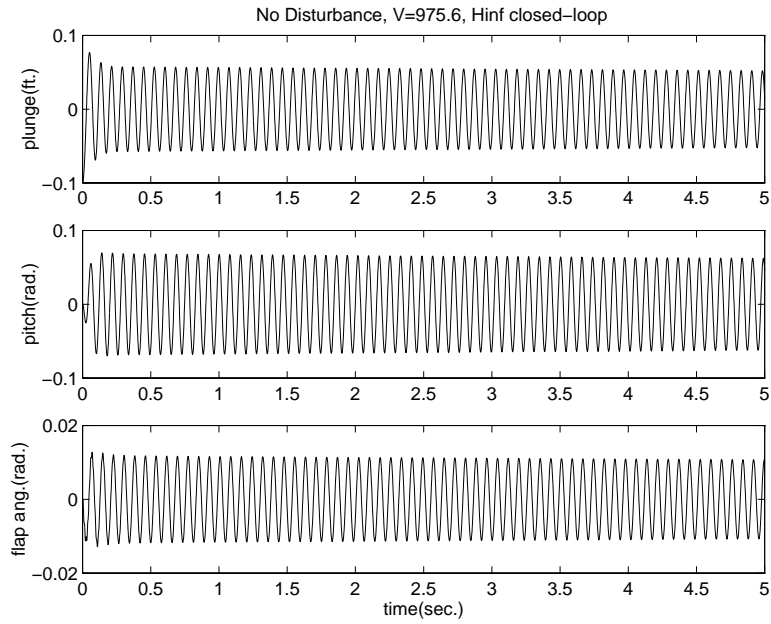


Figure 4.30: No Disturbance,  $V = 975.6 \text{ ft/sec}$ ,  $H^\infty$  Closed-Loop System

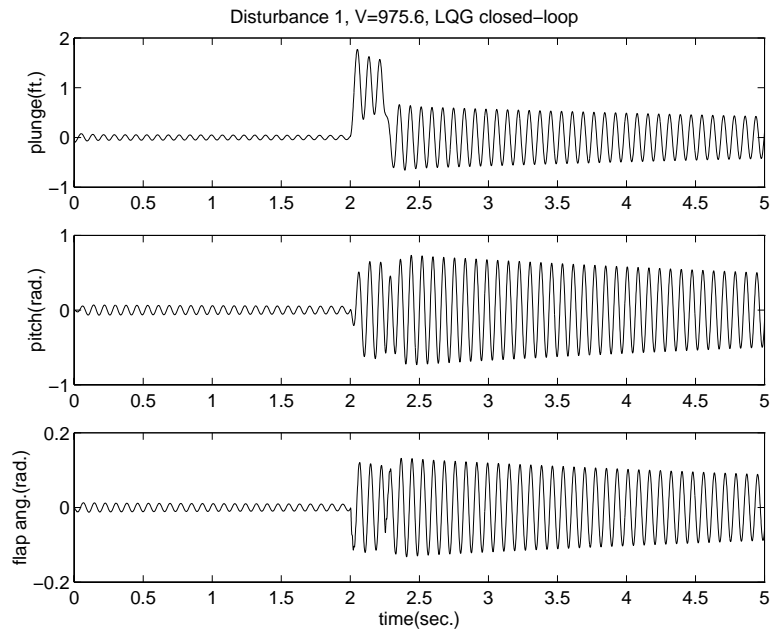


Figure 4.31: Disturbance 1,  $V = 975.6 \text{ ft/sec}$ ,  $LQG$  Closed-Loop System

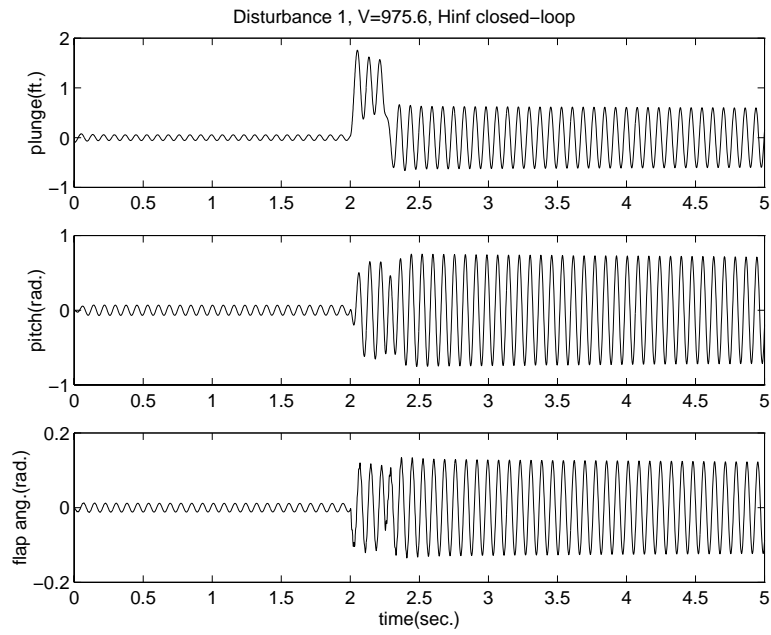


Figure 4.32: Disturbance 1,  $V = 975.6 \text{ ft/sec}$ ,  $H^\infty$  Closed-Loop System

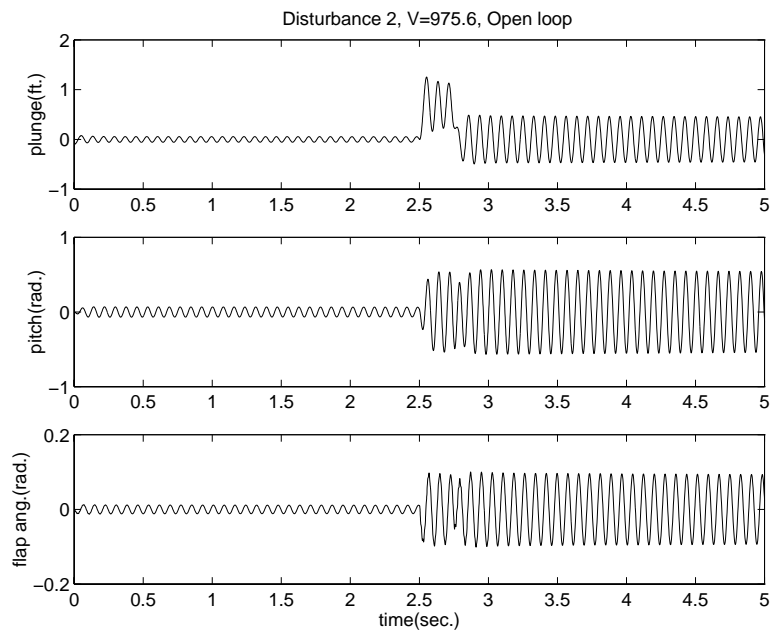


Figure 4.33: Disturbance 2,  $V = 975.6 \text{ ft/sec}$ , Open-Loop System

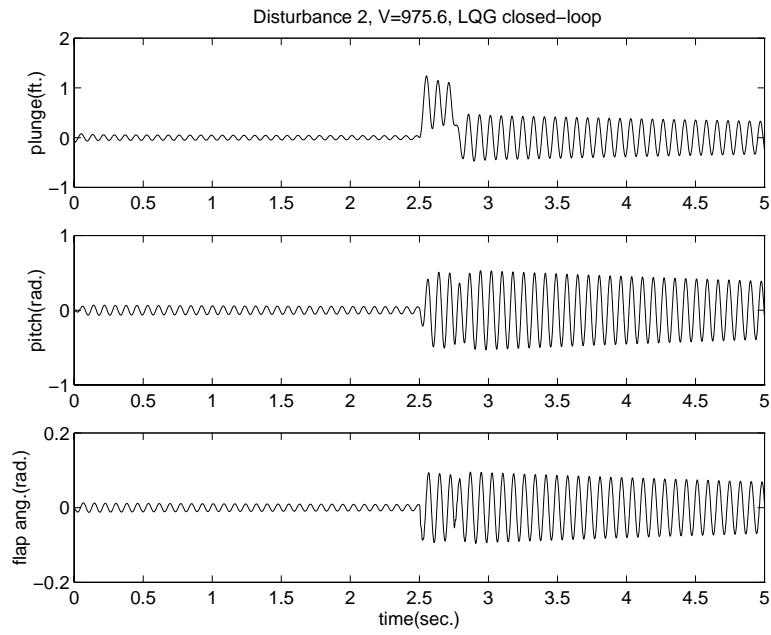


Figure 4.34: Disturbance 2,  $V = 975.6 \text{ ft/sec}$ , LQG Closed-Loop System

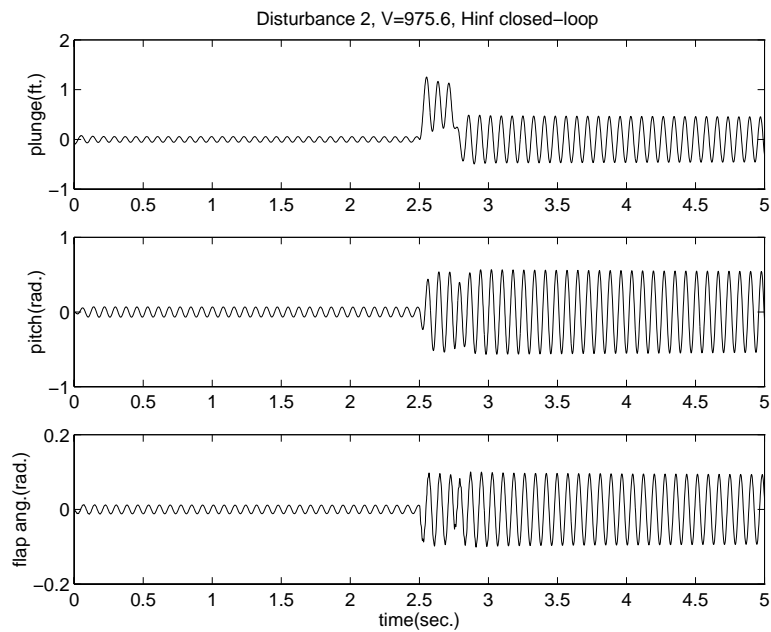


Figure 4.35: Disturbance 2,  $V = 975.6 \text{ ft/sec}$ ,  $H^\infty$  Closed-Loop System

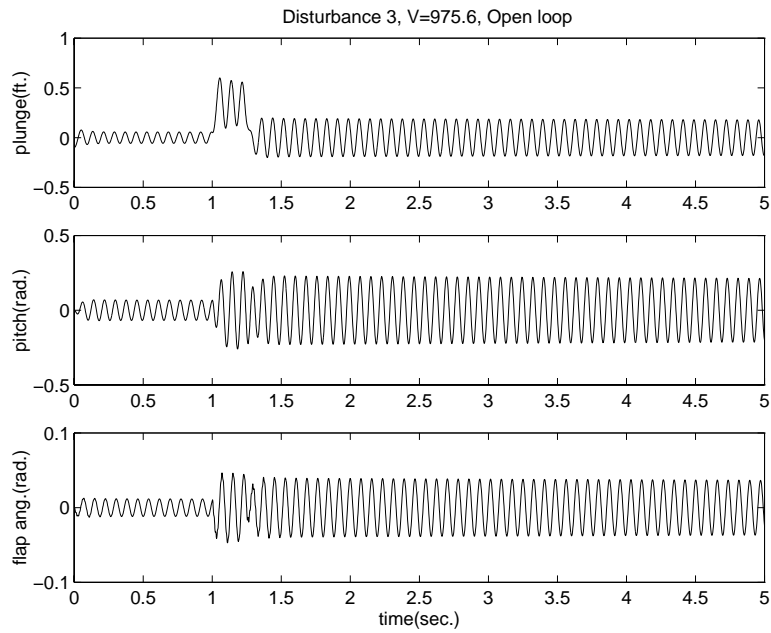


Figure 4.36: Disturbance 3,  $V = 975.6 \text{ ft/sec}$ , Open-Loop System

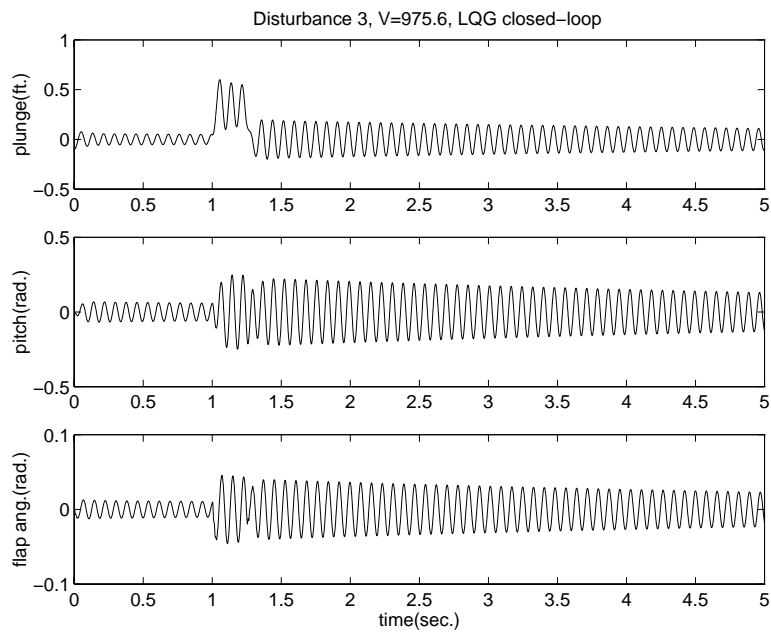


Figure 4.37: Disturbance 3,  $V = 975.6 \text{ ft/sec}$ , LQG Closed-Loop System

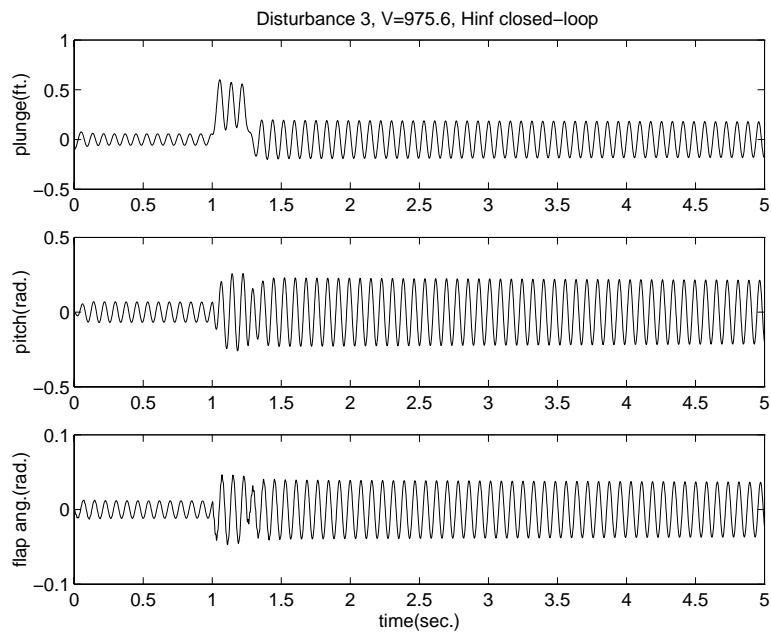


Figure 4.38: Disturbance 3,  $V = 975.6 ft/sec$ ,  $H^\infty$  Closed-Loop System

### 4.2.3 The Unstable Case

In this section simulations for the unstable system are presented and compared. Figures 4.8, 4.39 and 4.40 represent the plunge, pitch and flap angle of the open-loop,  $LQG$  closed-loop, and  $H^\infty$  closed-loop systems, respectively (at the unstable velocity  $V = 1000\text{ft}/\text{sec}$ ). Observe that the  $LQG$  and  $H^\infty$  controllers stabilize the system and have roughly the same performance. The main difference between the controllers is found in the flap angle and flap angle velocity. Figure 4.41 compares the flap-angle velocity for the  $LQG$  and  $H^\infty$  controlled systems. The  $LQG$  controller produces a sharp spike in the flap-angle velocity of approximately  $7\text{rad}/\text{sec}$ . The  $H^\infty$  control reduces this spike by approximately 50%. Also, the  $H^\infty$  controller requires half the energy of the  $LQG$  controller.

Figures 4.42 and 4.43 show the  $LQG$  and  $H^\infty$  closed-loop responses for the case of Disturbance 1. Again, the  $LQG$  and  $H^\infty$  controllers both stabilize the system. The main difference between the controllers is the flap-angle velocity. The  $H^\infty$  controller requires less energy than the  $LQG$ . This is evident from Figure 4.44.

Figures 4.45-4.47 show that similar results also hold for the simulation with Disturbance 2. However, the  $H^\infty$  controller does not attenuate the sinusoidal sensor noise in the flap-angle response.

Finally, Figures 4.49, 4.50 and 4.51 show the open-loop and closed-loop responses for the airfoil at the unstable velocity  $V = 1000\text{ft}/\text{sec}$  with Disturbance 3. The plunge state for the open-loop system is clearly affected by the gust and then becomes unbounded. This disturbance has a maximum amplitude of approximately  $1\text{ft}$ . Both controllers reduce the size of this disturbance by approximately 50%. As noted before, the  $H^\infty$  controller requires less energy than the  $LQG$  controller. This is shown in Figure 4.52. Figures 4.50 and 4.51 show a steady-state sinusoidal wave in the pitch and flap angle. This is due to the sensor noise as modeled by Disturbance 3. In this case, both the  $LQG$  and  $H^\infty$  controllers perform well. In the next chapter we address the issue of robustness.

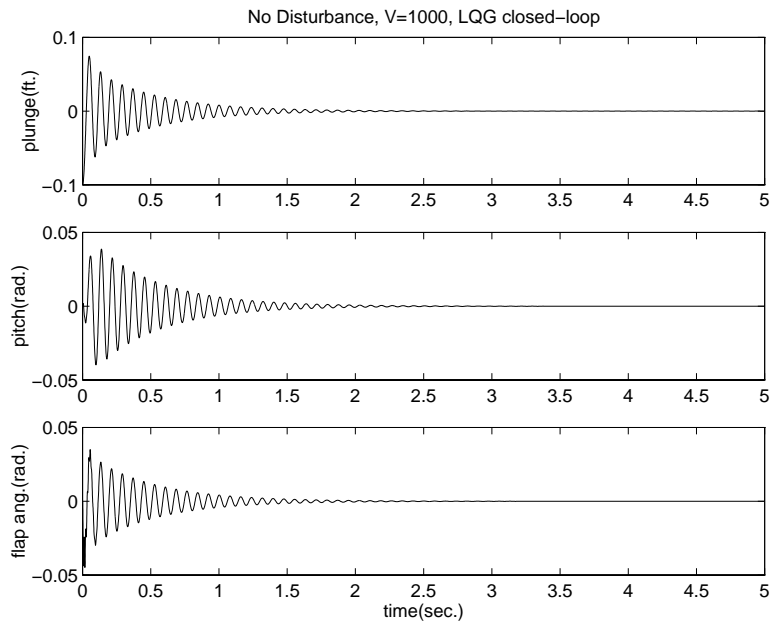


Figure 4.39: No Disturbance,  $V = 1000\text{ft}/\text{sec}$ ,  $LQG$  Closed-Loop System

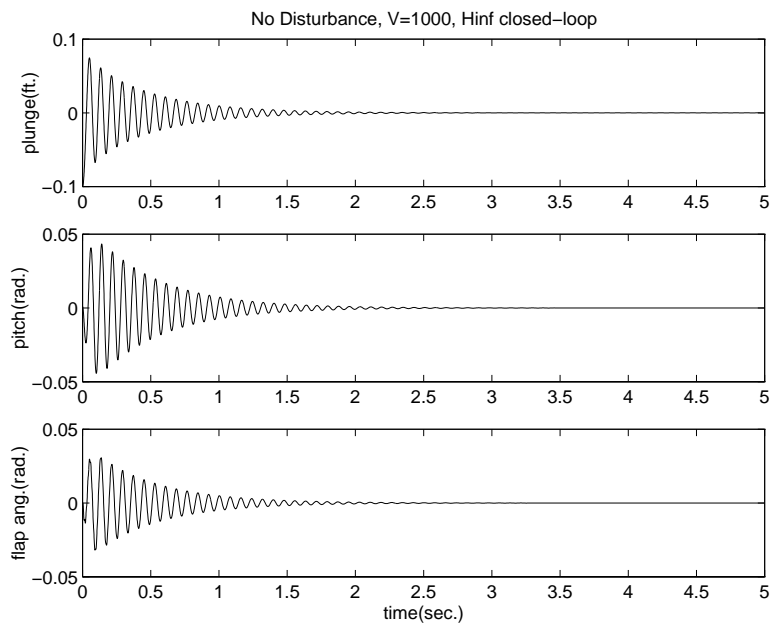


Figure 4.40: No Disturbance,  $V = 1000\text{ft}/\text{sec}$ ,  $H^\infty$  Closed-Loop System

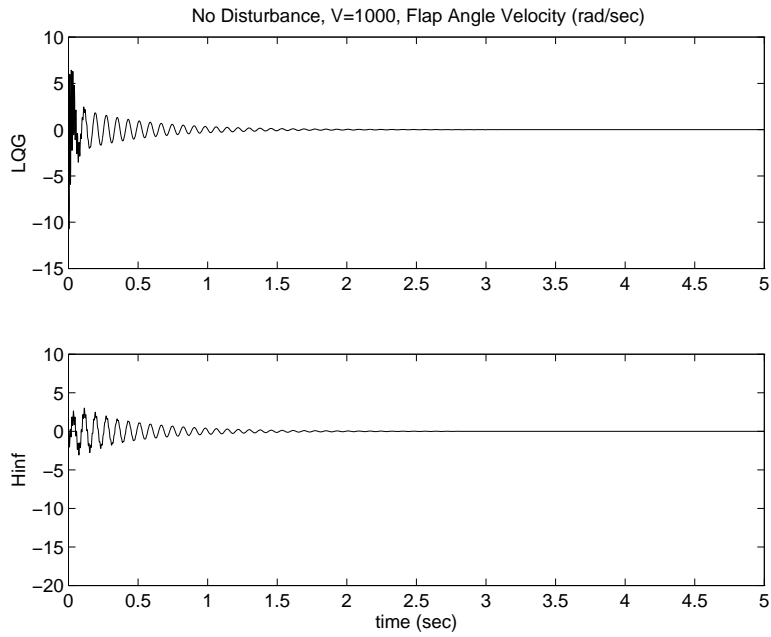


Figure 4.41: No Disturbance,  $V = 1000 ft/sec$ ,  $\dot{\beta}$

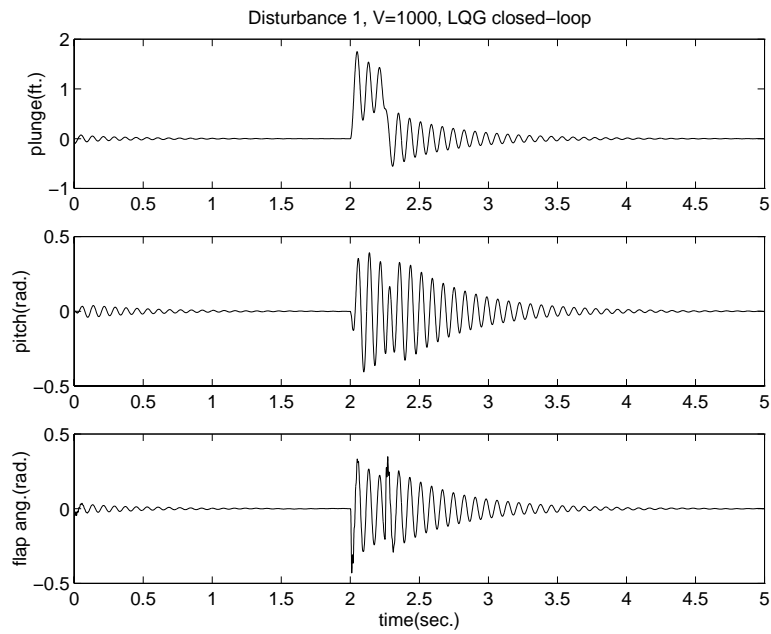


Figure 4.42: Disturbance 1,  $V = 1000 ft/sec$ , LQG Closed-Loop System

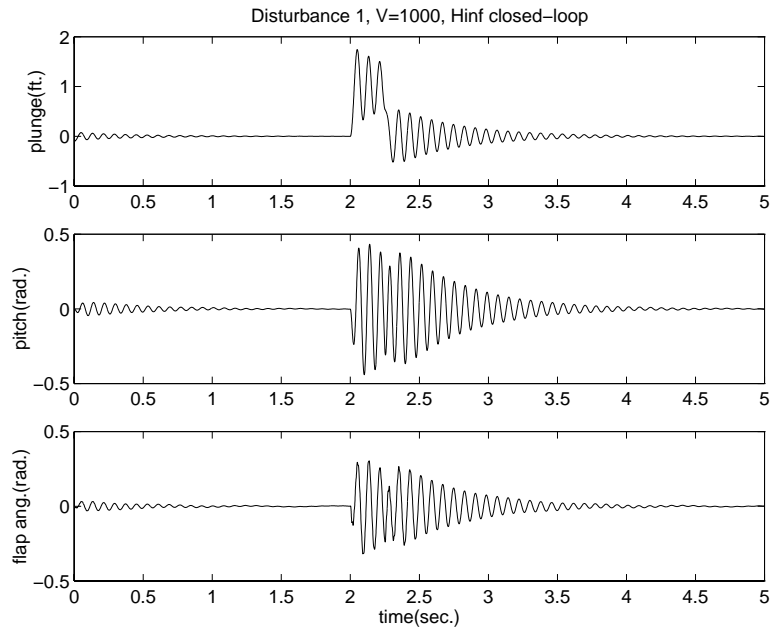


Figure 4.43: Disturbance 1,  $V = 1000 \text{ ft/sec}$ ,  $H^\infty$  Closed-Loop System

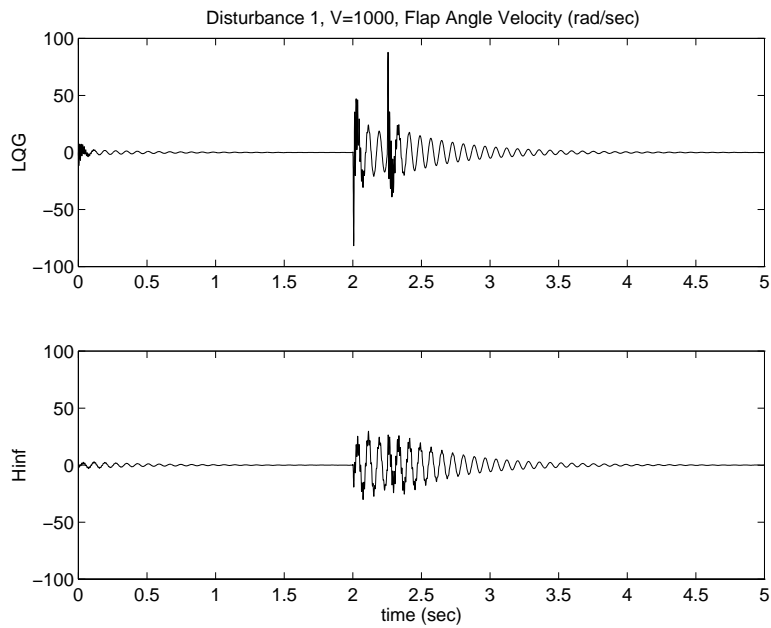


Figure 4.44: Disturbance 1,  $V = 1000 \text{ ft/sec}$ ,  $\dot{\beta}$

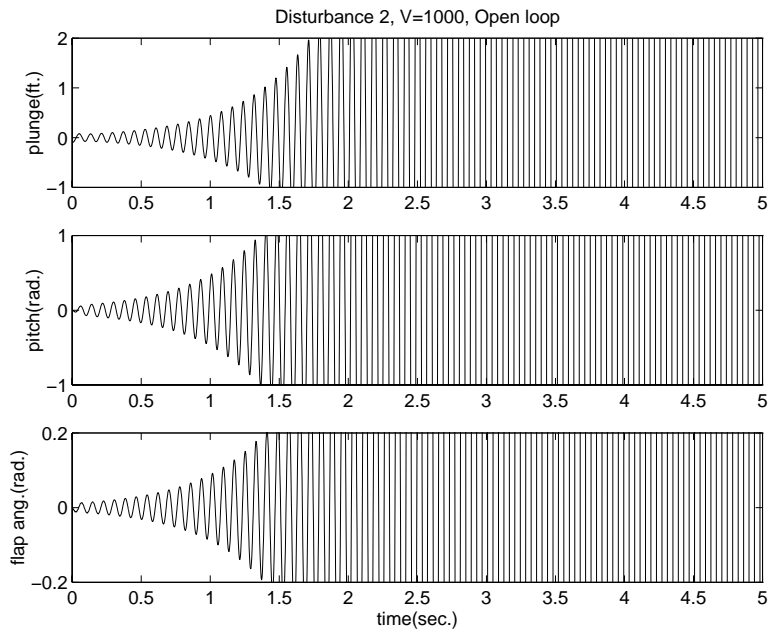


Figure 4.45: Disturbance 2,  $V = 1000\text{ft}/\text{sec}$ , Open-Loop System

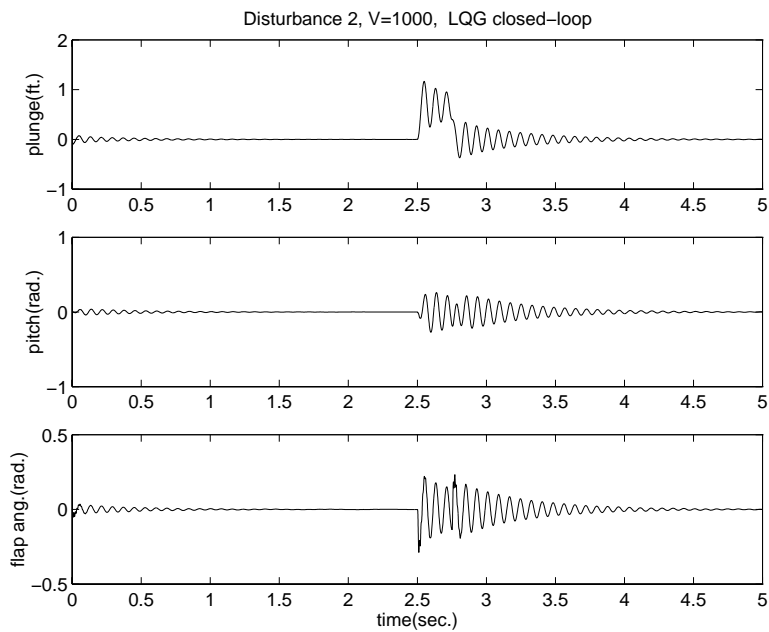


Figure 4.46: Disturbance 2,  $V = 1000\text{ft}/\text{sec}$ , LQG Closed-Loop System

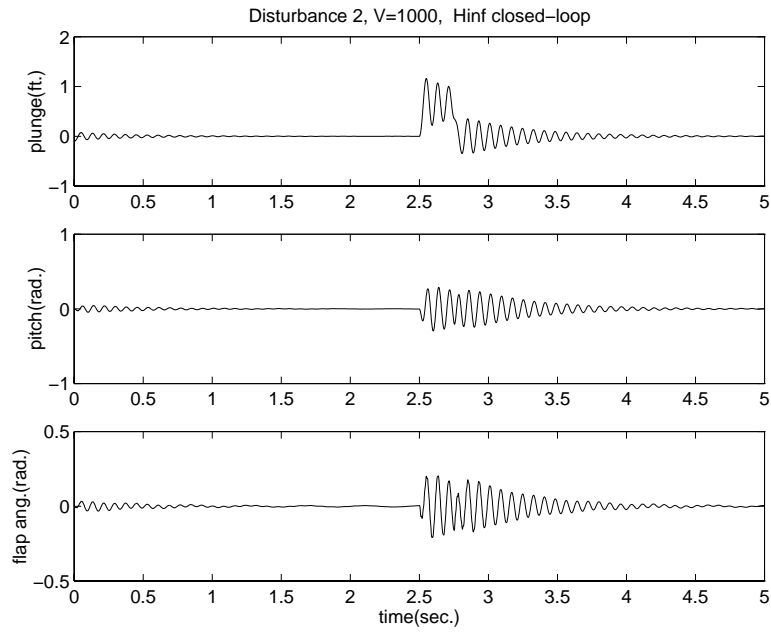


Figure 4.47: Disturbance 2,  $V = 1000 \text{ ft/sec}$ ,  $H^\infty$  Closed-Loop System

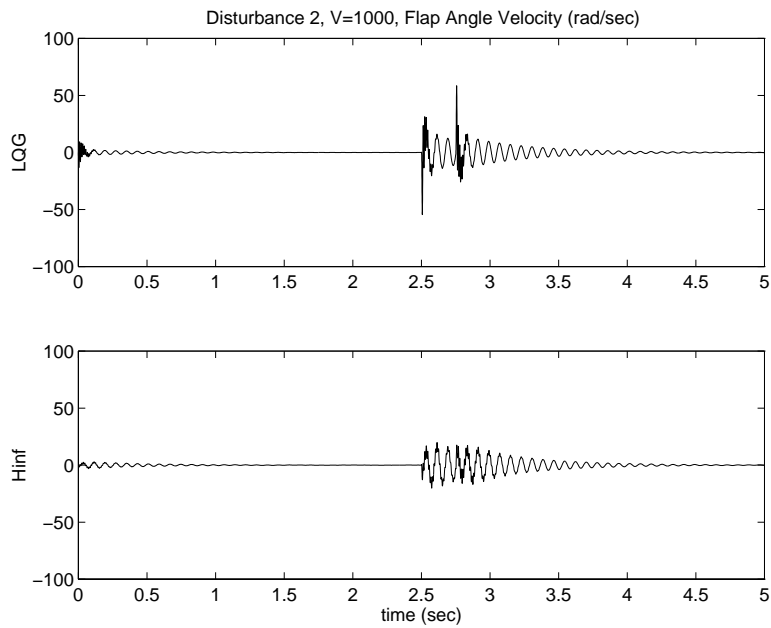


Figure 4.48: Disturbance 2,  $V = 1000 \text{ ft/sec}$ ,  $\dot{\beta}$

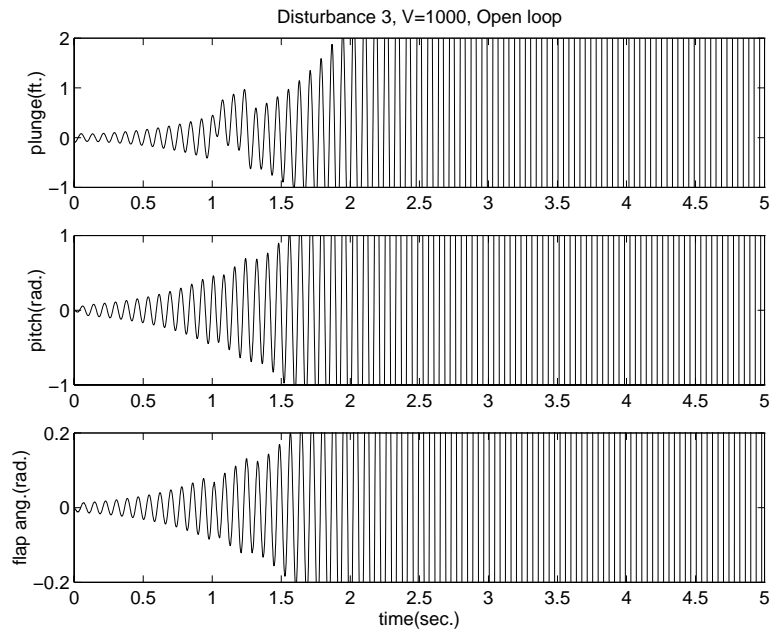


Figure 4.49: Disturbance 3,  $V = 1000\text{ft}/\text{sec}$ , Open-Loop System

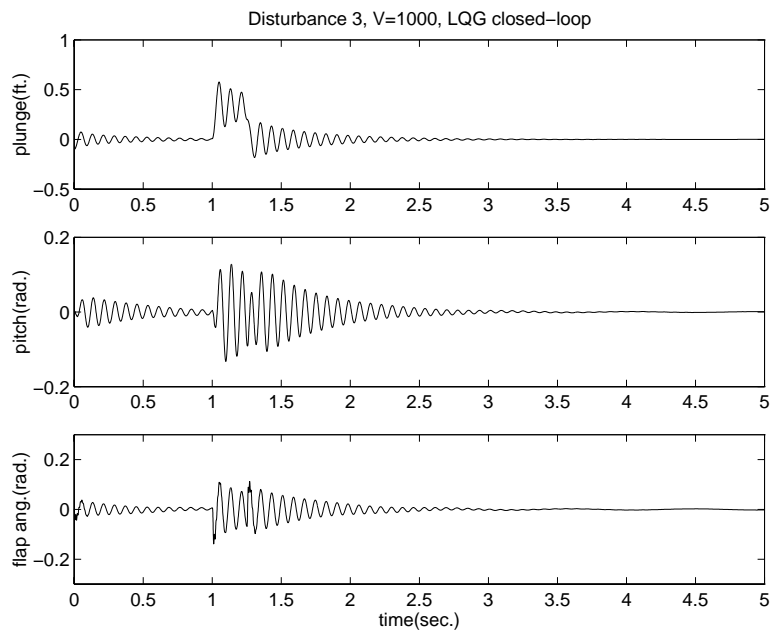


Figure 4.50: Disturbance 3,  $V = 1000\text{ft}/\text{sec}$ , LQG Closed-Loop System

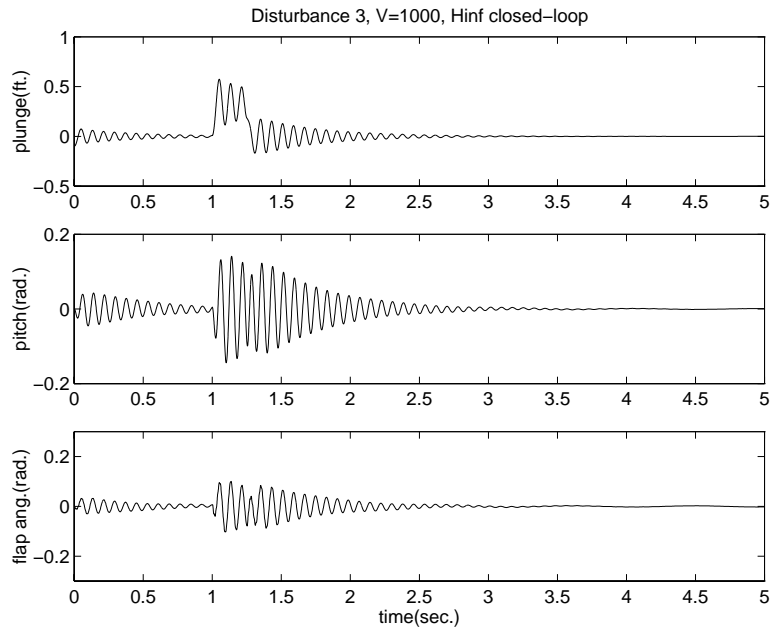


Figure 4.51: Disturbance 3,  $V = 1000 \text{ ft/sec}$ ,  $H^\infty$  Closed-Loop System

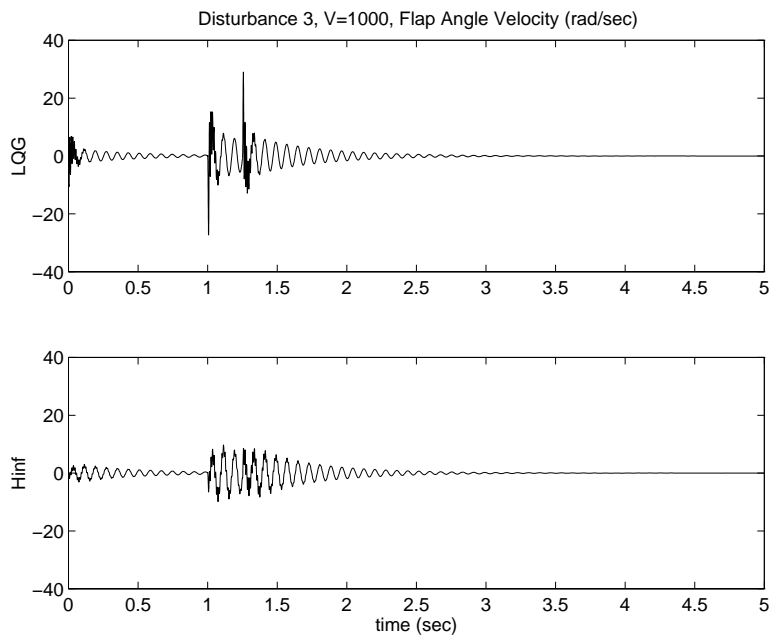


Figure 4.52: Disturbance 3,  $V = 1000 \text{ ft/sec}$ ,  $\dot{\beta}$

### 4.3 Remarks on Controller Performance

The open-loop,  $LQG$  closed-loop and the  $H^\infty$  closed-loop systems have been numerically implemented. Several simulations were run for each of the open-loop and closed-loop systems with no disturbance,  $\vec{w}(t) = \vec{0}$ , at three different velocities. Then three random disturbances were introduced to test the controllers.

For the stable case, it was shown that the controllers provided essentially the same performance as the open-loop system. In particular, the eigenvalues of the three systems have the same spectral range. In the marginally stable cases, the  $H^\infty$  controller had little affect on the system. The performance of the  $H^\infty$  controller could be improved by selecting different weights in the design. However, we chose the same weights as for the  $LQG$  design in order to make consistent comparisons.

Comparing the two controllers for the unstable velocity, the performance of the  $H^\infty$  and  $LQG$  controllers were similar. The major difference between the two systems was found in the energy required to implement the control. In each case, the  $LQG$  controlled system produced sharp spikes in the flap angle and flap-angle velocity. Comparing the flap-angle velocities for the  $LQG$  and  $H^\infty$  controlled systems, one sees that the  $H^\infty$  controller used approximately 50% of the energy used by the  $LQG$  controller. Finally, we observed that both reduce the disturbance due to the wind gust.

Although we see that the  $LQG$  and  $H^\infty$  controllers produce similar performance, the question of robustness has not been addresses. This is the subject of the following chapter.

# Chapter 5

## Analysis of Robustness

The singular value is a useful tool for robust analysis. For singular value analysis, a plant-perturbation system in the frequency domain is used. Plant-perturbation systems consist of a plant model, denoted  $M(j\omega)$ , and a perturbation model, denoted  $\Delta(j\omega)$ . In this paper, the plant is either the open-loop system, the *LQG* closed-loop system or the  $H^\infty$  closed-loop system at the various velocities. The perturbation is the additive disturbance consisting of a wind gust and sensor noise. When using a plant-perturbation system in the frequency domain the Singular Value Robust Stability theorem [2] provides a measure for robustness.

**Theorem 1** *The  $M$ - $\Delta$  system is stable for any stable  $\Delta$  satisfying*

$$\bar{\sigma}[\Delta(j\omega)] < \frac{1}{\bar{\sigma}[M(j\omega)]} \quad (5.1)$$

for all  $\omega \in R$ .

Defined earlier,  $\bar{\sigma}(A)$  is the maximum singular value of the matrix  $A$ . Necessity holds for the weakened sense in that there is some  $\Delta$  with  $\bar{\sigma}[\Delta(j\omega)] \geq \frac{1}{\bar{\sigma}[M(j\omega)]}$  such that the closed-loop system is not asymptotically stable. To apply the Singular Value Robust Stability Theorem it is necessary to transform the state-space open-loop and closed-loop systems to the frequency domain. The Laplace transform is used for this transformation.

In the frequency domain the open-loop system becomes

$$z = (C_1(sI - A)^{-1}B_1 + D_{11})w \quad (5.2)$$

or in terms of the transfer function that maps the disturbance input  $w$  to the controlled output  $z$ ,

$$T_{zw}^{ol} = C_1(sI - A)^{-1}B_1 + D_{11}. \quad (5.3)$$

For the  $LQG$  closed-loop system (3.26) the transfer function mapping  $w$  to  $z$  is

$$T_{zw}^{LQG} = C_{LQG}(sI - A_{LQG})^{-1}B_{LQG} + D_{LQG}. \quad (5.4)$$

Finally, referring to equation (3.47), the  $H^\infty$  closed-loop transfer function is given by

$$T_{zw}^{H^\infty} = C_{H^\infty}(sI - A_{H^\infty})^{-1}B_{H^\infty} + D_{H^\infty}. \quad (5.5)$$

For the analysis here we use the three plants  $M = T_{zw}^{ol}$ ,  $M = T_{zw}^{LQG}$  and  $M = T_{zw}^{H^\infty}$ .

Figures 5.1 and 5.4 are the singular value Bode plots of the open-loop system at  $V = 950ft/sec$  and  $V = 975.6ft/sec$ . Figures 5.2, 5.3 and 5.5 - 5.8 are the singular value Bode plots of the  $LQG$  and  $H^\infty$  closed-loop systems at the three velocities. From Figure 5.1 the  $H^\infty$  norm of the open-loop system at  $V = 950ft/sec$  is estimated to be

$$\|T_{zw}^{ol}\|_\infty \approx -70dB = 0.000316227.$$

Applying Theorem 1, the system is guaranteed to remain stable for

$$\|\Delta\|_\infty < 3162.$$

From this, one can see the system is naturally robust. Now we quantitatively compare the  $LQG$  and  $H^\infty$  closed-loop systems.

In Figures 5.2 and 5.3 the maximum singular values of the  $LQG$  and  $H^\infty$  closed-loop systems at  $V = 950ft/sec$  are estimated to be

$$\|T_{zw}^{LQG}\|_\infty \approx -20dB = .1$$

and

$$\|T_{zw}^{H^\infty}\|_\infty \approx -80dB = .0001,$$

respectively. Therefore, the  $LQG$  closed-loop system is guaranteed to remain stable for

$$\|\Delta\|_\infty < 10$$

and the  $H^\infty$  closed-loop system is guaranteed to remain stable for

$$\|\Delta\|_\infty < 1000.$$

From Figures 5.5 and 5.6 the maximum singular values for the  $LQG$  and  $H^\infty$  systems are estimated to be

$$\|T_{zw}^{LQG}\|_\infty = -10dB = .3162$$

and

$$\|T_{zw}^{H^\infty}\|_\infty = -80dB = .0001,$$

respectively. Therefore, the  $LQG$  closed-loop system is guaranteed to remain stable for

$$\|\Delta\|_\infty < 3.162.$$

and the  $H^\infty$  closed-loop system is guaranteed to remain stable for

$$\|\Delta\|_\infty < 1000.$$

Finally, we consider the unstable case,  $V = 1000ft/sec$ . Figures 5.7 and 5.8 the maximum singular values for the  $LQG$  and  $H^\infty$  closed-loop systems are estimated to be

$$\|T_{zw}^{LQG}\|_\infty = 15dB = 5.6234$$

and

$$\|T_{zw}^{H^\infty}\|_\infty = -.9dB = .901,$$

respectively. Therefore, the  $LQG$  closed-loop system is guaranteed to remain stable for

$$\|\Delta\|_\infty < .1778$$

and the  $H^\infty$  closed-loop system is guaranteed to remain stable for

$$\|\Delta\|_\infty < 1.12.$$

In each case the stability margin of the  $H^\infty$  closed-loop system is greater than the stability margin of the  $LQG$  closed-loop system. The  $H^\infty$  controller provides a more robust closed-loop system. As mentioned before, the closed-loop systems can be driven unstable by a perturbation  $\Delta$  with  $\|\Delta\|_\infty \geq \frac{1}{\|M\|_\infty}$ . In the case of the  $LQG$  closed-loop system at  $V = 1000ft/sec$  it would only take a perturbation of size

$$\|\Delta\|_\infty \geq .1778$$

to drive the system unstable. This is provided the disturbance acts upon the correct input. One can see that the  $LQG$  controller does not provide a very robust closed-loop system. The  $H^\infty$  controller is roughly an order of magnitude more robust. The weakness of the singular value for robust analysis is the fact that it does not specify which input channel will cause instability in the system. The structured singular value is used to address this weakness. This is left for further study.

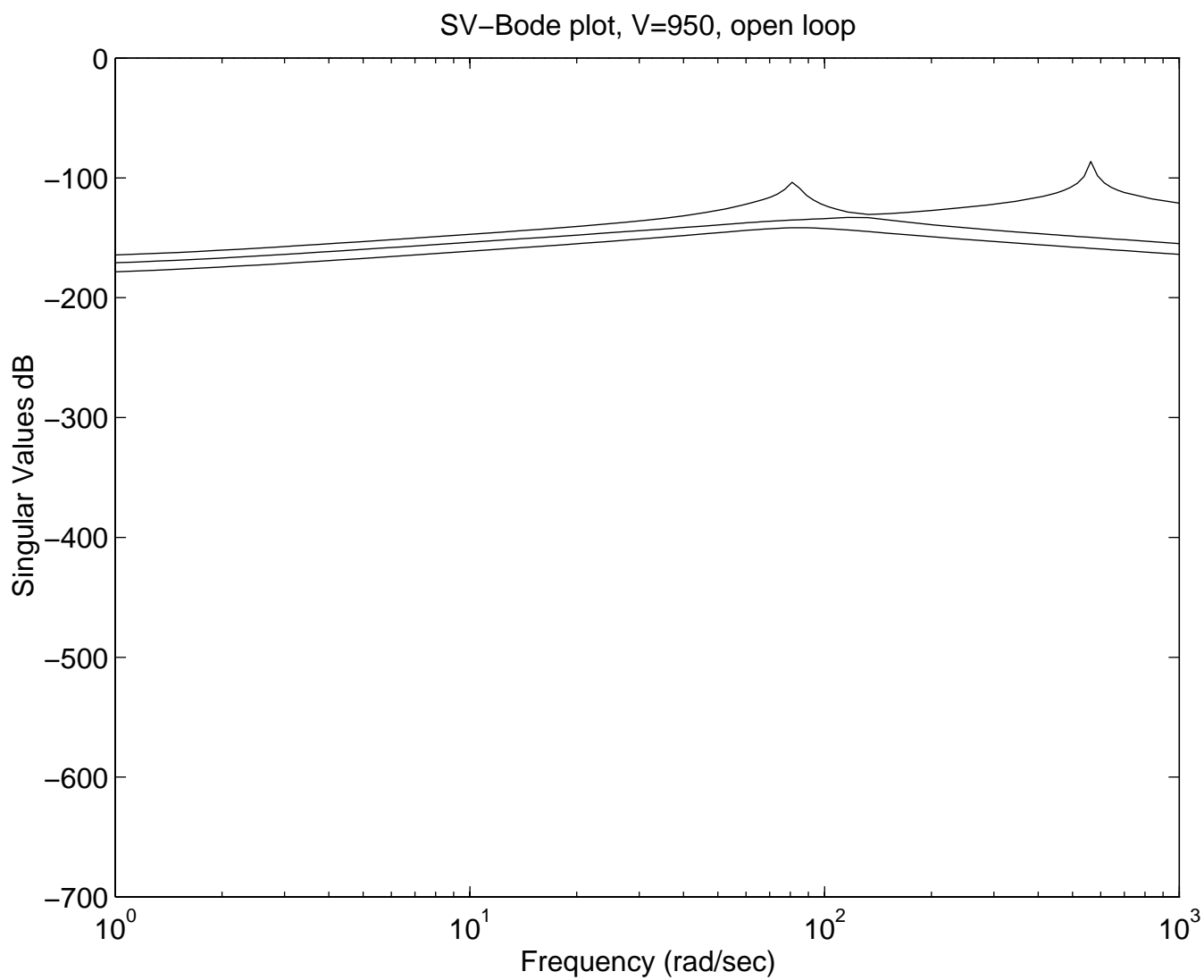


Figure 5.1: Singular Values, Open-Loop System,  $V = 950 ft/sec$

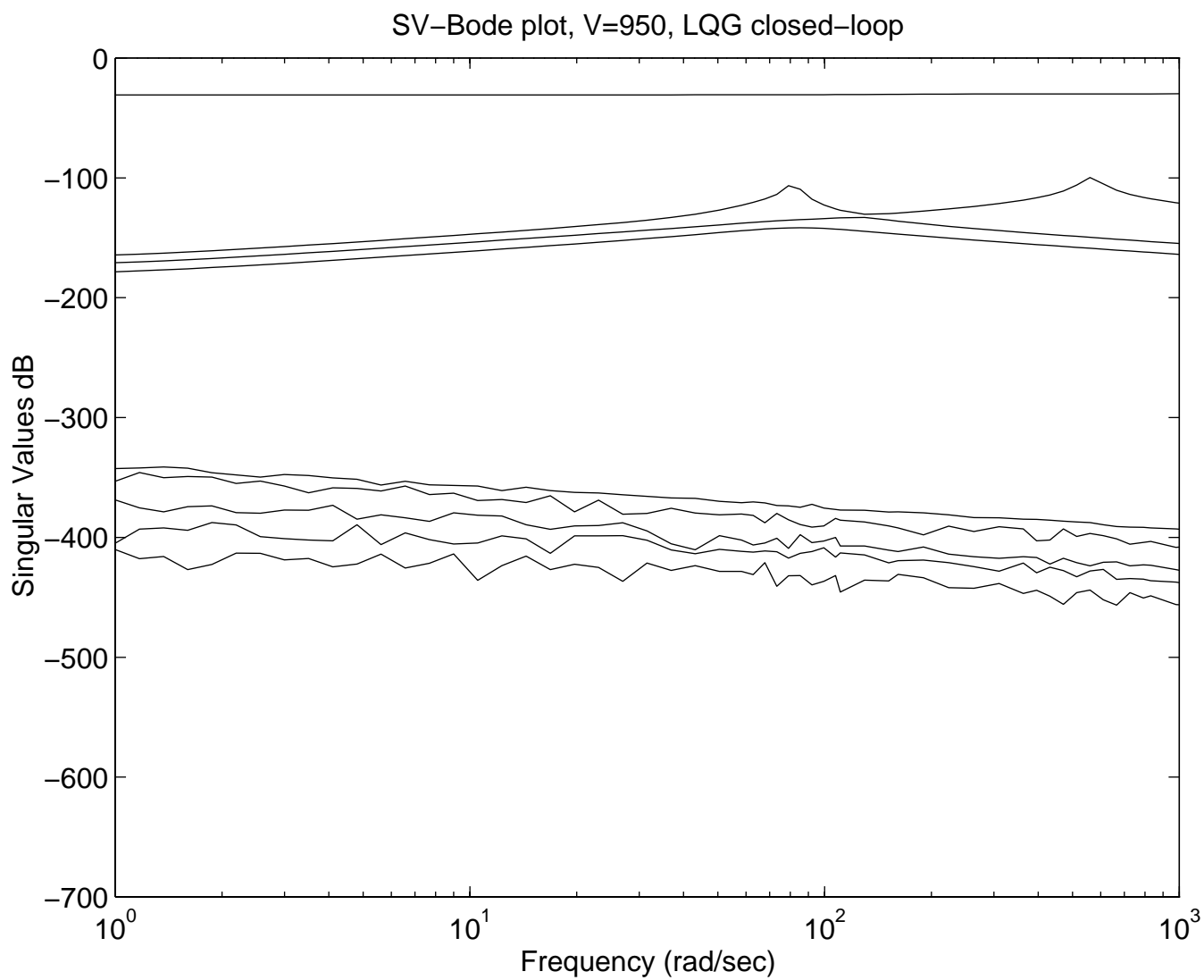


Figure 5.2: Singular Values, *LQG* Closed-Loop System,  $V = 950 ft/sec$

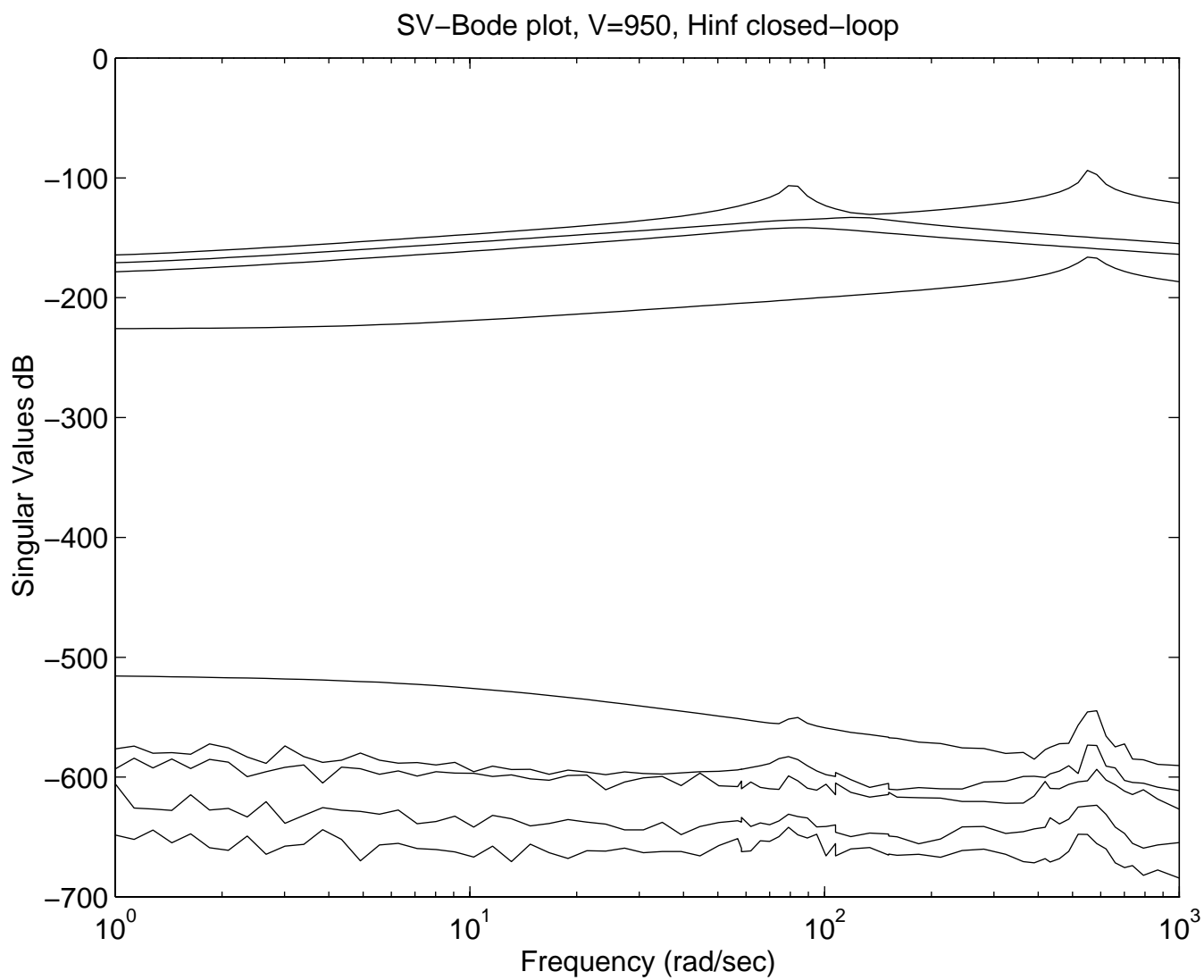


Figure 5.3: Singular Values,  $H^\infty$  Closed-Loop System,  $V = 950 \text{ ft/sec}$

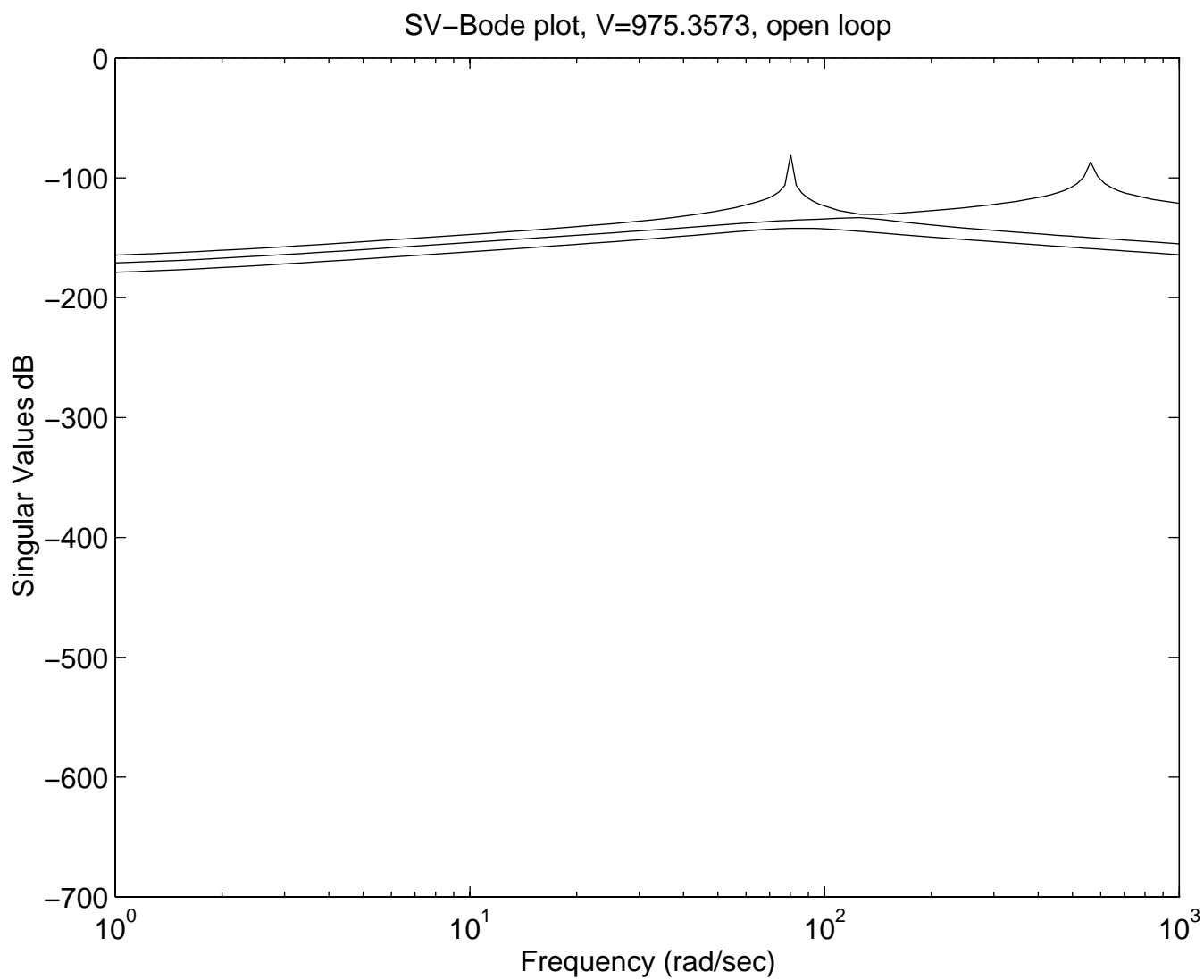


Figure 5.4: Singular Values, Open-Loop System,  $V = 975.6 \text{ ft/sec}$

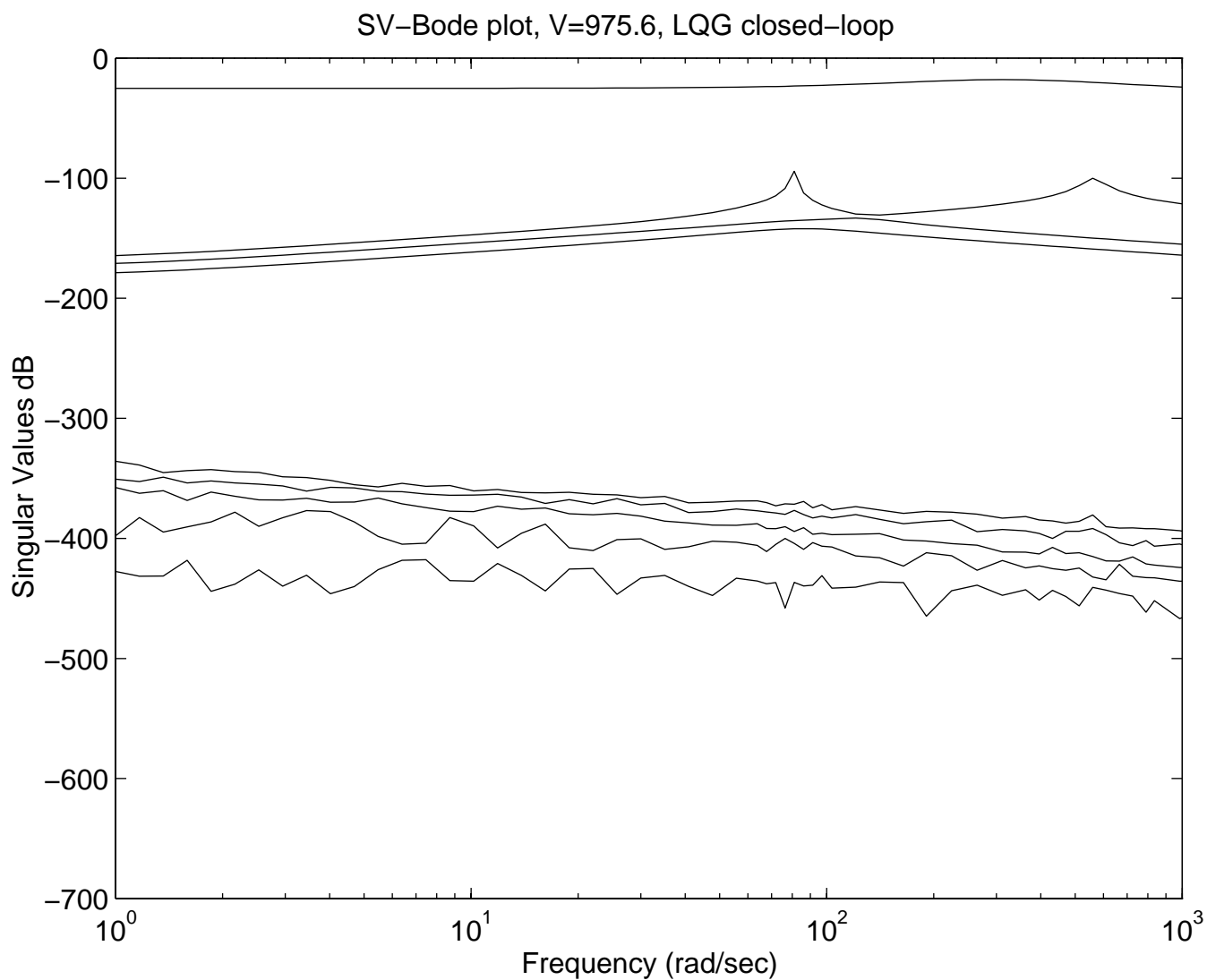


Figure 5.5: Singular Values, *LQG* Closed-Loop System,  $V = 975.6 \text{ ft/sec}$

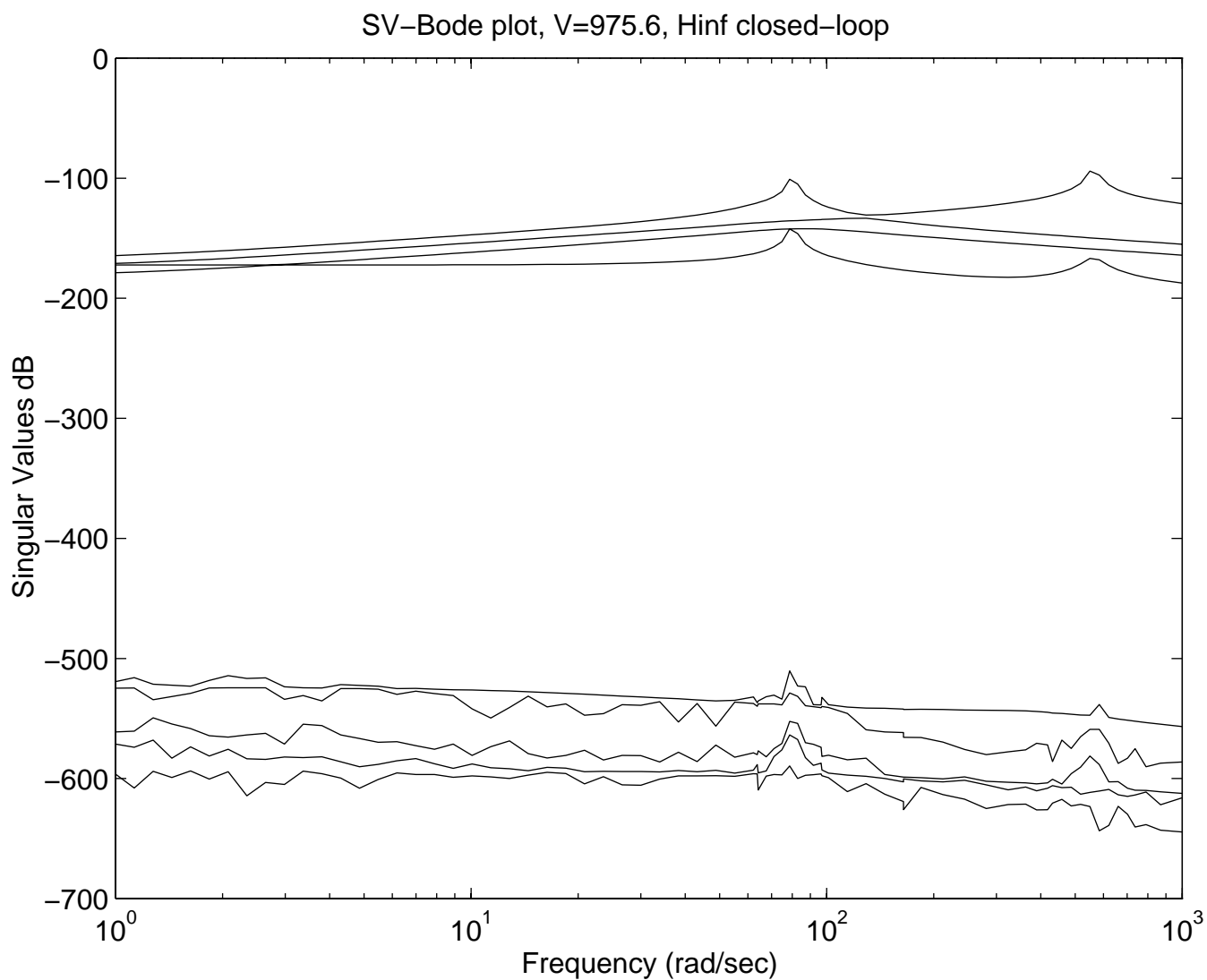


Figure 5.6: Singular Values,  $H^{\infty}$  Closed-Loop System,  $V = 975.6 \text{ ft/sec}$

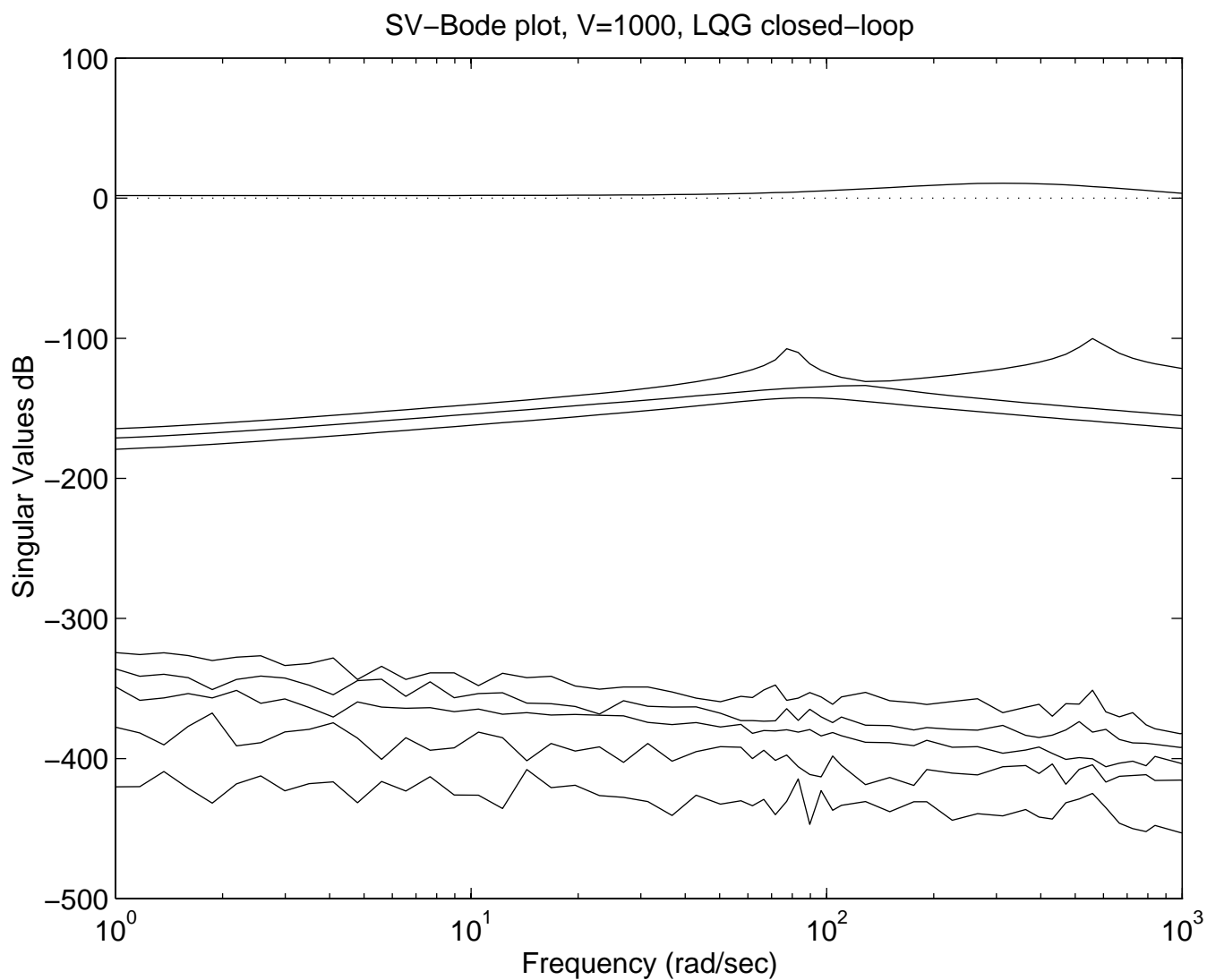


Figure 5.7: Singular Values, *LQG* Closed-Loop System,  $V = 1000 \text{ ft/sec}$

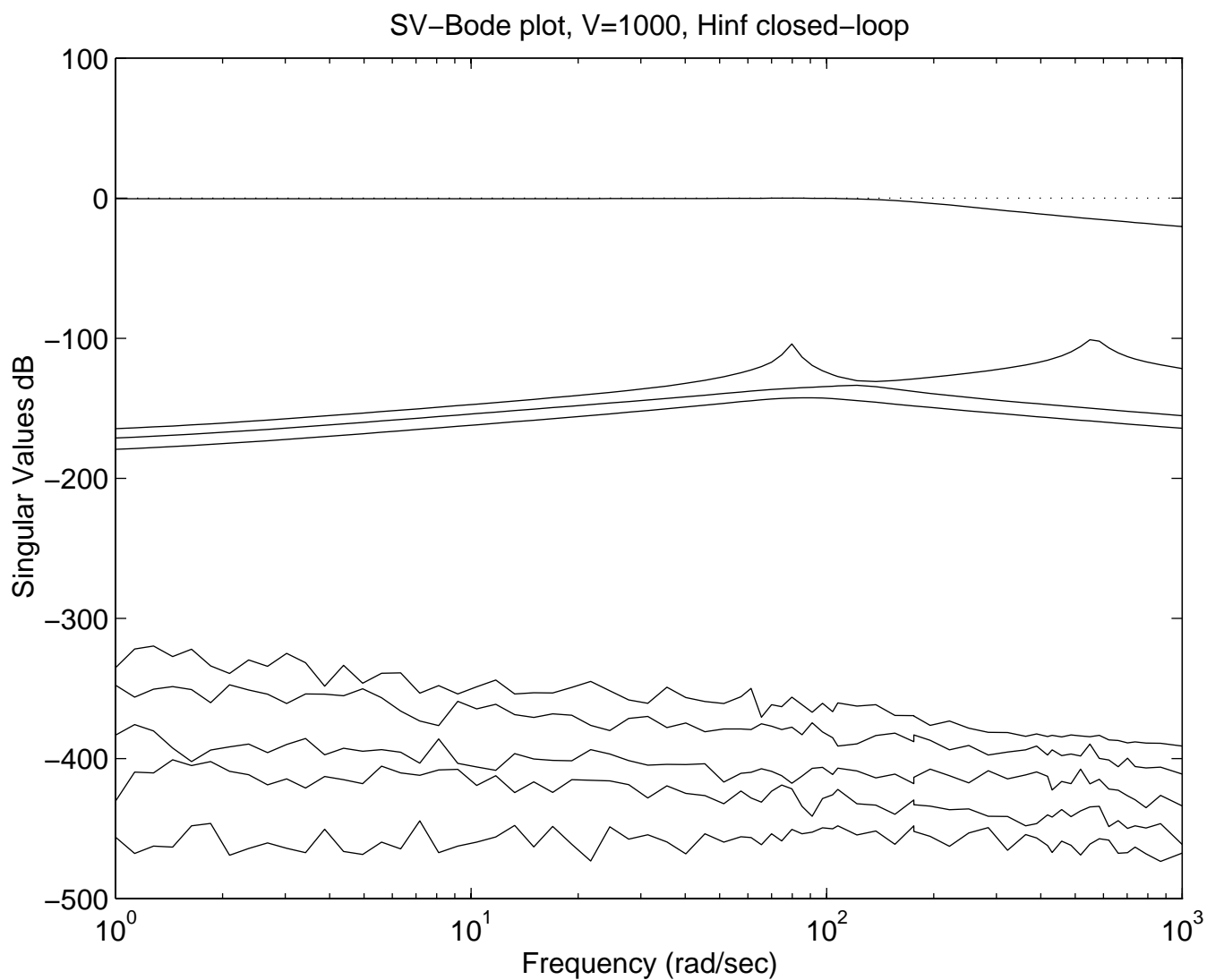


Figure 5.8: Singular Values,  $H^{\infty}$  Closed-Loop System,  $V = 1000 ft/sec$

# Chapter 6

## Conclusions

In this paper we applied  $LQG$  and  $H^\infty$  control methods to a flutter problem for a 2-D airfoil. Using the dynamical system (2.18),  $LQG$  and  $H^\infty$  control methods were applied and simulated. Disturbances were introduced to test the controllers.

The simulations produced the following observations. The  $H^\infty$  controller had little affect on system (2.18) at the flutter speed. This could be corrected through proper weighting. Also, for the unstable system, the  $H^\infty$  controller used less energy than the  $LQG$  controller.

For robust analysis the Singular Value Robust Stability Theorem [2] was reviewed and applied. The  $H^\infty$  controller provided a more robust closed-loop system than the  $LQG$  controller. One result showed the  $LQG$  to be very non-robust. The  $LQG$  closed-loop system at  $V = 1000ft/sec$  could be driven unstable by a disturbance of size greater than or equal to .1778. Structured singular value analysis would be needed to identify the channel leading to the loss of stability.

Even though this study accomplished the goals of applying and analyzing  $LQG$  and  $H^\infty$  control methods several questions remain for further study. One area of study is in proper weighting for this dynamical system. Finding better weighting for this system could provide better performance. The other area of study is investigating structured singular values for better control synthesis and analysis. Structured singular values would identify the least robust input channels and better control laws could be synthesised using specific loop shaping.

# Appendix A

## Symbols

$A$	state-space system matrix corresponding to the state vector, $x$
$A_i$	aerodynamic-lag states ( $i = 1, 2$ )
$A_{ii}$	submatrix of $A$
$A_0$	compensator matrix
$a_i$	random amplitudes ( $i = 1, 6$ )
$\alpha$	pitch angle
$B$	control input matrix
$B_1$	state-space matrix corresponding to the disturbance-input, $w$ ; aerodynamic-lag state
$B_2$	state-space matrix corresponding to the control-input, $u$ ; aerodynamic-lag state
$b$	semichord
$\beta$	controlling flap angle
$\beta_i$	coefficients in exponent in two-term approximation to the Wagner function( $i = 1, 2$ )
$c$	distance of control flap from shear center
$C_1$	controlled output matrix corresponding to the state vector, $x(t)$
$C_2$	measured output matrix corresponding to the state vector, $x(t)$
$D_{11}$	controlled output matrix corresponding to the disturbance input, $w(t)$
$D_{12}$	controlled output matrix corresponding to the control input, $u(t)$
$D_{21}$	measured output matrix corresponding to the disturbance input, $w(t)$
$D_{22}$	measured output matrix corresponding to the control input $u(t)$
$E\{\}$	expectation operator
$G$	state-space matrix corresponding to the gust-input, $w_1$ ; stable Laplace matrix
$h$	plunge
$I_\alpha$	moment of inertia for airfoil
$I_\beta$	moment of inertia for control flap
$J_{LQG}$	LQG cost function

$K$	stiffness matrix; stabilizability gain matrices
$K_\alpha$	stiffness of pitch spring; pitch spring
$K_\beta$	stiffness of flap spring; flap spring
$K_h$	stiffness of plunge spring; plunge spring
$K_c$	controller gain matrix
$K_f$	filter gain matrix
$L$	lift; detectability gain matrices
$M$	pitching moment; mass matrix; terminal control matrix
$m$	mass of airfoil
$N$	measured output matrix corresponding to the sensor noise input, $w_2$
$P$	solution to the ARE(3.15)
$p_i$	random numbers determining various periods ( $i = 1, 2$ )
$\phi_i$	aerodynamic constants
$Q$	$C_1^* C_1$
$R$	$D_{12}^* D_{12}$
$R_i$	constants ( $i = 1, 10$ )
$\rho$	air density
$S$	solution to the FARE(3.16)
$S_\alpha$	static moment of airfoil
$S_\beta$	static moment of control flap
$\bar{\sigma}$	maximum singular value
$T$	torque of flap spring
$T_{zw}$	closed-loop system with disturbance input $w(t)$ and output $z(t)$
$t$	time
$\Theta$	correlation matrix
$\theta$	white, Gaussian sensor noise
$u(t)$	control input
$V$	velocity of airfoil; LQR cost function
$V_f$	flutter speed
$w(t)$	disturbance input consisting of $w_1$ and $w_2$
$w_G$	vertical gust velocity
$w_L(t)$	lift impulse function
$w_M(t)$	moment impulse function
$w_f(t)$	control flap impulse function
$w_1(t)$	gust input vector
$w_2(t)$	sensor-noise input vector

$x(t)$	state vector
$x_A(t)$	column vector of aerodynamic state variables
$\hat{x}(t)$	state estimator
$\Xi$	correlation matrix
$\xi$	white, Gaussian plant noise
$Y$	column vector of plunge, pitch and flap displacement
$y(t)$	measured output
$Z_i$	$(i = 1, 4)$
$z(t)$	controlled output

# Appendix B

## Constants and Matrices

$$A_{11} = -[M' + \pi\rho b^2 Z_1]^{-1} \pi\rho b^2 Z_2 \quad (\text{B.1})$$

$$A_{12} = -[M' + \pi\rho b^2 Z_1]^{-1} (K + \pi\rho b^2 Z_3) \quad (\text{B.2})$$

$$A_{13} = -[M' + \pi\rho b^2 Z_1]^{-1} \pi\rho b^2 Z_4 \quad (\text{B.3})$$

$$A_{21} = [I_{3 \times 3}], A_{22} = [0_{3 \times 3}], A_{23} = [0_{3 \times 4}] \quad (\text{B.4})$$

$$A_{31} = \left[ \begin{array}{ccc|ccc} R_1 & R_2 & R_3 & A_{11} + & \left[ \begin{array}{ccc} 0 & R_4 & R_5 \end{array} \right] \\ R_1 & R_2 & R_3 & A_{11} + & \left[ \begin{array}{ccc} 0 & R_4 & R_5 \end{array} \right] \\ R_6 & R_7 & R_8 & A_{11} + & \left[ \begin{array}{ccc} 0 & R_9 & R_{10} \end{array} \right] \\ R_6 & R_7 & R_8 & A_{11} + & \left[ \begin{array}{ccc} 0 & R_9 & R_{10} \end{array} \right] \end{array} \right], \quad (\text{B.5})$$

$$A_{32} = \left[ \begin{array}{ccc|c} R_1 & R_2 & R_3 & A_{12} \\ R_1 & R_2 & R_3 & A_{12} \\ R_6 & R_7 & R_8 & A_{12} \\ R_6 & R_7 & R_8 & A_{12} \end{array} \right] \quad (\text{B.6})$$

$$A_{33} = \left[ \begin{array}{cccc} \left[ \begin{array}{cccc} \frac{-\beta_1 V}{b} & 0 & 0 & 0 \\ 0 & \frac{-\beta_2 V}{b} & 0 & 0 \\ 0 & 0 & \frac{-\beta_1 V}{b} & 0 \\ 0 & 0 & 0 & \frac{-\beta_2 V}{b} \end{array} \right] & + & \left[ \begin{array}{ccc|c} R_1 & R_2 & R_3 & A_{13} \\ R_1 & R_2 & R_3 & A_{13} \\ R_6 & R_7 & R_8 & A_{13} \\ R_6 & R_7 & R_8 & A_{13} \end{array} \right] \end{array} \right] \quad (\text{B.7})$$

$$M = \begin{bmatrix} bm & S_\alpha & S_\beta \\ bS_\alpha & I_\alpha & I_\beta + (S_\alpha bc) \\ bS_\beta & I_\beta + (S_\beta bc) & I_\beta \end{bmatrix} \quad (\text{B.8})$$

$$K = \begin{bmatrix} bK_h & 0 & 0 \\ 0 & K_\alpha & 0 \\ 0 & 0 & K_\beta \end{bmatrix} \quad (\text{B.9})$$

$$\begin{aligned} Z_1 &= \begin{bmatrix} L_{\ddot{h}} & L_{\ddot{\alpha}} & L_{\ddot{\beta}} \\ M_{\ddot{h}} & M_{\ddot{\alpha}} & M_{\ddot{\beta}} \\ T_{\ddot{h}} & T_{\ddot{\alpha}} & T_{\ddot{\beta}} \end{bmatrix}, \quad Z_2 = \begin{bmatrix} L_{\dot{h}} & L_{\dot{\alpha}} & L_{\dot{\beta}} \\ 0 & M_{\dot{\alpha}} & M_{\dot{\beta}} \\ T_{\dot{h}} & T_{\dot{\alpha}} & T_{\dot{\beta}} \end{bmatrix} \\ Z_3 &= \begin{bmatrix} 0 & L_\alpha & L_\beta \\ 0 & 0 & M_\beta \\ 0 & T_\alpha & T_\beta \end{bmatrix}, \quad Z_4 = \begin{bmatrix} L_{B_1} & L_{B_2} & 0 & 0 \\ 0 & 0 & 0 & 0 \\ 0 & 0 & T_{A_1} & T_{A_2} \end{bmatrix} \end{aligned} \quad (\text{B.10})$$

$R_1$	$=$	$b^2/V$
$R_2$	$=$	$b^2/V$
$R_3$	$=$	$\phi_2 b^2/2\pi V$
$R_4$	$=$	$V$
$R_5$	$=$	$\phi_1 V/\pi$
$R_6$	$=$	$\phi_8 b^3/\pi V$
$R_7$	$=$	$\phi_8 b^3/\pi V$
$R_8$	$=$	$\phi_2 \phi_8 b^3/2V\pi^2$
$R_9$	$=$	$\phi_8 Vb/\pi$
$R_{10}$	$=$	$\phi_1 \phi_8 Vb/\pi^2$

Table B.1: List of  $R$ 's

$\Phi_1(\phi)$	$= \pi - \phi + \sin \phi$
$\Phi_2(\phi)$	$= (\pi - \phi)(1 + 2 \cos \phi) + \sin \phi(2 + \cos \phi)$
$\Phi_3(\phi)$	$= \pi - \phi + \sin \phi \cos \phi$
$\Phi_4(\phi)$	$= (\pi - \phi)2 \cos \phi + \sin \phi \frac{2}{3}(2 + \cos^2 \phi)$
$\Phi_5(\phi)$	$= \sin \phi(1 - \cos \phi)$
$\Phi_6(\phi)$	$= 2(\pi - \phi) + \sin \phi \frac{2}{3}(2 - \cos \phi)(1 + 2 \cos \phi)$
$\Phi_7(\phi)$	$= (\pi - \phi)(\frac{1}{2} + 2 \cos \phi) + \sin \phi \frac{1}{6}(8 + 5 \cos \phi + 4 \cos^2 \phi - 2 \cos^3 \phi)$
$\Phi_8(\phi)$	$= (\pi - \phi)(-1 + 2 \cos \phi) + \sin \phi(2 - \cos \phi)$
$\Phi_9(\phi)$	$= (\pi - \phi)(1 + 2 \cos \phi) + \sin \phi \frac{1}{3}(2 + 3 \cos \phi + 4 \cos^2 \phi)$
$\Phi_{10}(\phi)$	$= \Phi_{31}(\phi) \cdot \Phi_5(\phi)$
$\Phi_{11}(\phi)$	$= \Phi_2(\phi) \cdot \Phi_3(\phi)$
$\Phi_{12}(\phi)$	$= (\pi - \phi)^2(\frac{1}{2} + 4 \cos^2 \phi) + (\pi - \phi) \sin \phi \cos \phi(7 + 2 \cos^2 \phi)$ $+ \sin^2 \phi(2 + \frac{5}{2} \cos^2 \phi)$
$\Phi_{31}(\phi)$	$= \pi - \phi - \sin \phi$

Table B.2: List of  $\Phi$ 's

$\alpha_1$	$= .0165$
$\alpha_2$	$= .335$
$b$	$= 3ft$
$\beta_1$	$= .041$
$\beta_2$	$= .32$
$c$	$= 1.0$
$I_\alpha$	$= 6.04868 \frac{slug-ft.^2}{ft.}$
$I_\beta$	$= .151217 \frac{slug-ft.^2}{ft.}$
$K_\alpha$	$= I_\alpha * 100^2$
$K_\beta$	$= I_\beta * 500^2$
$K_h$	$= m * 50^2$
$m$	$= 2.6883 \frac{slugs}{ft.}$
$\rho$	$= .002378 * 1$
$S_\alpha$	$= 1.61298 * 1.0 \text{ slugs}$
$S_\beta$	$= .10081 * 1.0 \text{ slugs}$
$V_f$	$= 975.6ft/sec$

Table B.3: List of Constants

# Appendix C

## MATLAB Codes

flutter.m

```
% M-file that generates the disturbance-input system
% and applies the control schemes.
%Inputs: Velocity(ft/sec) and gust begin time.
```

buildsys

```
global A B1 B2 C1 C2 D11 D12 D21 D22 G Q R w0 wg0 ...
        Alqr Blqr Clqr Dlqr Kc Kf Blqg Alqg Clqg Dlqg ...
        Ahinf Bhinf Chinf Dhinf tstep g1 g2 g3 a1 a2 ...
        a3 a4 a5 a6 p1 p2
tstep = input('tstep =')
runlqr
runlqg
runhinf
```

```
g1 = 3*10^8;
g2 = 10;
g3 = 0;
```

```
a1 = 15;
a2 = 8;
a3 = 2;
a4 = .6;
a5 = .2;
a6 = .0015;
```

```
p1 = 5;
```

```
p2 = 10;
```

```
buildsys.m
```

```
%Builds matrices for the disturbance-input system.
```

```
constnt
```

```
phi
```

```
tees
```

```
arrs
```

```
ells
```

```
emms
```

```
zees
```

```
mkprime
```

```
biga
```

```
bmatrix
```

```
cmatrix
```

```
dmatrix
```

```
weight
```

```
clear
```

```
load velocity
```

```
load amatrix
```

```
load bmatrix
```

```
load cmatrix
```

```
load dmatrix
```

```
load weight
```

```
initials
```

```
save sysmats V A B1 B2 C1 C2 D11 D12 D21 D22 G Q R w0 wg0
```

```
clear
```

```
load sysmats
```

cnstnt.m

```
%Constants for flutter problem.
b = 3;
c = 1;
V = input('velocity =')
%Vflutter at .6 flap = 975.35728157184669
m =2.6883;
Row = .002378*1;
ALPHA1 = .0165;
ALPHA2 = .335;
SALPHA = 1.61298*1.0;
SBETA = .10081*1.0;
IALPHA = 6.04868;
IBETA = .151217;
KH = m*50^2;
BETA1 = .041;
BETA2=.32;
KALPHA = IALPHA*100^2;
KBETA = IBETA*500^2;
save velocity V
```

phi.m

```
%Calculates phi's and sets the location of the flap angle.
```

```
xflap=.6;
Phi=acos(-xflap);
Phi1 = pi - Phi + sin(Phi);
Phi2 = (pi - Phi)*(1 + 2*cos(Phi)) + sin(Phi)*(2 + cos(Phi));
Phi3 = pi - Phi + sin(Phi)*cos(Phi);
Phi4 = (pi - Phi)*2*cos(Phi) + sin(Phi)*2/3*(2 + (cos(Phi))^2);
Phi5 = sin(Phi)*(1 - cos(Phi));
Phi6 = 2*(pi - Phi) + sin(Phi)*2/3*(2-cos(Phi))*(1 + 2*cos(Phi));
Phi7 = (pi - Phi)*(.5 + 2*cos(Phi)) + sin(Phi)*(1/6)*(8 + 5*cos(Phi)
+...
4*cos(Phi)^2 - 2*cos(Phi)^3);
Phi8 = (pi - Phi)*(-1 + 2*cos(Phi)) + sin(Phi)*(2-cos(Phi));
Phi9 = (pi - Phi)*(1 + 2*cos(Phi)) + sin(Phi)*1/3*(2 + 3*cos(Phi) +...
4*(cos(Phi))^2);
```

```

Phi31= pi - Phi - sin(Phi);
Phi10= Phi31 * Phi5;
Phi11= Phi2 * Phi3;
Phi12= (pi - Phi)^2 * (.5 + 4*cos(Phi)^2) + (pi - Phi) * sin(Phi)*...
cos(Phi)*(7 + 2*(cos(Phi))^2) + (sin(Phi))^2*(2 + 2.5*(cos(Phi))^2);

```

tees.m

```

% Generates T's in the Z matrices.
% b, V, ALPHA1, and ALPHA2 defined in CNSTNT.M
% Phi's generated in PHI.M

```

```

TH2 = (b^2/(2*pi))*Phi4;
TALPHA2 = (b^2/(4*pi^2))*Phi7;
TBETA2 = (b^2/(4*pi^2))*Phi12;
TH1 = (V*b/pi)*Phi2;
TALPHA1 = (V*b/pi)*(Phi9/2 + Phi8);
TBETA1 = (V*b/(2*pi^2))*(Phi11 + Phi2*Phi8);
TH0 = 0;
TALPHA0 = (V^2/pi)*Phi8;
TBETA0 = (V^2/pi^2)*(Phi10 + Phi1*Phi8);
TA1 = -V*ALPHA1/b;
TA2 = -V*ALPHA2/b;

```

arrrs.m

```

% Generates R values for the A matrix.
% R's are called from BIGA.M
% b and V are defined in CNSTNT.M
% Phi's are created in PHI.M

```

```

R1 = b^2/V;
R2 = b^2/V;
R3 = (b^2/(2*pi*V))*Phi2;
R4 = V;
R5 = V/pi *Phi1;
R6 = (b^3/(pi*V))*Phi8;
R7 = (b^3/(pi*V))*Phi8;
R8 = (b^3/(2*V*pi^2))*Phi2*Phi8;
R9 = (V*b/pi)*Phi8;

```

```
R10 = (V*b/pi^2)*Phi1*Phi8;
```

```
ells.m
```

```
% Generates the L values for the Z matrices.  
% b V ALPHA1, and ALPHA2 are defined in CNSTNT.M  
% Phi's are defined in PHI.M
```

```
LH2 = b;  
LALPHA2 = b/2;  
LBETA2 = (b/(2*pi))*Phi4;  
LH1 = 2*V;  
LALPHA1 = 3*V;  
LBETA1 = (V/pi)*(Phi3 + Phi2);  
LH0 = 0;  
LALPHA0 = 2*(V^2)/b;  
LBETA0 = (2*(V^2)/(pi*b))*Phi1;  
LB1 = -2*V*ALPHA1/b;  
LB2 = -2*V*ALPHA2/b;
```

```
emms.m
```

```
% Generates the M values for the Z matrices.  
% b and V defined in CNSTNT.M  
% Phi's defined in PHI.M
```

```
MH2 = (b^2)/2;  
MALPHA2 = (3*b^2)/8;  
MBETA2 = ((b^2)/(4*pi))*Phi7;  
MH1 = 0;  
MALPHA1 = V*b;  
MBETA1 = (V*b/(2*pi))*Phi6;  
MHO = 0;  
MALPHA0 = 0;  
MBETA0 = ((V^2)/pi)*Phi5;
```

```
zees.m
```

```
%Generates the Z matrices used in building the A matrix
```

```

Z1 = [LH2 LALPHA2 LBETA2; MH2 MALPHA2 MBETA2; TH2 TALPHA2 TBETA2];
Z2 = [LH1 LALPHA1 LBETA1; 0 MALPHA1 MBETA1; TH1 TALPHA1 TBETA1];
Z3 = [0 LALPHA0 LBETA0; 0 0 MBETA0; 0 TALPHA0 TBETA0];
Z4 = [LB1 LB2 0 0; 0 0 0 0; 0 0 TA1 TA2];

```

mkprime.m

```

%Builds the mass and stiffness matrices used in building matrix A.
% b, m SALPHA, SBETA, IALPHA, IBETA, c, KH, KALPHA, KBETA all are
% defined in CNSTNT.M

```

```

MPRIME = [ b*m SALPHA SBETA; b*SALPHA IALPHA IBETA+(SBETA*b*c);
          b*SBETA IBETA+(SBETA*b*c) IBETA];

```

```

KPRIME = [b*KH 0 0; 0 KALPHA 0; 0 0 KBETA];

```

```

global MPRIME KPRIME

```

biga.m

```

% Generates the A matrix from the submatrices A11 through A33.
% This is the A matrix used in y = A*x.
% R's are defined in ARRS.M
% MPRIME and KPRIME defined in MKPRIME.M
% Row, b, V are defined in CNSTNT.M
% Z's are defined in ZEES.M
% BETA1 and BETA2 defined by CNSTNT.M

```

```

A11 = -1*inv(MPRIME + (pi*Row*(b^2)*Z1)) * pi*Row*(b^2)*Z2;
A12 = -1*inv(MPRIME + (pi*Row*(b^2)*Z1)) * (KPRIME + pi*Row*(b^2)*Z3);
A13 = -1*inv(MPRIME + (pi*Row*(b^2)*Z1)) * pi*Row*(b^2)*Z4;
A21 = eye(3);
A22 = zeros(3);
A23 = zeros(3,4);
A31 = [[R1 R2 R3]*A11 + [0 R4 R5]; [R1 R2 R3]*A11 + [0 R4 R5];
        [R6 R7 R8]*A11 + [0 R9 R10]; [R6 R7 R8]*A11 + [0 R9 R10]];

```

```

A32 = [[R1 R2 R3]*A12; [R1 R2 R3]*A12; [R6 R7 R8]*A12; [R6 R7 R8]*A12];
A330=eye(4);
A330(1,1)=-BETA1*V/b;
A330(2,2)=-BETA2*V/b;
A330(3,3)=-BETA1*V/b;
A330(4,4)=-BETA2*V/b;
A33 = [A330 + [[R1 R2 R3]*A13; [R1 R2 R3]*A13; [R6 R7 R8]*A13; [R6 R7
R8]*A13]];

```

```

% Building the A matrix from the submatrices above
A = [A11 A12 A13; A21 A22 A23; A31 A32 A33];

```

```

save amatrix A

```

```

bmatrix.m

```

```

% B matrices used in the control system,
% xdot =Ax + B1w + B2u.
% MPRIME called from MKPRIME.M.
% IBETA set in CNSTNT.M.

```

```

G = [(pi*Row*(b^2)/V)*(inv(MPRIME + (pi*Row*(b^2)*Z1)))*...
      eye(3); zeros(7,3)];

```

```

B1 = [G zeros(10,6)];

```

```

bbb0=[0 0 1];
bbb1=[0 0 0];
bbb2=[0 0 0 0];
bbb0=inv(MPRIME)*bbb0';
B2=(1/IBETA)*[bbb0' bbb1 bbb2]';

```

```

save bmatrix G B1 B2

```

```

cmatrix.m

```

```

% Creates state matrices C1 and C2

```

```

C1 = [eye(10); zeros(1,10)];
C1(7,7) = .0001;

```

```
C1(8,8) = .0001;  
C1(9,9) = .0001;  
C1(10,10) = .0001;
```

```
C2=27*[eye(6) zeros(6,4)];
```

```
save cmatrix C1 C2
```

```
dmatrix.m
```

```
%Creates the disturbance-input matrices D11 and D21. Also  
%the control-input matrices D12 and D22.
```

```
D11 = [zeros(11,9)];
```

```
D21 = [zeros(6,3) eye(6)];
```

```
D12 = [zeros(10,1); 1];
```

```
D22 = [zeros(6,1)];
```

```
save dmatrix D11 D21 D12 D22
```

```
weight.m
```

```
%creates the weighting matrices Q and R
```

```
Q = C1'*C1;
```

```
R = D12'*D12;
```

```
save weight Q R
```

```
initials.m
```

```
%Initial conditions for solving odes  
global w0 wg0
```

```
w0 = zeros(10,1);
```

```
w0(1)=.05;  
w0(2)=-.01;  
w0(3)=.005;  
w0(4)=-.1;  
w0(5)=.001;  
w0(6)=-.0001;
```

```
wg0=zeros(20,1);  
wg0(1)=.05;  
wg0(2)=-.01;  
wg0(3)=.005;  
wg0(4)=-.1;  
wg0(5)=.001;  
wg0(6)=-.0001;  
wg0(11)=.045;  
wg0(12)=-.005;  
wg0(13)=.0045;  
wg0(14)=-.09;  
wg0(15)=.0015;  
wg0(16)=-.00009;
```

```
runlqr.m
```

```
%Set up and run the LQR problem
```

```
global Alqr Blqr Clqr Dlqr fk
```

```
Kc=lqr(A,B2,Q,R);  
Alqr = A-B2*Kc;  
Blqr = G;  
Clqr = C1+D12*Kc;  
Dlqr = zeros(11,3);
```

```
runlqg.m
```

```
%Set up and run the LQG problem.
```

```
global Alqg Blqg Clqg Dlqg Kf Xi Theta acpl bcpl ccpl dcpl
```

```
Xi = eye(10);
```

```
Theta = eye(6);
```

```
Kftran = lqr(A',C2',Xi,Theta);
```

```
Kf=Kftran';
```

```
Alqg = [A -B2*Kc; Kf*C2 A-(B2*Kc)-(Kf*C2)];
```

```
Blqg = [B1; Kf*D21];
```

```
Clqg = [C1 -D12*Kc];
```

```
Dlqg = D11;
```

```
acpl = [A-B2*Kc-Kf*C2];
```

```
bcpl = [Kf];
```

```
ccpl = [-Kc];
```

```
dcpl = [zeros(1,6)];
```

```
runhinf.m
```

```
%runs the hinf controller for the flutter problem
```

```
global Ahinf Bhinf Chinf Dhinf
```

```
[acph, bcph, ccph, dcph,Ahinf,Bhinf,Chinf,Dhinf,hinfo,ak,b1k,b2k,...  
c1k,c2k,d11k,d12k,d21k,d22k]=hinf(A,B1,B2,C1,C2,D11,D12,D21,D22);
```

```
gustep.m
```

```
% Step function that turns on gust at
```

```
% specified time (tstep). Used in GUST.M
```

```
function z=gustep(tt)
```

```
global tstep
```

```
z=0;
```

```
if tt>tstep
```

```
z=1;
```

```
end
```

```
if tt > tstep + .25
```

```
z=0;
```

```
end
```

```
rhs.m
```

```
%Solves the right-hand side, Ax.
```

```
function y=rhs(t,w)
```

```
global A tstep G g1 g2 g3
```

```
y=A*w + G*[g1*gustep(t);g2*gustep(t); g3*gustep(t)];
```

```
rhslqg.m
```

```
% Solves the right-hand side, Alqg.
```

```
% Uses the LQG controller, gust and
```

```
% sensor noise are added
```

```
function y=rhslqgn(tn,wn)
```

```
global Alqg tstep Blqg g1 g2 g3 a1 a2 a3 a4 a5 a6 p1 p2 Noise
```

```
Noise = [a1*cos(p1*tn); a2*cos(p1*tn); a3*cos(p2*tn); a4*cos(p2*tn);  
         a5*cos(p2*tn); a6*cos(p2*tn)];
```

```
y=Alqg*wn + Blqg*[g1*gustep(tn); g2*gustep(tn); g3*gustep(tn); Noise];
```

```
rhshinf.m
```

```
%sets up rhside for ode45 to solve the Hinf closed loop matrix
```

```
function y = rhshinf(tn,wn)
```

```
global Ahinf Bhinf tstep g1 g2 g3 a1 a2 a3 a4 a5 a6 p1 p2 Noise
```

```
Noise = [a1*cos(p1*tn); a1*cos(p1*tn); a3*cos(p1*tn); a4*cos(p2*tn);  
         a5*cos(p2*tn); a6*cos(p2*tn)];
```

```
y = Ahinf*wn + Bhinf*[g1*gustep(tn); g2*gustep(tn); g3*gustep(tn);  
Noise];
```

# Bibliography

- [1] B.D.O. Anderson and J.B. Moore *Optimal Control: Linear Quadratic Methods*, Prentice Hall, 1990
- [2] R.Y. Chiang and M.G. Safonov *Robust Control Toolbox User's Guide*, The Math Works, Inc., 1992
- [3] P. Dorato, C. Abdallah and V. Cerone, *Linear-Quadratic Control: An Introduction*, Prentice Hall, 1995.
- [4] E.H. Dowell, *A modern course in aerolasticity*, Sijthoff and Noordhoff, 1978
- [5] J.C. Doyle, "Guaranteed margins for LQG regulators," *IEEE Trans. Automat. Contr.* AC-23 1978: 756-757.
- [6] J.C. Doyle, K. Glover, P. Khargonekar, B. Francis, "State-Space Solutions to Standard  $H_2$  and  $H_\infty$  Control Problems" *IEEE Transactions on Automatic Control* Vol 34, No. 8, 1989: 831-846
- [7] A. Grace, A. Laub, J. Little, and C. Thompson, *Control System Toolbox User's Guide*, The Math Works, Inc., 1992
- [8] Micheal Green and David Limebeer, *Linear Robust Control*, Prentice Hall, Englewoods Cliffs, New Jersey, 1995.
- [9] Shana Olds, *Modeling and LQR Control of a Two-Dimensional Airfoil*, MS Thesis, Virginia Tech, 1997.
- [10] Ihnseok Rhee and Jason L. Speyer, "A Game Theroetic Controller and its Relationship to  $H^\infty$  and Linear-Exponential-Gaussian Synthesis," *Proceedings of the Conference on Decision and Control* Tampa FLA 1989 :909-915.
- [11] Kemin Zhou with J. Doyle and K. Glover, *Robust and Optimal Control*, Prentice Hall, 1996

- [12] Darrell L. York. *Analysis of Flutter and Flutter Suppression Via An Energy Method*, MS Thesis, Virginia Tech, 1980.

# Vita

Thomas Bail was born in Washington D.C. on May 18th, 1973. He grew up in a Navy family and got the chance to live in many unique parts of the world. He graduated from Virginia Tech in May 1995 with a B.S. in Mathematics (Applied Computational Option) and a minor in Physics. To complete an M.S in Applied Mathematics, he remained at Virginia Tech and studied under Dr. John Burns. After graduation he will be working for Hughes Missiles Systems in the Guidance, Navigation, and Control department.